Thesis in Biomedical and Pharmaceutical Sciences

Identification of small molecules targeting the tetrameric interface of lactate dehydrogenases for enhanced therapeutic strategies

Chiara Brustenga

Pr. Raphaël Frédérick & Pr. Pierre Sonveaux

2024

Remerciements

I thank my supervisor, Prof. **Raphaël Frédérick**, for welcoming me into his laboratory for my master thesis and giving me the opportunity to start this long journey. Your trust allowed me to pursue my PhD and provided me with the scientific autonomy I needed. These five years have been immensely enriching for me, both scientifically and personally. The opportunity to move to a new city and learn a new language has been life-changing. I will always be grateful for the opportunity you gave me.

I want to thank my co-promoter, **Prof. Pierre Sonveaux**, for always supporting and encouraging me. Our scientific discussions were not only interesting but also incredibly helpful. What I appreciate even more is his humanity and the time he took to listen and care about his students. His support and kindness have meant a lot to me, and I am truly grateful for everything he has done.

I would like to warmly thank **Prof. Giulio Muccioli**, **Prof. Joris Messens**, and **Prof. Bart De Spiegeleer** for guiding me with their suggestions and discussions since my first year. Your insights and support have been invaluable. I also extend a huge thank you to **Prof. Filippo Minutolo** and **Prof. Serge Van Calenbergh** for accepting to be part of my jury and for their precious suggestions in helping me finalize this pathway. Thank you all for the time you have dedicated reading my manuscript. I really appreciate it.

Asia, ton aide au laboratoire, tes câlins et ta joie de vivre ont été essentiels. Je te remercie de t'être occupée de moi, d'avoir toujours été disponible et de m'avoir toujours fait sentir comme à la maison. Tu es une amie spéciale.

Ayham, your scientific (and moral) support have been invaluable this past year, and I thank you immensely for it. I am certain that your great passion and intelligence will lead you to achieve great things in the future, and I wish you all the best in realizing all your projects.

Benjamin, I am glad to have shared these last few months with you at the CMFA. Thank you for the time you dedicated to me and for the help I have found in your scientific advices. I also want to thank you for your incredile positivity.

Caroline, merci pour ton soutien au cours de ces années. Je suis sûre que ta détermination te mènera loin, je te souhaite le meilleur pour ton avenir.

Un merci à **Darius**, car malgré ton sifflement, malgré tes QR codes et photos collés sur mon bureau et malgré les moments difficiles que tu m'as fait passer à la cafétéria (whistle)... tu as été un collègue/ami unique. Merci d'avoir toujours apporté la bonne humeur au CMFA.

Esra, le CMFA a beaucoup de chance de t'avoir et je suis extrêmement chanceuse maintenant de t'avoir comme amie. Merci pour ta merveilleuse bonté d'âme, pour ton soutien constant (scientifique et autre) et pour être toujours prête à aider tout le monde. J'ai hâte de faire de nouveaux voyages ensemble.

Thank you, **Ferran**, for the constant support and for the invaluable scientific discussions we had. Even though it was for a brief period, you became an indispensable part of the CMFA, and I am very grateful to have had you on the team.

Un merci à **François**, pour ton extrême gentillesse et pour le temps passé à me donner des conseils précieux. To **Yongua**, it was a pleasure working with such a positive and cheerful person. You are greatly missed at the CMFA. Grazie a te, **Giuditta**, per le nostre chiacchierate tra un esperimento e l'altro e per avermi sempre supportata e ascoltata durante questi anni.

Juhans, je ne te remercierais pas d'avoir voulu me faire aimer les pâtes au poulet ou pour les créations que tu laissais sur mon bureau quand je partais mais... Je dois absolument te remercier pour tous les rires et les conseils scientifiques que tu m'as donnés. Ce fut un plaisir de partager le bureau avec toi et de voler tes frites.

Karine, ta bonne humeur contagieuse et tes précieux conseils scientifiques ont rendu le temps que nous avons passé ensemble au laboratoire et à l'exterieur très agréable. Je sais que de nombreux succès t'attendent et je serai heureuse de celébrer chacun d'entre eux avec toi.

Marine1, thank you for being a supportive friend, for always standing by my side and for holding my hand, especially during this last period (and I really needed it). You have been my karaoke partner, my TV series marathon buddy, but most importantly, you are the Gabriella to my Troy.

Marine2, merci pour ton soutien constant et de ta positivité infaillible. Merci de m'avoir écoutée répéter à chaque fois, pour tes conseils, pour avoir chanté avec moi à chaque karaoké et pour avoir eu la patience de m'aider avec le français. Maintenant, il y a toujours une belle petite voix en moi qui me dit "c'est parti".

Thank you, **Quentin**, for your patience and the time you dedicated to me. Our discussions and your scientific advice have been invaluable, and I have been really lucky to have you as a colleague this past year (except when you where beating me to baby-foot). I will always be happy to chat about books and recommend new Italian dishes for you to try.

One of the biggest thanks goes to you, **Perrine**. You know well that when I say I wouldn't have made it this far without you, I am being extremely sincere. You have been an exceptional colleague and an irreplaceable friend. Your scientific and moral support has been fundamental. I see many more victories together at "What the Tune" in our future.

Romain, je te remercie car discuter de science avec toi a toujours été enrichissant et instructif. Merci pour tous les rires que tu m'as faits faire, pour m'avoir présenté Dark Romain, mais surtout, pour m'avoir donné l'honneur de participer à la création du Mono Liso. Je t'en serai toujours reconnaissante.

Séraphin, en toi, j'ai trouvé un collègue toujours prêt à aider mais surtout un ami avec qui parler. Merci pour les rires (MDR), pour les “outfit of the day” et pour le soutien constant. Malheureusement, la mayonnaise sur les lasagnes continuera à me donner des haut-le-coeur.

I have been lucky enough to be part of a second amazing lab, and I want to thank everyone who has been a part of it over these years: **Tania**, grazie per tutto l’aiuto scientifico, per il sostengno in questi anni e per essere diventata una preziosa amica. **Justine**, thank you for all your support and kindness, and especially for bringing Babu into my life. **Thibaut and Alan**, thank you (grazie) for the time and help you have given me. It has been a true pleasure working (and laughing) with you. **Justin**, It was nice to chat with you (science and non) during these past years. I’m sure you will do amazing things in the future. **Ilaria**, grazie per la tua estrema gentilezza, ti auguro tutto il meglio. **Barbara**, thank you for our incredible victory in the “banana team”. Thank you also to **Marie**, **Loïc**, **Mauricio**, **Marine**, **Matteo, Laurane and Emmanuel,** it was a pleasure to meet all of you.

A huge thank you to **Mégane** and **Magdalena**, with whom I had the pleasure to collaborate over these years. Your scientific help has been invaluable, and it has been a pleasure discussing with you during this time. I also want to thank **Prof. Wouters** and **Prof. Fillet** for the interesting discussions that have increased the value of the project.

Thank you to the people who shared with me the first phase of this journey: **Léopold**, thank you for welcoming me into the LDH team from day one and for trusting me and my work. **Maxime**, thank you for the time and advices you gave me. **Arina** and **Alice**, it was a pleasure chatting with you and sharing good times both in and out of the lab. **Julien**, it was a pleasure sharing the office and chatting with you (except hearing "It's a Small World" all the time). **Bouazza** Merci pour ta gentillesse.

Thank you to everyone I have met over these years at the LDRI: **Valentina**, **Giulia, Mingchao** thank you for all the laughes and the moments toghteher. Thank you to our neighborhood, the REMA team: **Natacha**, **Caner**, **Chloe**, **Jérôme**. A special thanks to **Nicolas** and **Lionel** for all your help and patience during my fights with the NMR-STD.

Un grazie speciale va ad un gruppo di persone che è diventata la mia famiglia qui a Bruxelles: **Martina**, sei come un bellissimo corgi che rallegra le mie giornate. Il tuo sostengo (mentre vedevamo fenicotteri e non) e le nostre serate, sono state fondamentali. **Stefania**, grazie per esserci stata dal giorno uno e grazie perché nonostante io sia la peggiore partner di shopping sei stata di costante sostegno. Grazie al mio “pat-pat”, **Elia**, perchè con le tue lezioni di empatia sei sempre riuscito a strapparmi un sorriso tra le lacrime. **Matteo**, grazie per assecondarmi nel mangiare formaggio senza pentirci e perchè da cinque anni continui a regalarmi risate e pizzoccheri. **Andrea**, grazie per so(u)pportarmi e per aprirmi la porta di casa pure quando ti costringo a vedere programmi discutibili.

Alessio (AAOO), grazie per il grande e costante sostegno, e per le risate che mi hai regalato in questi anni.

Paola, **Ramona** sono grata a questa esperienza per avermi fatta incontrare voi due. Mi avete accompagnata durante questo percorso con una gentilezza, sostegno ed affetto incredibile. Le nostre chiacchierate sono una boccata d’ aria fresca e vi ringrazio per essere diventate il mio piccolo porto sicuro.

To the best neighbor and sports partner I could have wished for, **Yasmine**. Thank you for always listening to (and comforting) me, for our (therapeutic) evening infusions and for never leaving me alone to watch and comment on silly shows. Your friendship has been invaluable over these years.

Grazie alle persone con le quali sono cresciuta e che nonostante la lontananza sono diventate ancor più vicine: **Sara** e **Giulia**, le mie colonne portanti. Ai miei fratelli acquisiti **Antonio**, **Francesco**, **Edoardo** e **Daniele**. **Federica** e **Francesca**, questo traguardo é anche vostro. Alla mia sostenitrice più grande, **Edith**, sono fortunata ad averti. Grazie a **Marco**, **Daniele**, **Marta**, **Flavia**, **Serena, Irene, Cecilia**.

I am grateful to this PhD journey for bringing me to you. Thank you, **Flo**, for your patience and the immense support you have given me over these years. Thanks for the happiness you've brought into my life and for always being close to me, even from distance. The world of capybaras now has two more fans. Merci aussi à ta famille (et à Joe) pour leur gentillesse et leur soutien.

Zio, averti qui a Bruxelles è stato fondamentale. Non sono sufficenti i ringraziamenti per l'aiuto, il supporto e l'avermi fatto sentire a casa ogni volta che ne avevo bisogno. Ti ringrazio dal profondo del mio cuore. **Zia Della**, la positività e la tua forza d'animo sono un esempio per me. I tuoi messaggi mi hanno sempre strappato dei sorrisi proprio quando ne avevo più bisogno. Un grazie infine alle mie due splendide **nonne**.

A voi due il grazie più grande. **Mamma**, **Babbo** il vostro continuo sostegno mi ha dato l'energia per affrontare i momenti più difficili. Grazie per aver dato le carezze a **Pulce** che non potevo dare, per accogliermi ogni volta con un supplì ed un enorme abbraccio. Avervi come genitori é la mia fortuna.

Abbreviations

^{18}F-FDG	^{18}F-fluorodeoxyglucose
3-PG	3-phosphoglycerate
Acetyl-CoA	Acetyl coenzyme A
ACL	ATP citrate lyase
ADME	Absorption, distribution, metabolism and excretion
Akt	Serine-threonine kinase AKT
Arg1	Arginase 1
bFGF	Basic fibroblast growth factor
BL	Burkitt lymphoma
BS3	Bis(sulfosuccinimidyl)suberate
CAF	Cancer-associated fibroblast
CETSA	Cellular thermal shift assay
CIC	Mitochondrial citrate carrier
dG	London dispersion energy scoring function
DHAP	Dihydroxyacetone phosphate
DSF	Differential scanning fluorimetry
EC_{50}	Half maximal effective concentration

EGFR	Epidermal growth factor receptor
ELISA	Enzyme-linked immunosorbent assay
EMT	Epithelial–mesenchymal transition
FDA	Food and Drug Administration
FID	Free induction decay
G6P	Glucose-6-phosphate
GLUT	Glucose transporter
Gm	Gomesine
GPD1	Glycerol-3-phosphate dehydrogenase 1
HBP	Hexosamine biosynthesis pathway
HCC	Hepatocellular carcinoma
HIF-1	Hypoxia-inducible factor-1
HK	Hexokinase
HRE	Hypoxia response element
IC_{50}	Half-maximal inhibitory concentration
IKK	IκB kinase
IL-8	Interleukin-8
IPTG	Isopropyl-β-D-1-thiogalactopyranoside
ITC	Isothermal titration calorimetry

ITF	Intrinsic tryptophan fluorescence
IV	Intravenous
K_D	Dissociation constant
K_i	Inhibition constant
Km	Michaelis-Menten constant
LDH	Lactate dehydrogenase
LDH-Hfl	Full length LDH-H
LDH-Htr	Truncated LDH-H
LiP-MS	Proteolysis-coupled mass spectrometry
LogP	octanol-water partition coefficient
MCT	Monocarboxylate transporter
MDH	Malate dehydrogenase
MDS	Molecular dynamics simulation
MMP	Matrix metalloproteinase
MOE	Molecular operating environment
MP	Mass photometry
MST	Microscale thermophoresis
MW	Molecular weight
NADPH	Nicotinamide adenine dinucleotide phosphate

nanoDSF	Nano different scanning fluorimetry
NF-κB	Nuclear factor kappa light-chain-enhancer of activated B cells
NMR-STD	Saturation transfer-different nuclear magnetic resonance
NSCLC	Non-small-cell lung cancer
OAA	Oxaloacetate
OXPHOS	Oxidative phosphorylation
PAINS	Pan-assay interference compounds
PET	Positron emission tomography
PFK	Phosphofructokinase
PHD2	Prolyl hydroxylase-2
pH_e	Extracellular pH
PHGDH	Phosphoglycerate dehydrogenase
PI3K	Phosphoinositide 3-kinase
PIP_3	Phosphatidylinositol3,4,5-trisphosphate
PKM2	pyruvate kinase M2
PO	*Per os*
PPI	Protein-protein interaction
PPP	Pentose phosphate pathway
PTEN	Phosphatase and tensin homolog

RBC	Red blood cell
RCC	Renal cell carcinoma
R_{gyr}	Radius of gyration
RMSD	Root mean square deviation
ROS	Reactive oxygen species
SAR	Structure-activity relationship
SDS-PAGE	Sulfate-polyacrylamide gel electrophoresis
SEC	Size-exclusion chromatography
SEC-MALS	SEC with multi-angle light scattering
SHMT	Serine hydroxymethyltransferase
SSP	Serine synthesis pathway
SSRI	Serotonin re-uptake inhibitor
STAT3	Signal transducer and activator of transcription 3
TALDO	Transaldolase
TCA	Tricyclic antidepressant
TCAC	Tricarboxylic acid cycle
TIGAR	TP53-inducible glycolysis and apoptosis regulator
TKTL1	Transketolase-like 1
TRIC	Temperature-related intensity-change in fluorescence

UDP-GlcNAc	Uridine diphosphate *N*-acetylglucosamine
V-ATPase	Vacuolar ATPase
VEGF	Vascular endothelial growth factor
VEGFR2	VEGF receptor 2

Table of Contents

1. Preamble 18

2. Introduction 21

2.1 Cancer Metabolism 21

2.2 LDH family and physiological roles 29

2.2.1 LDH family and catalytic properties 29

2.2.2 Significance of LDH quaternary structures 34

2.3 LDH involvement in cancer metabolism 38

2.3.1 LDHs orchestrating metabolic symbiosis and autophagy 38

2.3.2 Lactate promotes cancer cell invasiveness, tumor angiogenesis and epigenetic regulation. 42

2.4 Targeting cancer metabolism 45

2.4.1 LDHs as metabolic anticancer targets 47

2.4.2 Challenges for *in vivo* LDH inhibition 49

2.4.3 Towards allosteric inhibition 55

2.4.4 Towards homomeric disruption 62

3. Methods for targeting protein self-assembly 73

3.1 Applied techniques targeting protein self-assembly 73

3.1.1 Nano differential scanning fluorimetry 73

3.1.2 Microscale thermophoresis 74

3.1.3 NMR STD 76

3.1.4 Mass photometry 77

3.1.5 SEC-MALS 79

3.1.6 Cellular engagement assay 81

3.1.7 Isothermal titration calorimetry 82

3.1.8 Native polyacrylamide gel electrophoresis 83

3.1.9 Enzyme-linked immunosorbent assay (ELISA) 84

3.1.10 Intrinsic fluorescence assays 85

4. General context, preliminary work and objective 86

4.1 General context 86

4.2 Preliminary work 87

4.3 Objectives 88

5. Results: Chapter 1 91

5.1 Introduction 92

5.2 Result and discussion 93

5.2.1 Primary screening using nanoDSF 93

5.2.2 Hit validation 96

5.2.3 Hit Characterization 100

5.3 Preliminary conclusion 107

5.4 Experimental section 108

5.4.1 General 108

5.4.2 Virtual Screening and library selection 108

5.4.3 Protein production 109

5.4.4 NanoDSF 110

5.4.5 Nuclear Magnetic Resonance 110

5.4.6 MST 111

5.4.7 Denaturation assay 112

5.5 Supporting information 113

6. Results: Chapter 2 117

6.1 Introduction 117

6.2 Results and discussion 120

6.2.1 Elaboration of a focused library of antidepressant and antihistaminic drugs 120

6.2.2 Biophysical characterization 121

6.2.4 Exploring binding interactions: Insights from structural analysis. 130

6.2.3 Cellular target engagement profiling of selected compound in Cancer Cell 134

6.3 Preliminary conclusion 135

6.4 Experimental section 137

6.4.1 General 137

6.4.2 Protein production 137

6.4.3 Nano DSF 137

6.4.4 MST 138

6.4.5 enzymatic assay 139

6.4.6 Dissociation-reassociation assay 139

6.4.7 NMR STD 140

6.4.8 Co-crystallographic studies 141

6.4.9 *In silico* study 141

6.4.10 Cellular toxicity assays 142

6.4.11 Cellular engagement assay 143

6.5 Supporting information 144

7. General discussion and perspectives 150

7.1 Major outcomes of the thesis 150

7.2.1 Probing disruption: Assessing the influence of identified Hits on LDH activity and structure 154

7.2.2 Is the anti-proliferative effect of our LDH inhibitors in cancer cells LDH-dependent? 158

7.3 Perspectives 159

7.3.1 Probing metabolic shift unveiling the impact of LDH inhibition. 159

7.3.2 Optimization of fluoxetine for a novel library of small molecules inhibitors 162

7.3.3 Unlocking synergy: Development of dual inhibitors for enhanced LDH targeting 164

7.3.4 Mimicking the *N*-Terminal arm: insights from foldamer design 168

8. References 171

1. Preamble

Cancer is a disease in which malignant cells acquire the capabilities of overcoming organism safeguard and collaborating to satisfy tumor bioenergetic needs. In this context, exploiting uncommon metabolic pathways is one of the most frequent strategies for malignant cells to survive and to participate in tumor growth, proliferation, and invasiveness. This PhD thesis aims to disrupt one of these mechanisms by targeting lactate dehydrogenases (LDHs), crucial enzymes in the regulation of carbon metabolism. In their tetrameric form, these enzymes catalyze the interconversion of pyruvate + NADH + H^+ to lactate + NAD^+, thus driving tumorigenicity by regulating intracellular pH, the redox balance and autophagy, and fostering lactate-fueled respiratory pathways within the dynamic metabolic landscape of cancer cells [1-4].

Previous attempts to target these enzymes by academic and industrial groups have been unsuccessful, which can be largely attributed to a challenging active site druggability. Recognizing the critical significance of LDHs in cancer, we pioneered an alternative strategy consisting in targeting a novel site of the proteins located at their oligomeric interfaces, resulting in tetramer disruption and subsequent LDH inactivation (**Figure 1**). To achieve this goal, we conducted extensive research using purified enzymes, various biophysical methods, and *in cellulo* assays. We identified hits and achieved a comprehensive 360-degree characterization of their mode of action. Our findings open the door to proving the binding of these molecules, which were not originally developed as anticancer drugs, to LDHs. The promising perspectives emerging from this work are closely tied to the long-term clinical outcome of cancer patients.

The present manuscript starts with an introduction emphasizing the role of LDHs in cancer metabolic adaptations, particularly their involvement in the collaboration of heterogeneous cancer cell populations. Subsequent sections delve into historical efforts to target LDHs, putting in perspective the power of our new strategy, and the state-of-heart technology used to characterize protein-protein interactions. The results section outlines the screening methods and different techniques used in pursuing our objectives. It is presented through two articles: the first one [5] focuses on the strategy that we developed for identifying and characterizing novel LDH inhibitors. The second addresses the characterization of the core structure of two recently identified FDA-approved compounds within the antidepressant and antihistaminic classes as LDH inhibitors. These findings indicate their potential action at the tetrameric interface. It further provides unprecedented information about their binding efficacy, including in cellular environments. The final sections engage in a discussion and offer perspectives to the work, underlining the significant possibilities that our achievements could provide in advancing cancer research and patient outcomes.

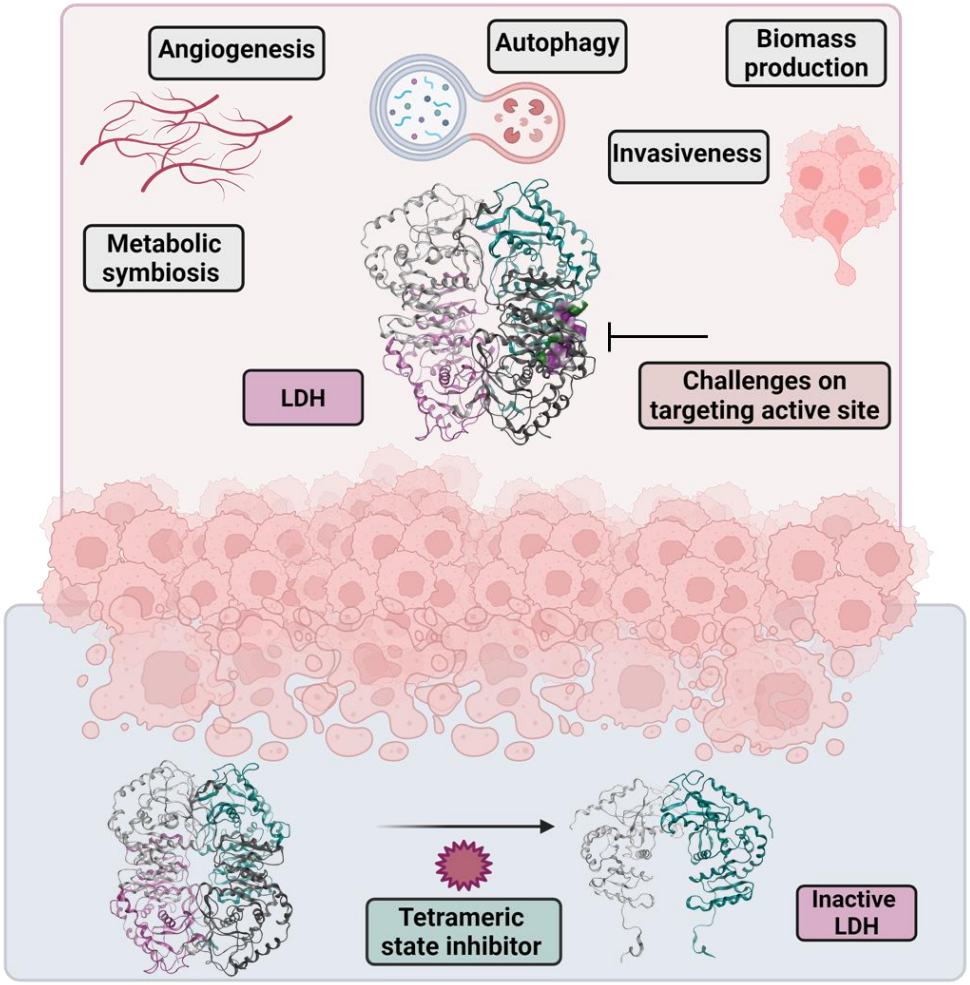

Figure 1. Implications of LDHs in cancer growth and innovative strategy to inhibit its activity. The upper part of the figure illustrates the various cancer processes in which LDH is involved, including autophagic, metabolic symbiosis and angiogenesis. It also highlights the challenges associated with targeting the enzyme active site showed in LDH-1 crystallographic structure (PDB: 1t2f). The lower part of the figure presents our novel strategy for inhibiting LDH by targeting its oligomeric interfaces. This approach aims to disrupt tetramer formation, leading to the dissociation of LDH into an inactive conformation state. The figure was generated using Biorender.

2. Introduction

2.1 Cancer Metabolism

Cancer is a heterogenous disease, and this fundamental characteristic extends to cancer metabolism [6]. Metabolic flexibility allows cancer cells to reprogram classical processes in order to satisfy the bioenergetic and biosynthetic requirements of uncontrolled proliferation, thus activating uncommon metabolic processes that could be targeted therapeutically.

Otto Warburg in the 1920's first observed that some malignant cells avidly take up and consume glucose independently of oxygen availability, rewiring glycolysis to lactate fermentation instead of to the tricarboxylic acid cycle (TCAC) and oxidative phosphorylation (OXPHOS) [6, 7]. This phenomenon took the name of "the Warburg Effect" or "Aerobic Glycolysis" and reshaped our understanding of cancer biology. At a first glance, such metabolic shift is surprising, as glycolysis alone generates only 2 mol of ATP per mol of glucose, while its coupling to the TCAC cycle and OXPHOS generates up to 38 mol of ATP per mol of glucose. However, adopting glycolysis as a main mode of energy production is associated to a faster conversion of glucose into pyruvate and lactate, and, therefore, to a high rate of ATP production. It offers biosynthetic advantages.

While proliferating cancer cells are generally a minority in clinical tumors, cancer cells in general also have to deal with an insufficient blood supply, creating hypoxic areas. Hypoxia stands out as a key driver for the adoption of a glycolytic phenotype. Hypoxic cells indeed undergo a pivotal metabolic adaptation referred to as "the glycolytic switch", a process in which

glycolysis is uncoupled from respiration, establishing itself as the primary pathway for ATP production. To induce the switch, hypoxia activates hypoxia-inducible factor-1 (HIF-1), a transcription factor that binds to hypoxia response elements (HREs) in the promoter region of target genes, inducing their expression. Among metabolic enzymes and transporters, HIF-1 promotes the expression of glucose transporters (GLUTs), hexokinases 1 and 2 (HK1 and HK2), pyruvate kinase M2 (PKM2), LDH-A, and lactate/proton symporter monocarboxylate transporter 4 (MCT4) [8, 9] (**Figure 2**).

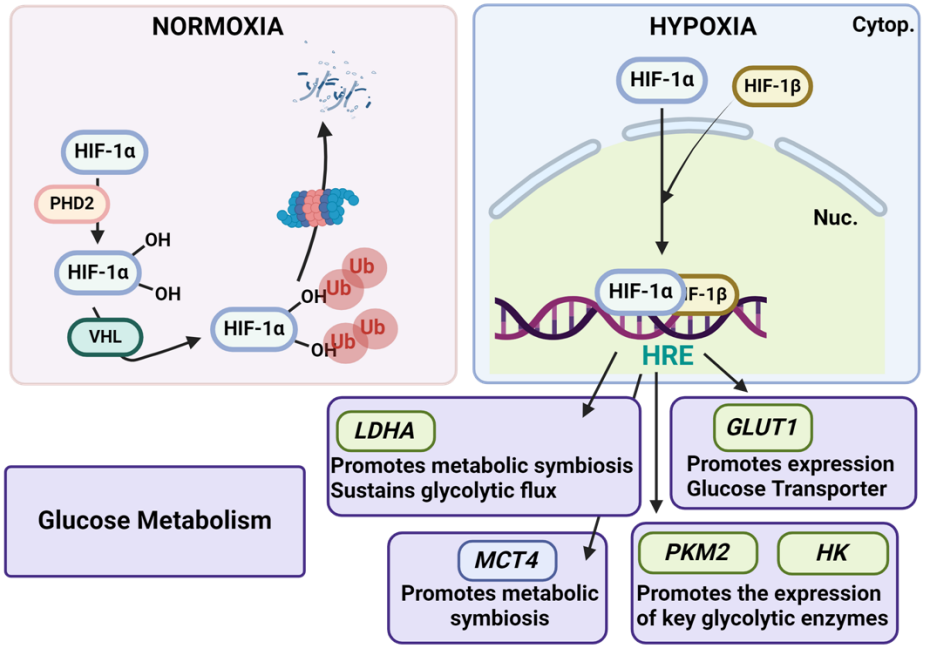

Figure 2. Hypoxia-induced activation of HIF-1 and its effects on metabolic enzymes and transporters impacting glucose metabolism. Illustration of the differential cellular responses to oxygen availability, focusing on glucose metabolism. On the left, under normoxic conditions, PHD2 hydroxylates HIF-1α, marking it for ubiquitination by VHL protein and subsequent degradation by the proteasome. On the right, in a hypoxic environment, the lack of oxygen inhibits PHD2 activity, preventing HIF-1α degradation. Stabilized HIF-1α dimerizes with HIF-1β, and the complex translocates to the nucleus. There, it binds to hypoxia response elements (HREs) in the promoter regions of target genes, driving the expression of various metabolic enzymes and transporters. This HIF-induced gene expression enhances glucose metabolism to support cancer cell survival and growth. The Figure was generated using Biorender. Abbreviations: HIF-1α/HIF-1β- Hypoxia-inducible factor-1; PHD2- Prolyl hydroxylase-2; VHL- Von Hippel-Lindau; Ub- Ubiquitin; HRE- Hypoxia response element; *LDHA*- Lactate dehydrogenase A; *GLUT1*- Glucose transporter1; *PKM2*- pyruvate kinase M2; *HK*- Hexokinase; *MCT4*- monocarboxylate transporter 4.

This adaptation not only facilitates the survival of cancer cells under low oxygen conditions, but it also contributes to the increased glucose uptake observed in most cancers [7]. Noteworthy, increased glucose consumption is a cancer biomarker detectable through positron emission tomography (PET) imaging by monitoring the uptake of glucose analogue tracer ^{18}F-FDG PET [7, 10]. Currently, this non-invasive method is extensively used for the clinical detection of cancers and to monitor progression [10].

To satisfy the heightened demand for glucose by glycolytic cells, various pathways coordinate to orchestrate an elevation in glucose uptake. Notably dysregulation of the phosphoinositide 3-kinase (PI3K) pathway and a loss of function of tumor suppressor phosphatase and tensin homolog (PTEN) sequentially promote phosphatidylinositol-3,4,5-trisphosphate (PIP_3) accumulation, the recruitement and activation of serine-threonine kinase AKT (Akt) [11], the activation of phosphofructokinase-2 (PFK-2, an enzyme catalyzes the production of fructose-2,6-biphosphate, an allosteric activator of glycolytic enzyme PFK-1)[12], and potentiates the activity of hexokinase 2 (HK2, which catalyzes the phosphorylation of glucose to impede its efflux from cells) [13, 14]. Moreover, the activation of oncogenes, such as Akt, Myc, and Ras, can further enhance the expression of GLUT1. This concerted action not only ensures the prevention of glucose leakage from cells, but it also enhances glucose uptake, which can occur independently of hypoxia [15-17] (**Figure 3**).

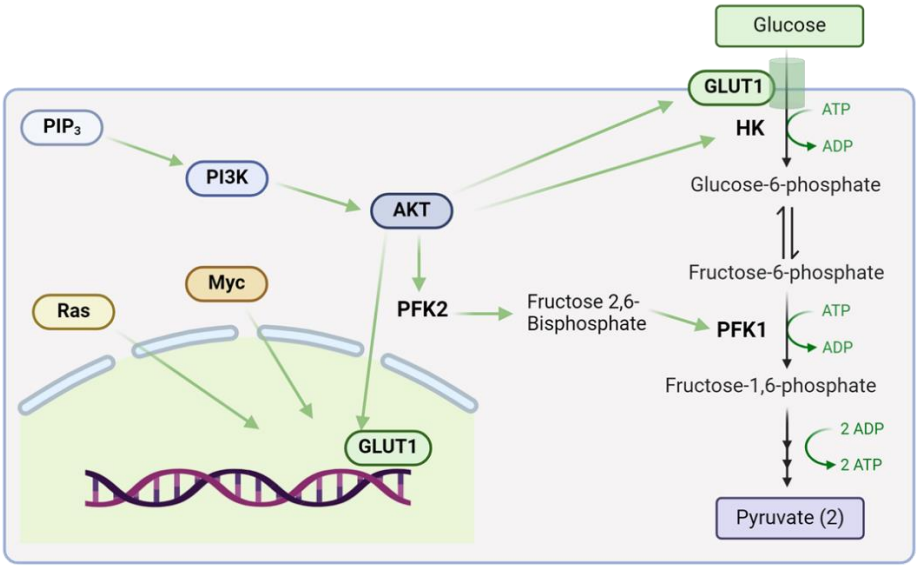

Figure 3. Cancer cells orchestrate an increase in glucose uptake. This figure illustrates how cancer cells enhance glucose uptake through dysregulation of the PI3K pathway, leading to PIP3 accumulation. PIP3 activates AKT, which in turn enhances the activity of PFK-2, accelerating glycolysis, and HK2, preventing glucose efflux. Oncogenes like Akt and Myc further increase GLUT1 expression, boosting glucose uptake. Green arrows represent positive regulatory effects. Black arrows represent glycolysis metabolic steps. The Figure was generated using Biorender. Abbreviations: GLUT1- Glucose transporter 1; HK- Hexokinase; PFK2- Phosphofructokinase; ATP- Adenosine triphosphate; ADP- Adenosine diphosphate; AKT- Serine-threonine kinase AKT; PIP3- Phosphatidylinositol-3,4,5-trisphosphate; PI3K- Phosphoinositide 3-kinase.

For proliferating cancer cells, the advantage of adopting a glycolytic metabolism can be found in the need to fulfill a high anabolic demand. Carbon derived from glucose is indeed needed to generate nucleotides, nicotinamide adenine dinucleotide phosphate (NADPH) and lipids, *i.e.*, biomass required for growing processes. Glycolysis can thus be viewed as a biosynthetic hub, as several glycolytic intermediates can fuel anabolic pathways. Glucose-6-

phosphate (G6P) serves as critical nodal point in cancer metabolism, as it can be directed either to glycolysis or to the pentose phosphate pathway (PPP) depending on metabolic needs (**Figure 4**). When it fuels the PPP, G6P serves to generate ribose-5-phosphate (for *de novo* nucleotide synthesis) [7] and NADPH [18], which is critical for a range of biosynthetic processes, including the synthesis of fatty acids and nucleotides. Activation of the PPP thereby significantly contributes to support the biomass production necessary for relentless cancer cell proliferation. Notably, PPP enzymes transketolase-like 1 (TKTL1) and transaldolase (TALDO) are often overexpressed in cancer [19, 20]. Downstream of G6P in the glycolytic pathway, fructose-6-phosphate can be redirected towards hexosamine biosynthesis (HBP), which ultimately leads to the production of amino sugar uridine diphosphate *N*-acetylglucosamine (UDP-GlcNAc). UDP-GlcNAc serves as a precursor for the biosynthesis of glycoproteins and glycoconjugates [21, 22]. Dihydroxyacetone phosphate (DHAP), the next glycolytic intermediate, can fuel glycerol-3-phosphate dehydrogenase 1 (GPD1) to produce glycerol-3-phosphate for the synthesis of various phospholipids necessary to build up cellular membranes [23]. Finally, 3-phosphoglycerate (3-PG) can be redirected towards the serine synthesis pathway (SSP), which further promotes anabolic cancer cell growth. The enzymatic activities of phosphoglycerate dehydrogenase (PHGDH) and serine hydroxymethyltransferase (SHMT, converting serine into glycine) are increased in some cancer types, which provides one-carbon units involved in nucleotide synthesis [24, 25].

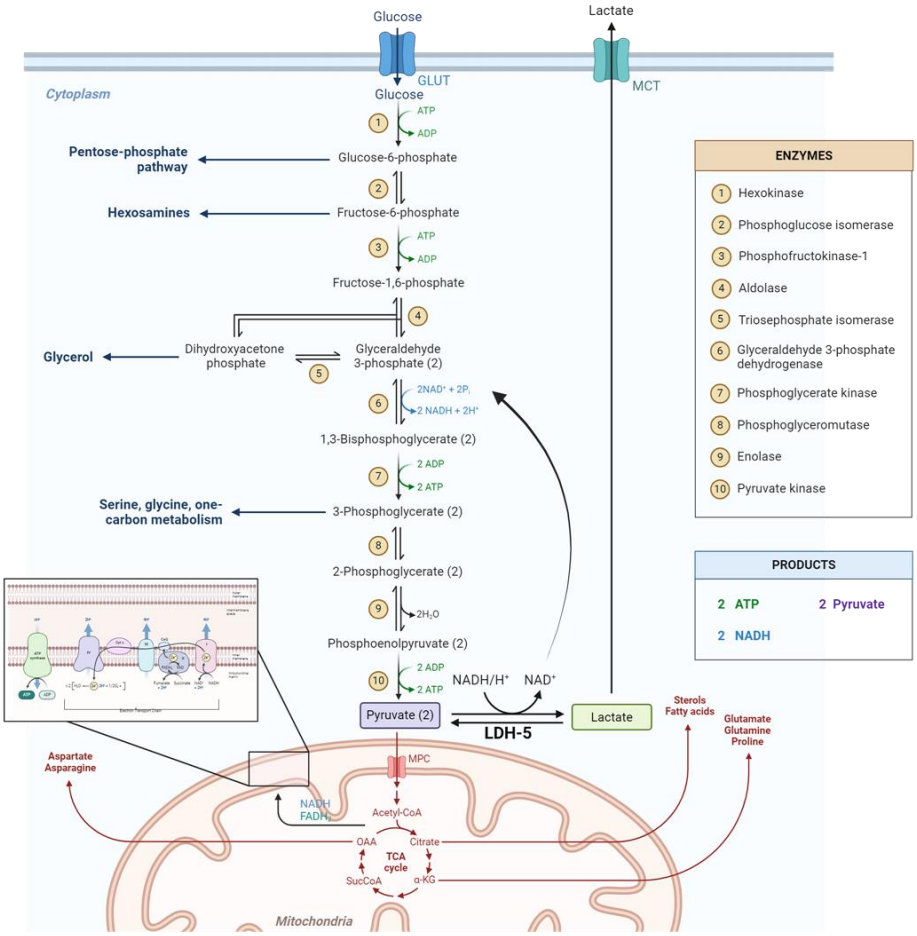

Figure 4. Glycolytic biomass synthesis and TCAC dynamics in cancer cell proliferation. The schematic illustrates the joint efforts of glycolysis and the tricarboxylic acid cycle in supporting tumor biomass production. Glycolysis intermediates fuel anabolic pathways: Glucose-6-phosphate (G6P) is diverted to either glycolysis or the pentose phosphate pathway (PPP). Fructose-6-phosphate supports hexosamine biosynthesis, while dihydroxyacetone phosphate (DHAP) contributes to phospholipid synthesis. 3-phosphoglycerate (3-PG) aids serine synthesis. The TCAC cycle, via cataplerosis, generates lipid and amino acid precursors. Citrate is converted to acetyl-CoA for fatty acid synthesis, and glutamine replenishes TCAC intermediates. The Figure was generated using Biorender.

Beyond glycolysis, the TCAC cycle is also crucial for producing building blocks for lipids and amino acids, a process called cataplerosis (**Figure 4**). Citrate can be exported from mitochondria to the cytosol *via* the mitochondrial citrate carrier (CIC), where ATP citrate lyase (ACL) breaks it into oxaloacetate (OAA) and acetyl coenzyme A (Acetyl-CoA). Acetyl-CoA is a precursor of cholesterol and fatty acids, while OAA supplies amino acid building blocks [26]. To sustain TCAC cycle activities, proliferating cancer cells use glutamine to generate α-ketoglutarate, which feeds into the TCAC cycle to replenish OAA stores [27]. In a glioblastoma cell model, it was demonstrated that by condensing acetyl-CoA derived from glucose with OAA derived from glutamine, the cells primarily synthesize fatty acids and lipids using carbon from glucose [28]. Meanwhile, 60% of glutamine was metabolized into lactate. This implies a malic enzyme flux high enough to supply the NADPH needed for fatty acid synthesis.

Cellular heterogeneity is a prevalent trait within solid tumors, particularly between oxidative and glycolytic phenotypes. This complex system not only poses a challenge for effective therapeutic interventions, but also highlights the importance of better understanding the inner workings at the molecular level. In the upcoming chapter, we will focus on the central role played by LDHs in orchestrating these metabolic dynamics. These enzymes regulate the balance between oxidative and glycolytic states, offering an interesting avenue for further exploration. Our focus on studying these proteins is driven by the potential insights it holds for developing targeted strategies to disrupt metabolic dependencies, offering new opportunities for anticancer therapeutics.

2.2 LDH family and physiological roles

2.2.1 LDH family and catalytic properties

LDHs constitute a family of intracellular enzymes that form homo or hetero-tetramers by the arrangement of two sub-units, LDH-M and LDH-H, encoded by two different genes; *LDH-A* on chromosome 11 and *LDH-B* on chromosome 12, respectively [2]. The association of LDH-H and M may lead to the formation of 5 active tetrameric isoforms: LDH-1 (H4), LDH-2 (H3M1), LDH-3 (H2M2), LDH-4 (H1M3) and LDH-5 (M4) [1] (**Figure 5**). They all catalyze the reversible redox conversion of pyruvate + NADH + H^+ to lactate + NAD^+. Among them, homotetramers LDH-1 and LDH-5 exhibit the highest metabolic activities. Because *LDH-A* (but not *LDH-B*) is a HIF-1-target gene, LDH-5 expression is predominant in hypoxic conditions when lactate fermentation is essential for energy generation [29]. Conversely, LDH-1 prevails in aerobic metabolism.

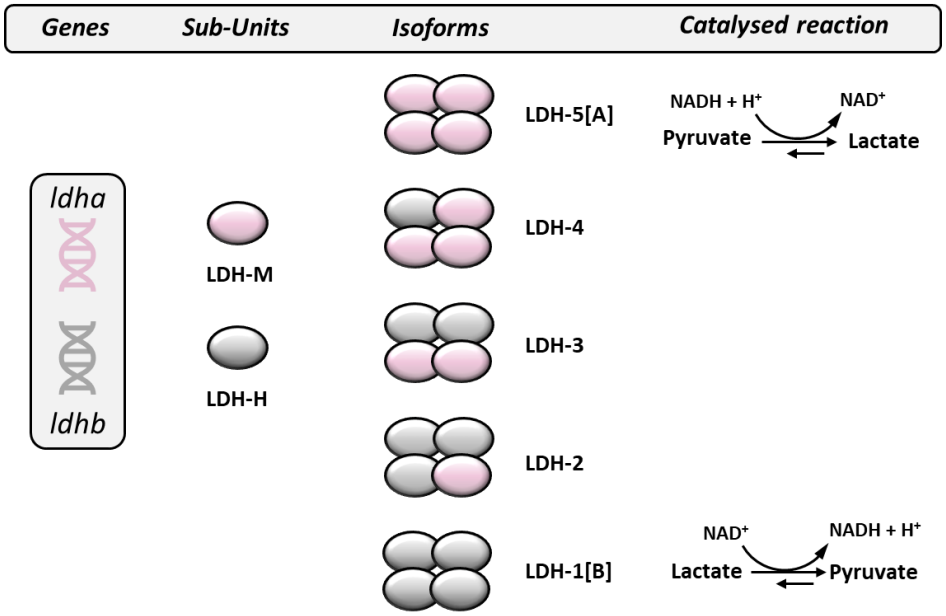

Figure 5. LDH family, structures and functions. Eukaryotic LDHs are encoded by two genes, *LDHA* and *LDHB*. The association of the two subunits LDH-M and LDH-H may give rise to five isoforms: LDH-5 (preferentially catalysing the reduction of pyruvate to lactate), LDH-4, LDH-3, LDH-2 and LDH-1 (preferentially catalysing the oxidation of lactate to pyruvate).

LDH-1 and LDH-5 exhibit a shared identity of 75% and a homology of 89% [30]. Both enzymes contain three primary domains. The first domain encompasses residues 20-162 and 248-266. It features a 'Rossman fold' [31] characterized by three parallel β-strands enclosing two α-helices (**Figure 6**). In this region, NAD(H) initiates the binding process with specific amino acids, facilitating substrate entry into the 'active site loop' (residues 99-110) located at the interface of two domains, thus initiating the catalytic reaction. For human LDH-5, the process starts with the interaction between NADH and His-195 (**Figure 7**). Critical residues, including Arg-109, Asp-165 and Arg-

171, are involved in essential interactions that are necessary for the geometric arrangement [32]. At the catalytic site, Arg-109 forms a hydrogen bond with the carbonyl group of pyruvate, triggering the closure of 'active site loops', thus preventing solvent access and inhibiting hydride exchange during the catalytic reaction. This interaction constrains pyruvate in the correct conformation. In human LDH-1, analogous roles are played by His-193, Arg-106, Asp-166 and Arg-169 [33]. The catalytic site of LDHs is highly conserved among the isoenzymes [34]. Differences in catalytic activities are attributed to variations in the net charge of residues within the active site of each enzyme. Specifically, the role of His-195 in LDH-5 and His-193 in LDH-1 is noteworthy, as these residues facilitate the proton transfer crucial for the reversible conversion of pyruvate to lactate. The distinct pKa values of these residues result in differing substrate affinities [33]. His-193 indeed interacts much strongly with pyruvate and lactate in LDH-1 compared to His-195 in LDH-5, which is reflected by a lower K_m of LDH-1 (0.12 and 4.1 mM) compared to LDH-5 (0.46 and 14.3 mM) for pyruvate and lactate, respectively [33, 35] . Interestingly, the pyruvate concentrations needed for optimal LDH-5 activity further inhibit LDH-1 activity (LDH-1 Ki = 3,900 µM; LDH-5 Ki = 770 µM), orienting the reaction [36]. Despite these differences, one isoenzyme has the capacity to compensate for the inhibition or genetic disruption of the other [37]. The second LDH primary domain comprises amino acids 163-247 and 267-331 [1] (**Figure 6**). The substrate-binding cavity is located between the two first domains, where the 'active site loop' closes upon binding [1]. The final domain corresponds to the *N*-terminal sequence (residues 1-19), adopting an extended conformation and encircling the adjacent subunit within the tetrameric structure. It serves as an anchor,

preserving the relative position and distance between two subunits, thereby contributing to structural stability [38] (**Figure 6**). This region corresponds to the tetramerization domain also investigated by our group [30]. It will be discussed in the next chapters together with another tetramerization area corresponding to residues 54-76 [39].

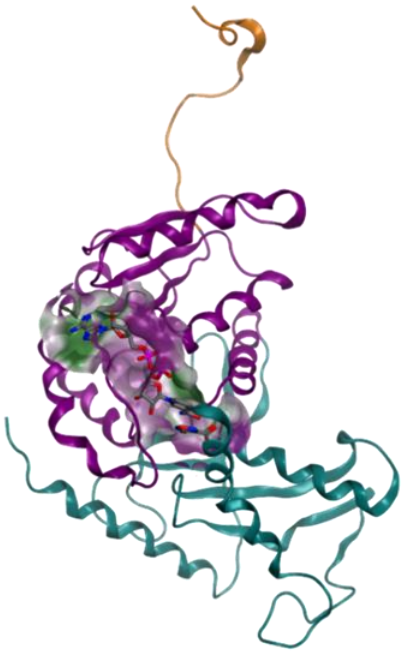

Figure 6. Structure of LDH-H. The picture corresponds to the LDH-H subunit (PDB ID: 1I0Z). Highlighted are the three LDH domains: the tetramerization domain in orange (residues 1-19), the substrate-binding domain in green (163-247) and (267-333), and the cofactor-binding domain in violet (20-162-162) and (248-266). Cofactor (NADH) and substrate analogue (oxamic acid) are represented in the catalytic pocket (99-110). The molecular surface of the polar active site is shown, with violet highlighting polar and green lipophilic regions. Figure was generated using the MOE software.

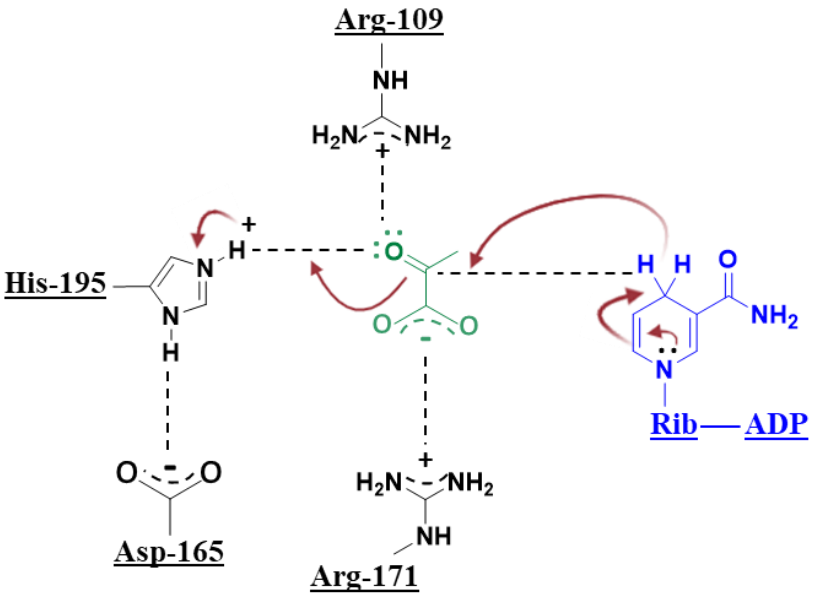

Figure 7. Representation of the LDH-5 catalytic reaction. The substrate (pyruvate) is represented in green, and the cofactor (NADH) in blue. Red arrows correspond to electron transfers. The most important residues contributing to the catalytic activity (Arg-109, Asp-168, Arg-171 and His-195) are shown.

The different isoforms are not homogeneously distributed between organs and tissues, with LDH forms rich in M subunits being prevalent in skeletal muscles, while the forms rich in H are prevalent in the heart and in the brain. The different localization of the various LDH isoforms is believed to reflect the metabolic environment of the tissue itself. The so called "aerobic-anaerobic theory" postulates that tissues enriched in H-containing isoforms are more suited to an aerobic metabolism, while more glycolytic tissues preferentially express M-containing isoforms [1]. Under normal conditions, different LDH isozyme patterns do not appear to serve distinct physiological roles. However, during intense exercise and episodes of

accrued metabolic demand, LDHs can deviate from their usual equilibrium and express specific, differentiated functions. For example, LDH-5 plays a crucial role in overworking skeletal muscles facing hypo-oxygenation and characterized by an increased demand for glucose [40]. It efficiently supports anaerobic glycolysis by facilitating lactate production to regenerate NAD^+, thereby sustaining a high glycolytic flux. Once produced, lactate is secreted and can serve to nourish the heart by fueling of the TCAC cycle, a process primarily facilitated by LDH-1 [41].

In tumors, elevated pyruvate production by glycolytic cancer cells fuels LDH-5 (LDH-M4) that catalyzes the conversion of pyruvate + NADH + H^+ to lactate + NAD^+. This reaction buffers the cytosolic pH and produces NAD^+, used as a cofactor by glycolytic enzyme glyceraldehyde-3-phosphate dehydrogenase (GAPDH) to maintain an elevated glycolytic flux [42]. Lactate together with protons is then exported through MCTs, which elevates lactate concentration and acidity in the tumor microenvironment (TME) [43]. Conversely, oxidative cancer cells can take up lactate from the lactate-rich TME, a process facilitated by MCT1 [26]. They preferentially express LDH-1 (LDH-H4) that catalyzes the reverse reaction, oxidizing lactate to pyruvate. Consequently, LDH-1 promotes lactate-fueled respiration, autophagy and angiogenesis in cancer, while LDH-5 rather supports high rates of both aerobic and anaerobic glycolysis [3, 26].

2.2.2 Significance of LDH quaternary structures

The crystal structures of LDH-1 and LDH-5 reveal tetramers comprising dimers of dimers, with the anchoring of the *N*-terminal arm (residues 1-19)

playing a central role in this association [44]. This peptidic sequence binds to two adjacent pockets of two different monomers between Leu-3 and Leu-7 of the arm and Leu-178, Val-206, Val-209, Val-211 and Trp-227 in one monomer, and Leu-300 and Val-303 in the other monomer. Blast alignment of LDH-1 and LDH-5 sequences (**Figure 8**) reveals a high level of similarity between the two tetrameric sites. As a result, achieving specificity in targeting either isoform poses a challenge when focusing on this particular site. Several reports underscore the significance of this sequence from both structural and functional perspectives. For instance, the characterization of artificial dimers of porcine LDH-5 lacking the first 34 *N*-terminal amino acids demonstrated their inactivity in comparison to the active tetrameric form [45]. Zheng *et al.* [46] further demonstrated that when the first 5 (LD5) or 10 (LD10) amino acids were removed, the ability of LDH-5 to refold after denaturation in an acidic buffer was diminished compared to the wild-type native enzyme (RW-LD). Complementing structural studies, in-depth investigation was conducted that highlighted critical roles of individual amino acids in the *N*-terminal arm. For examples, mutating Leu-3 with a proline (L3P) to destabilize the α-helix resulted in a less stable tetramer, and introducing glutamic acid instead of Ile-8 (I8E) to disrupt the β-sheet fully prevented tetramer formation in aqueous solution [47]. Our team also previously sought to better characterize the interaction between the *N*-terminal domain of human LDH-H and the tetramerization site: biophysical analyses and crystallographic data revealed that Leu-3, Leu-7 and Ile-8 are required for association, as their replacement with alanine or glycine led to a loss of interaction [30]. We further identified a novel LDH-H tetramerization site at residues 54-76 [39]. An alanine scan was conducted where substituting either Glu-62 or Phe-72 by alanine

prevented tetramer formation and resulted in LDH-1 existing as dimers in solution [39]. The L71A variant exhibited a mass photometry (MP) profile indicating a mixture of tetramers and dimers. A detailed description of the characterization of these two tetrameric sites is provided in Chapter 2.4.4.

Despite the fact that each subunit of LDH contains an active site with all the necessary structural features for proper functionality, the tetrameric state is imperative for full activity. Molecular dynamics studies (MDS) indeed showed that a proper cooperation between subunits and the correct folding of the tetramer are necessary for the appropriate closure of the active site loop, preventing water from accessing to the catalytic site and disrupting hydride exchange [48]. These studies further supported the significant contribution of binding energies to the dimerization of dimers, potentially impacting both enzyme assembly and catalytic functions [46, 47]. Building on previous work in our laboratory, it was demonstrated that truncating the last 19 *N*-terminal residues of human LDHs resulted in weaker dimeric activity compared to the native tetramer [30] (Detailed in paragraph 2.4.4, Figure 11).

This fundamental structural characterization coupled with the recognized role of LDHs in cancer metabolism laid the ground for pioneering inhibitor discoveries based on a novel strategy targeting the LDH tetramerization site [30, 39, 49].

a

```
LDH-H 1    ATLKEKLIAPVAEEEATVPNNKITVVGVGQVGMACAISILGKSLADELAL   50
           ||||::||..:.:||.| |.|||||||||.||||||||||.|.|||||||
LDH-5 1    ATLKDQLIYNLLKEEQT-PQNKITVVGVGAVGMACAISILMKDLADELAL   49

LDH-1 51   VDVLEDKLKGEMMDLQHGSLFLQTPKIVADKDYSVTANSKIVVVTAGVRQ  100
           |||:||||||||||||||||:|||||:.|||:||||||:|::||||.||
LDH-5 50   VDVIEDKLKGEMMDLQHGSLFLRTPKIVSGKDYNVTANSKLVIITAGARQ   99

LDH-1 101  QEGESRLNLVQRNVNVFKFIIPQIVKYSPDCIIIVVSNPVDILTYVTWKL  150
           ||||||||||||||:||||||.:|||||:|.:::||||||||||||.||:
LDH-5 100  QEGESRLNLVQRNVNIFKFIIPNVVKYSPNCKLLIVSNPVDILTYVAWKI  149
```

b

Sequence/ amino acid	LDH-1/LDH-5	Methods	Results	Ref
RW-LD (wild-type) Depletion of: LD5 (ATLKD) LDH10 (ATLKDQLIYN)	LDH-M	Dissociation-reassociation	Activity restored: RW-LD: 20% LD5: 15% LD10: 7%	[46]
E62A-L71A-F72A	LDH-H	Alanine scan Mass photometry	Dimer behavior	[39]
L3A-L7A	LDH-H	Alanine scan NMR WaterLOGSY	Loss of interactions	[30]

I8A	LDH-H	Nano DSF	Destabilization of the oligomeric state	[30]

Figure 8. Essential amino acid depletion disrupts LDH tetrameric structures. (**a**) Human LDH-1 and LDH-5 [1-150/149] sequences aligned and compared using the EMBOSS Needle alignment software [50]. The middle line represents the alignment results were " | " account for identity, " . " accounts for a deletion or a difference in the sequence, and " : " for a positive score. Tetramerization sites (residues 1-19 and 55-77) are reported in light blue. Amino acids or sequences fundamental to maintain a tetrameric form are highlighted or underlined in pink. (**b**) Table reporting the fundamental amino acids involved in LDH tetramerization.

2.3 LDH involvement in cancer metabolism

2.3.1 LDHs orchestrating metabolic symbiosis and autophagy

In stark contrast to normal cells, cancer cells exhibit a remarkable metabolic plasticity that enables them to thrive in nutrient-deprived environments and adapt their metabolism depending on substrate availability. Spatially, the tumor microenvironment displays heterogeneous characteristics, with distinct bioenergetic needs and metabolic behaviors being evident in areas proximal to perfused blood vessels compared to the core of the tumor (**Figure 9**). Glycolytic cancer cells predominantly reside in poorly perfused areas and at the tumor core where oxygen limitation and nutrient scarcity create a challenging milieu for survival. These cells are highly dependent on glucose, and their viability is compromised under conditions of glucose starvation [51].

In response to the hypoxia-driven upregulation of HIF-1 activity, LDH-5 plays an important role in glycolytic cancer cells. By reducing pyruvate, the

end product of glycolysis, to lactate, LDH-5 facilitates NAD^+ regeneration, which is needed for sustaining upstream glycolytic reactions. LDH-5 activity accelerates in glycolytic compared to oxidative cancer cells (in which NAD^+ oxidation primarily occurs through OXPHOS), resulting in a stable NAD^+/NADH balance that is crucial for preserving redox homeostasis and promoting cellular proliferation and growth [26, 52]. Such activity is also facilitated by the phosphorylation of LDH-5 at tyrosine 10 (Y10). The tyrosine kinase receptor FGFR1 enhances LDHA activity by phosphorylating LDH-5 at both Y10 and Y83, thereby promoting the formation of the active LDHA isoenzyme and increasing its affinity for NADH[53]. LDH-5 further contributes to buffering the cytosolic pH by incorporating protons formed earlier in glycolysis into lactate anions, preventing metabolic acidosis [42]. Lactate export is facilitated by MCT4, a hypoxia-inducible lactate-proton symporter [54]. This double pH regulation is vital, as a slightly alkaline intracellular environment supports glycolysis. PFK1 is particularly sensitive to pH changes, and its activity increases with pH [55].

Conversely, oxygenated cancer cells relying on OXPHOS preferentially use lactate as an energy source despite glucose availability [26]. Extracellular lactate is imported by oxidative cancer cells in a process facilitated by MCT1. In the cytosol, LDH-1 oxidizes lactate to pyruvate, which then fuels the TCAC cycle and OXPHOS to generate ATP. This lactate shuttle mechanism optimizes glucose availability for glycolytic cancer cells located in nutrient-starved regions, promoting their survival. As a consequence, silencing MCT1 disrupts lactate-fueled respiration and indirectly induces glycolytic cancer cell death by virtue of glucose starvation, underscoring the crucial role of the LDHs-lactate-MCTs pathway in the metabolic symbiosis (**Figure 9**) [51, 56].

The clinical significance of lactate in various malignancy is underscored by studies revealing correlations between tumor lactate levels and the outcomes of human cancer patients [57].

A major advantage for oxidative cancer cells of using lactate preferentially to glucose is to promote autophagy [58], a process supporting cancer cell survival and proliferation through recycling damaged/oxidized cellular material. The LDH-1 reaction indeed produces protons in close proximity to lysosomes, as LDH-1 physically interacts with vacuolar ATPase (V-ATPase) [59], a proton pump expressed at the lysosomal membrane and being responsible for maintaining a low pH within lysosomes. LDH-1 activity was shown to acidify lysosomes, activate pH-dependent lysosomal acid hydrolases, and activate autophagy, whereas silencing the enzyme inhibited autophagy, slowed down cancer cells proliferation and induced apoptosis [3, 60]. In glycolytic cancer cells, LDH-5 converts pyruvate to lactate, and lactate can either be exported to support the metabolic symbiosis or be reoxidized to pyruvate by LDH-1. The reoxidation process drives lysosomal acidification in a similar way to what occurs in oxidative cancer cells, providing glycolytic cancer cells with an additional source of energy and biosynthetic materials. Brisson *et al.* [3] demonstrated that silencing *LDH-B* with siRNAs inhibited autophagy in both glycolytic and oxidative cancer cells. Comparatively, *LDH-A* silencing reduced the autophagic flux in glycolytic cancer cells only. These experiments underscored the role of LDH-1 in supporting autophagy in cancer.

Metabolic relationships within the tumor microenvironment extend to nonmalignant host cells, such as cancer-associated fibroblasts (CAFs) that can undergo a catabolic shift to support cancer cell metabolism. Studies have

shown that the presence of MCF7 breast cancer cells increased the autophagic activity of CAFs [61]. Glutamine released from autophagic CAFs to the TME, fueled the mitochondrial activity of MCF7 cells, protecting them from apoptosis through the overexpression of the multifunctional protein TP53-inducible glycolysis and apoptosis regulator (TIGAR).

The oxidative use of lactate is not exclusive to cancer cells. This mechanism is also observed in astrocytes, which provide lactate to neurons, forming an astrocyte-neuron lactate shuttle. Neurons express MCT2 and LDH-1, creating an ideal condition for the uptake and utilization of lactate as an energy substrate [62]. What distinguishes cancer cells is their limited metabolic options in hypoxic conditions where they heavily rely on glucose for survival, growth and proliferation. The notable reliance of hypoxic/glycolytic cancer cells on the metabolic preferences of normoxic/oxidative cancer cells has prompted the development of strategies to disrupt the exchange of lactate, as detailed below.

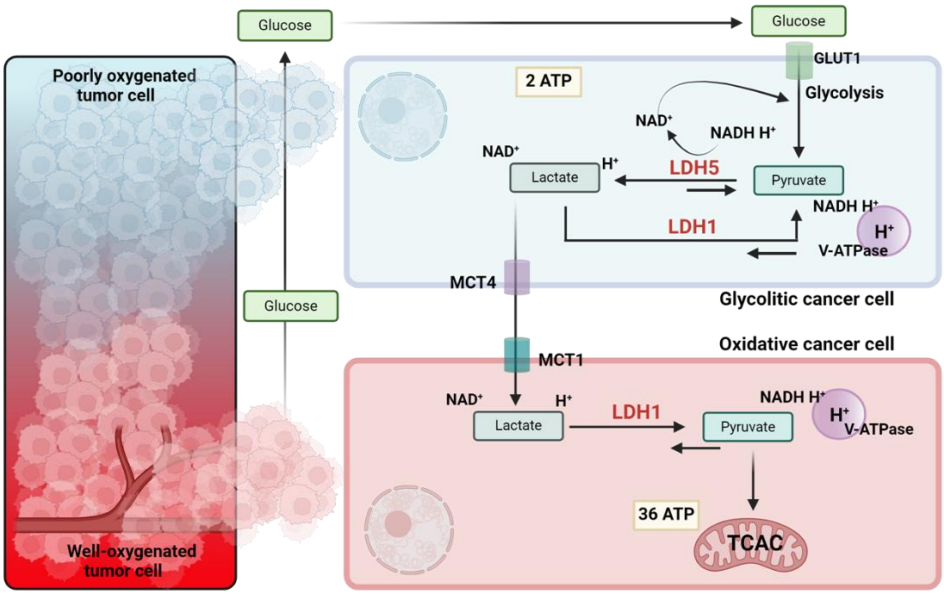

Figure 9. Lactate metabolism drives a metabolic symbiosis between oxidative and glycolytic cancer cells, further promoting lysosomal acidification and autophagy. The figure illustrates the metabolic interplay between glycolytic and oxidative cancer cells within the tumor microenvironment, influenced by oxygen gradients. A decreasing gradient of oxygen develops in tumors, notably with the distance from perfused blood vessels (left). Hypoxic/glycolytic cancer cells (blue) rely on GLUT1-facilitated glycolysis, producing lactate *via* LDH-5 and exporting it together with a proton through MCT4. Normoxic/oxidative cells (pink) use MCT1 to take up lactate and convert it back to pyruvate by LDH-1, supporting oxidative phosphorylation. LDH1-dependent lysosomal acidification, triggering autophagy, is present in both cell types. The Figure was generated using Biorender
Abbreviations: ATP- Adenosine triphosphate; GLUT1- Glucose transporter 1; LDH- Lactate dehydrogenase; MCT- Monocarboxylate transporter; NAD(H)- Nicotinamide adenine dinucleotide; V-ATPase- Vacuolar ATPase; TCAC- Tricarboxylic acid cycle.

2.3.2 Lactate promotes cancer cell invasiveness, tumor angiogenesis and epigenetic regulation.

Angiogenesis is a physiological process required during embryogenesis and wound healing, which oversees the development of new blood vessels from

existing ones [63, 64]. In solid tumors, new blood vessels are needed for delivering oxygen and nutrients to cancer and host cells [63]. Lactate recently emerged as a key player in this process. Inside cells that have the ability to import lactate, lactate is oxidized to pyruvate by LDH-1, and pyruvate competes with 2-oxoglutarate for prolyl hydroxylase-2 (PHD2), resulting in inhibition of the enzyme [65]. It has two main consequences. First, PHD2 inhibition in oxidative endothelial cells is responsible for a stabilization of the expression of IκB kinase (IKK), which leads to activation of transcription factor nuclear factor kappa-light-chain-enhancer of activated B cells (NF-κB). NF-κB translocates into the nucleus, initiating the transcription of a gene program that includes *IL-8* [66, 67]. Enhanced IL-8 synthesis, secretion and binding to its receptor triggers multiple signaling pathways, fostering angiogenic responses in endothelial cells and enhancing the proliferation and survival of cancer cells. This process accounts for a significant portion of the pro-angiogenic effects attributed to exogenous lactate. The second consequence of PHD2 inhibition by lactate is a stabilization of the expression of HIF-1α in oxidative cancer cells and in endothelial cells, thus activating transcription factor HIF-1 independently of hypoxia. In oxidative cancer cells, it stimulates the transcription of the *VEGFA* gene, hence the production and secretion of pro-angiogenic factor vascular endothelial growth factor (VEGF) [68]. In endothelial cells, HIF-1 activation by lactate enhances the transcription and expression of VEGF receptor 2 (VEGFR2), making them more responsive to extracellular VEGF. Basic fibroblast growth factor (bFGF) production and secretion are also enhanced [69]. Lactate can thus be viewed as a signaling agent whose activity depends on its conversion to pyruvate by LDH-1.

The link between an acidic TME and the aggressive invasive behavior of cancer cells is well established nowadays [70-72]. Following increased metabolism, H^+ production and efflux as well as CO_2 production are enhanced in cancers, resulting in an acidic extracellular pH (pH_e). Tumor pH_e typically ranges between 6.5 and 6.9 compared to normal tissues in physiologic conditions, where pH_e is 7.2-7.4 [43]. This acidic environment is toxic for normal cells, but no for those cancer cells that develop adaptive mechanisms to survive to acidity and gain an advantage to invade the surrounding place. Secretion of lactic acid is part of this process, activating matrix metalloproteinases (MMPs) and cathepsin proteinases, leading to tissue remodeling and local invasion [73]. In particular, an acidic extracellular environment induces a redistribution of cathepsin B towards the cancer cell surface from where the active form is secreted, which helps the cells to degrade the extracellular matrix and facilitates migration.

LDH-5 and lactate also play a role in cancer development through histone lactylation, a process that links cellular metabolism to gene regulation [74]. This modification alters the structure of chromatin, making it more accessible and driving the expression of genes involved in tumor progression and immune evasion, such as Arg1 (arginase 1)**,** IL-10 and VEGF are upregulated[74, 75]. Lactate enters in tumor-associated macrophages (TAMs) and induces histone lactylation, modifying the chromatin structure similarly. Through this mechanism, lactate promotes TAMs toward an M2-like state characterized by anti-inflammatory and pro-tumor activities, including the secretion of cytokines that suppress cytotoxic T cell and natural killer (NK) cell activities. This creates an environment that not only supports tumor cell proliferation, survival, and invasion, but also protects the tumor from immune

attack, facilitating tumor progression and immune evasion [76]. Lactate also inhibits histone deacetylases (HDACs), further modifying chromatin structure and gene expression [75]. This highlights a dual role of lactate in energy production and gene regulation, ultimately facilitating cancer development and progression.

Considering the diverse metabolic adaptations supporting cancer cell survival, extensive efforts have been dedicated to targeting key enzymes and transporters. LDHs are among them.

2.4 Targeting cancer metabolism

Given the strong metabolic reliance of tumors on glycolysis and their inherent population heterogeneity, targeting enzymes and transporters of this pathway has been recognized to be an appealing avenue for the development of new anticancer drugs. Attention has been directed towards metabolic enzymes and transporters that are overexpressed or on which cancer cells strongly depend. Studying glucose transporters GLUT1, GLUT2 and GLUT3 has yielded the identification of potent small molecule inhibitors, such as Glutor and BAY-876 [77, 78]. The extent to which these compounds possess the requisite pharmacokinetic properties for clinical advancement is a critical aspect yet to be tested. The increased expression of HK2 in cancer cells coupled with its crucial role as the initial step of the glycolysis pathway underscores its consideration as a potential therapeutic target. Inhibitors based on glucosamine derivatives have demonstrated nanomolar potency against HK2, and their binding at the catalytic pocket has been characterized through co-crystal structures [79]. However, there is currently a lack of *in vivo* efficacy

data for these inhibitors. Targeting PKM2 has also emerged as a promising strategy for anticancer therapy. PKM2 indeed drives metabolic reprogramming in cancer cells as a tetramer, supporting rapid tumor growth. Posttranslational modifications (acetylation of lysine-305) and Fructose-1,6-biphosphate (F16BP) can convert PKM2 in a less active dimeric form, redirecting glycolytic intermediates to fuel tumor development [80]. Additionally, an up-regulation of PKM2 expression by transcription factors like HIF-1 and c-Myc promotes cancer cell proliferation. Inhibiting PKM2 activity or promoting its active tetrameric form offers a potential approach to impede cancer growth and progression [81]. However, many PKM2 modulators failed to advance to clinical use due to issues such as their promiscuity and interference with assay outcomes caused by compounds known as pan assay interference compounds (PAINS), exhibiting a non-specific bioactivity [80]. Malate dehydrogenase (MDH), which exists as cytoplasmic and mitochondrial isoforms, is another metabolic enzyme involved in energy production and cell division. In cancer, MDH supports glycolysis and NAD^+ regeneration when LDH activity is inhibited. Despite its potential as a therapeutic target, there are currently no MDH inhibitors available on the market, largely due to challenges in achieving specificity [82]. Many known inhibitors target the NADH-binding site common to numerous enzymes, resulting in off-target effects and cytotoxicity to nonmalignant cells [83]. Nonetheless, the recent identification of an allosteric pocket in MDH offers a promising route for developing specific inhibitors [84]. Allosteric inhibitors like 4-(3,4-difluorophenyl)-thiazol-2-amine and its derivatives have shown potential by binding to sites distant from the active site, thus avoiding the issues associated with cofactor analogs. Further, the

decisive roles played by MCT1 and MCT4 in lactate exchange supporting cancer cell survival have been underscored. Studies conducted by Sonveaux and his colleagues [51, 54] have provided evidence of a metabolic switch occurring when MCT1 or MCT4 was knocked down, resulting in unwiring oxidative and glycolytic cell populations, ultimately leading to reduced cancer cell survival and necrosis. A potent MCT1 inhibitor is currently undergoing phase I clinical trials in patients with advanced-stage cancers [85]. The potential benefits of simultaneously inhibiting MCT1 and MCT4 are significant, given that most tumors express both transporters, but only a limited number of dual inhibitors have been discovered so far, and none have reached the market [54]. Concerns arise about specificity when targeting MCTs, as they transport various monocarboxylates, possibly leading to side effects [86, 87]. Despite these challenges, focusing on targeting lactate shuttling in cancer appears promising [88, 89].

2.4.1 LDHs as metabolic anticancer targets

Both LDH isoforms play important roles in the metabolic adaptability of cancer cells, which substantiates the significance of targeting them in anticancer approaches [90]. Initial research interest centered on inhibiting LDH-5, but subsequent endeavors have focused on developing LDH-1 inhibitors.

Analysis of LDH-5 expression across various types of cancers has revealed its overexpression at various stages along the cancerogenic pathway [2]. Consistently, *in vitro* and *in vivo* experiments have shown that silencing *LDHA* inhibits the migration and invasiveness of renal cell carcinoma (RCC)

cells by inhibiting the epithelial-mesenchymal transition (EMT) [91]. In a mouse model of non-small-cell lung cancer (NSCLC) featuring KRAS and EGFR mutations, suppressing LDH-5 expression resulted in reduced tumorigenesis and a regression of established tumors [92], which could find its origin in a decreased survival of hypoxic cancer cells [93]. Meanwhile, studies on LDH-1 have shown its upregulation in basal-like/triple-negative breast cancers [94]. It also accelerates the growth of lung tumors and promotes lysosomal acidification and autophagy in both oxidative and glycolytic cancer cells [3].

The current strategy to exploit LDHs as therapeutic targets involves the identification of pan inhibitors that would target all LDH isoforms simultaneously [95]. A pending question is whether complete inhibition of both isoforms would be associated to acceptable side effects. To our knowledge, patients lacking both LDH-1 and LDH-5 have not been identified so far, but cases of absence of one of the two isoforms have been reported. Patients with a complete deficiency of LDH-M show muscle rigidity and myoglobinuria after strenuous exercise, but no symptomatology under ordinary circumstances [96]. These effects are congruent to the critical role of LDH-5 in regenerating NAD^+ to maintain the glycolytic flow producing ATP in hypo-oxygenated contractile muscle cells. LDH-5 impairment results in ATP depletion, leading to membrane damage and impacting cytosolic proteins, such as myoglobin [96, 97]. Individuals lacking the LDH-1 subunit have been identified as well [98]. They do not exhibit symptoms, though occasional reports have indicated mild signs of hemolysis in some cases.

The modest symptomatology of LDH deficiency can be attributed to the presence of compensatory mechanisms. For example, in skeletal muscles, α-

glycerophosphate dehydrogenase steps in when LDH-5 is absent, converting glucose in α-glycerophosphate and glycerol while generating NAD^+ for continued metabolic functions [1, 99]. This does not prevent ATP levels to decrease under hypoxia, though. In erythrocytes, a lack of LDH-1 can be compensated by a NADH reoxidation system operated by NADH-methemoglobin reductase [1], wherein metabolites bypass the PPP and the ATP ratio is preserved. This type of observations suggest that a simultaneous inhibition of LDH-1 and LDH-5 is likely to activate compensatory mechanisms, thus limiting potential side effects when it comes to anticancer applications. This supports the development of pan LDH isoform inhibitors in addition to specific isoenzyme inhibitors. In line with this idea, Ždralević *et al.* [37] demonstrated that only a simultaneous knockdown of LDH-1 and LDH-5 (LDHA/B-KO) effectively decreased tumor colon adenocarcinoma and melanoma growth in xenograft mouse experiments. Under normoxia, LDH-deficient cancer cells did survive by switching to high-rate OXPHOS. However, this option is not possible under hypoxia, so that deficient cells died *in vitro*. Strategies adopted to target LDHs are reported in the next chapters.

2.4.2 Challenges for *in vivo* LDH inhibition

Intense efforts have been devoted to the development of LDH inhibitors, but the conversion of the associated findings towards preclinical and clinical studies is still inconclusive despite high inhibitory potencies [100-102]. This limitation can be partly explained by the orthosteric mode of inhibition of most of these compounds.

Unfavorable pharmacokinetics profile and lack of selectivity of existing compounds

The polar and solvent-exposed catalytic site of LDHs poses significant challenges for the development of new inhibitors. It is positioned at the interface of the tetramer and rich in cationic residues necessary for docking substrates and cofactors in a correct conformation. These characteristics impose the design of inhibitors harboring moieties that do not fit with an appropriate absorption, distribution, metabolism and excretion (ADME) profile.

Gossypol and its derivatives (**1**) are among the first reported LDH inhibitors [32] (**Table 1**). Gossypol is a polyphenolic binaphthyl sesquiterpene extracted from cotton seeds, acting on NAD^+/NADH-dependent enzymes, including LDHs. Even if it has been evaluated in Phase 1/2 clinical trials [103, 104], it induces severe side effects due to two functional aldehyde groups responsible for non-specific protein binding and inhibition [105]. Gossypol optimization yielded FX-11 (**2**), which was used to demonstrate that LDH-5 inhibition can arrest the progression of lymphomas and pancreatic tumor xenografts in mice [100] (**Table 1**). However, the presence of two catechol moieties argues for the possibility that additional, unintended effects of FX11 could contribute to its anticancer activity. Overall, Gossypol and FX-11 showed high reactivity but a lack of selectivity towards different dehydrogenases, such as malate and glutamate dehydrogenases [106, 107].

A fragment-based approach using different biophysical techniques has been pursued to identify small molecules inhibitors of LDH-5 [108]. All hits turned out to be NADH competitor molecules. As for other catalytic site

inhibitors, they harbored polar moieties needed for interacting at the catalytic pocket, suggesting that they mimicked the pyruvate-binding pattern [108]. The most active molecule was compound 9 (**3**) (**Table 1**) (IC_{50} = 0.120 µM) containing four hydroxyl groups that create a network of hydrogen bounds. The physiochemical properties of such compound are not optimal for cell penetration, and work remains to be done for the development of LDH inhibitors with acceptable ADME profiles.

Quinoline 3-sulfonamides (**4**) (**Table 1**) showed a low micromolar potency against LDHs [109]. Crystal structures nevertheless established their binding at the cofactor-binding site, which means that the development of this class of compounds also necessitates improvements of the ADME profile before *in vivo* efficacy studies [109].

The conservation of the sequence and structure of LDH catalytic sites with other NAD^+/NADH-dependent enzymes makes the production of selective inhibitors very challenging [1, 107]. Some Quinoline-3-sulfonamide derivatives achieved some selectivity for LDH-1, though, as they interacted with two amino acids residues that differ between LDH-1 and LDH-5 (Ala-98 *versus* Val-98 and Ile-116 *versus* Val-117, respectively).

Boudreau *et al.* [110] reported a high-throughput small-molecule screening resulting in the identification of a high potent hit against LDHs. GNE-140 (**5**) (**Table 1**) inhibits the biochemical activities of LDH-1 (IC_{50} = 5 nM) and LDH-5 (IC_{50} = 3 nM). The X-ray structure showed that this compound binds close to the NAD-binding area within the active site pocket of the enzymes, forming hydrogen bonds between its carbonyl oxygen atoms and Arg-168, His-192 and Asn-137. Interestingly, GNE-140 did not inhibit

other dehydrogenases (MDH-1 or -2) closely resembling LDHs, suggesting specificity. *In cellulo*, similar responses were observed in MIA PaCa human pancreatic cancer cells when comparing LDH-5 depletion to a treatment with GNE-140 (EC_{50} = 0.67 µM). However, this inhibitor did not progress to clinical trials due to ineffectiveness in inhibiting tumor growth in preclinical mouse studies, with no detectable alterations of any metabolite [110]. It is likely that the high clearance rate of the compound contributes to its *in vivo* inefficacy.

Recent studies brought interest on a novel class of pyrazol-based small molecules [111], with compound 63 (**6**) having a robust *in vitro* and *in cellulo* potency against LDHs (K_D = 0.111 nM; IC_{50} = 2.90 ± 0.3 µM in A673 cells and IC_{50} = 3.96 ± 0.68 µM in MiaPaCa-2 cells) (**Table 1**). Structure-activity relationship (SAR) studies have been conducted with the scaffold of the compound, obtaining a high resolution (1.6 Å) crystal structure. It revealed that the benzyl-sulfonamide substituent at position 4 of the pyrazole is involved in critical hydrogen bonds with Asp-140, Glu-191 and Ile-141 inside the active site pocket of LDHs. Introduction of a cyclopropyl group with a methylene spacer further created π-π interactions between the cyclopropyl group and active-site tyrosine Tyr-238. This structural modification aimed to enhance the binding affinity to the target. However, while the compound showed potent inhibition with similar IC_{50} values (27 nM for LDH-1 and 32 nM for LDH-5), it also exhibited some undesirable characteristics. One issue is related to its polar nature, which was intended to enhance interactions with the polar active site of the enzymes. Another is related to high clearance rates in mice and rats, which brings the necessity of improvements of the ADME profile before additional *in vivo* efficacy studies [109].

Table. 1 Overview of LDH active site inhibitors: Structure, mechanism of action and *in vitro*/*in cellulo* activity.

N°	Structure	LDH-5 (and LDH-1) inhibition	*In cellulo* activity	Mechanism of action
1	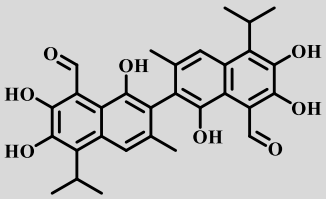	K_i = 1.9 (1.4) µM	Cytotoxic effects in different cancer cell lines	N.D.
2	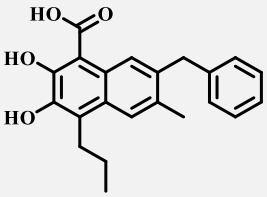	K_i = 0.05 (1.0) µM	Cytotoxic effects	N.D.
3	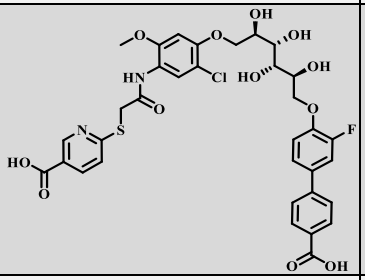	IC_{50} = 0.120 (N.D.) µM	N.D.	NADH competitive
4	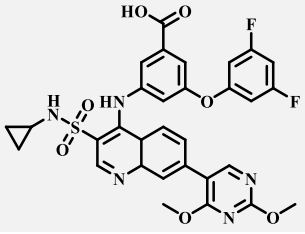	IC_{50} = 0.0026 (0.043) µM	EC_{50} on lactate production ranging from 0.4 to 30 µM across various cancer cell lines	NADH competitive

5	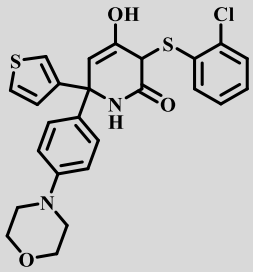	IC_{50} = 0.003 (0.005) µM	EC_{50} = 0.67 µM on lactate production (MIA PaCa-2)	NADH competitive
6	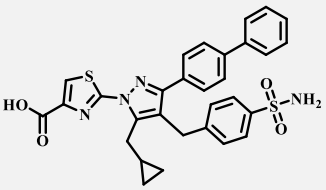	IC_{50} = 0.032 (0.027) µM	EC_{50} = 0.85 µM on lactate production (MIA PaCa-2)	NADH competitive
7	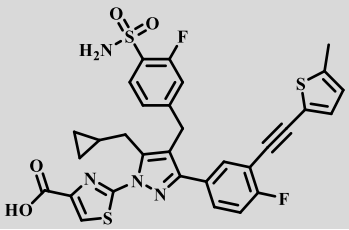	IC_{50} = 0.06 (0.03) µM	EC_{50} = 0.37 µM on lactate production (MIA PaCa-2)	NADH competitive

High LDH cellular expression

Another constraint for the development of LDH inhibitors is high LDH concentrations in cells (1-10 µM) [109]. Considering that each monomer is necessary to form the quaternary structure of the catalytic site, only the tetrameric form is active. Therefore, a 1:1 stoichiometry is necessary between active site-inhibitory molecules and monomers. Because $EC_{50} = K_i + ½ E_t$ (where K_i represents the inhibition constant and E_t is the total cellular enzyme concentration), an E_t significantly greater than the K_i would imply an enzymatic concentration much higher than the concentration of a compound required for half-maximal inhibition. E_t values for both LDH-1 and LDH-5 isozymes were determined to be in the µM range across various cancer cell

lines, which adds to the challenge of achieving potent catalytic inhibition in cells [109]. For example, Quinoline-3-sulfonamides (**4**) (**Table 1**) only achieved cellular EC_{50} values in the low micromolar range, contrasting with a nM potency on purified enzymes [109].

Optimization of the pyrazole-based series has been pursued, which led to the design of a small molecule (NCI-006) (**7**) that overcomes the issues relative to *in vivo* LDH inhibition [95, 111] (**Table 1**). This LDH-1/LDH-5 pan inhibitor is biochemically active at low µM concentrations (IC_{50} = 0.06 µM for LDH-5 and IC_{50} = 0.03 µM for LDH-1). Its EC_{50} for inhibiting lactate secretion by red blood cells (RBC) after *per os* (PO) and intravenous (IV) administration to mice was 2.1 µM and 1.6 µM, respectively. Following PO administration, NCI-006 failed to inhibit LDHs in Mia Paca-2 tumor-bearing mice, as the drug concentration measured in the tumor was < 4 µM and the level of LDHs in Mia Paca-2 cells is around 10-20 µM. IV administration improved the tumor drug concentration (to 15-20 µM) and *in tumor* LDH inhibition [111]. LDH inhibition reduced the growth rate of MIA PaCa-2 xenografts, with minimal impact on the body weight of mice.

2.4.3 Towards allosteric inhibition

Taking into consideration what has been described so far, the development of LDH inhibitors remains a challenge. Even if a successful identification of potent inhibitors has been achieved *in vitro*, *in cellulo* and/or *in vivo*, none of them has reached the market. To overcome the challenge on targeting its active site, efforts have also been recently devoted to successfully target the

allosteric site of LDHs using novel peptide-based and small molecule inhibitors.

Peptides and small molecules serve as LDH allosteric inhibitors.

Peptides have emerged as a key and versatile class of compounds in contemporary medicinal chemistry. Since 1920s, peptides have been isolated and introduced in therapeutic use (*e.g.* insulin) [112, 113]. Subsequently, both industry and academia have pursued research to evolve in this field. Remarkably, from 2016 to 2022, the Food and Drug Administration (FDA) approved 25 new peptides, encompassing a diverse array of cyclic, linear, and peptidomimic structures [114]. However, peptides have several limitations, notably their vulnerability to proteolysis and low bioavailability [115]. Medicinal chemistry has addressed these issues by exploring innovative routes of administration (*e.g.* co-formulation with permeation enhancers), incorporating stapling techniques, and using unnatural amino acids, particularly at proteolysis sites, as an effective strategy to extend their half-life [116, 117]. Short peptide sequences lack a defined structure in water, adopting a random arrangement in contrast with their binding targets usually recognized in a specific conformation [118]. To address this problem, stapling modifications have been used to constrain peptides in a more native-like conformation, hiding the peptide bonds and enhancing their resistance to proteases. Furthermore, the introduction of unnatural amino acids has shown promise in achieving better pharmacokinetics while also modulating peptide interactions with proteins [119].

In recent years, the development of peptide-based inhibitors against LDHs has garnered significant attention in the field of drug discovery [30, 38, 39, 49, 120]. Medicinal groups, particularly through the design and

characterization of these peptides, have disclosed novel potential allosteric sites for inhibition. The following example presents an instance of an allosteric peptide designed to interact with LDH-5. This specific peptide-based strategy serves as a preview, providing glimpse into the diverse array of peptide-based approaches that will be comprehensively addressed in the next chapter, particularly focusing on their use as homomeric disruptors.

Investigations conducted by Mark R. Woodford and his colleagues identified a peptide named FLCN-10 (**8**), (**Table 2**) derived from tumor suppressor protein folliculin. This peptide demonstrated allosteric inhibition of LDH, with immune precipitation analyses having revealed selectivity towards LDH-5 *versus* LDH-1 [121]. Binding analyses using fluorescence polarization anisotropy yielded promising results, displaying a potent inhibitory effect on LDH-5 activity. Proteolysis-coupled mass spectrometry (LiP-MS) further identified the binding site (residues 91-99, LVIITAGAR) to be distant from the active-site pocket (**Figure 11b**). It rather corresponded to the *N*-terminal portion of the LDH-5 catalytic loop, which could explain why FLCN-10 binding interfered with the accessibility of NADH to the active loop. Through optimization, an enhanced penetration of this peptide into cells and patient tumors was achieved, suggesting potential therapeutical applications that warrant further exploration [121].

Small molecules stand out as a major class of anticancer drugs, with the FDA having approved 89 of them for various oncology purposes [122, 123]. Unlike macromolecular drugs, small molecule drugs offer advantages in terms of pharmacokinetics, cost, patient adherence, and practical considerations for storage and transportation [123]. In contrast to peptides, they allow for easy oral administration and efficient systemic delivery. Their

diverse chemical structures enable modifications, enhancing drug properties and leading to the development of new compounds. Approaches for hit finding encompass both knowledge-based design utilizing existing information, and random screening exploring extensive compound libraries [124]. In the quest for LDH allosteric inhibitors, a blend of these approaches, both virtual and physical, resulted in the identification of promising inhibitors.

For instance, a biochemical high-throughput screening led to the identification of phthalimide (**Table 2, 9**) and dibenzofuran (**Table 2, 10**) derivatives targeting a specific allosteric site of LDH-5 [125] (**Figure 10**). They exhibit IC_{50} of 308 nM and 757 nM, respectively. Co-crystallization revealed that their binding site is located at the interface between two monomers, distant from the catalytic site. These two compounds bind the same pocket but protract in two different directions: the phthalimide derivative engages in a π-stacking interaction with Tyr-172 and extends until Lys-59, whereas the dibenzofuran derivative interacts with the same Tyr-172 but extends towards the other monomer where its sulfonamide moiety interacts with Ile-77 and Pro-75 (**Figure 12b**). Remarkably, minor conformational adjustments become evident upon binding. The most noteworthy change pertains to a repositioning of Arg-169, a critical factor in coordinating the substrate within the active site. Withdrawal of its guanidinium group hints at a substrate binding that is not well-suited, serving as a plausible explanation for the observed inhibition of the enzymatic activity. In accordance with strong inhibition, it is reasonable to conclude that this newly revealed binding site operates as an allosteric site, holding promise for further strategies aimed to inhibit LDH-5. Significantly, our research team

delved into the same region on the LDH-1 isoform [39]. Notably, peptides LP-22 and GP-16 that we identified perfectly match the same allosteric site in LDH-1. Our group has recognized this site as a novel tetramerization site.

Shibara *et al.* [126] reported another molecule selectively targeting LDH-1 at a novel allosteric site. Screening more than 345.000 compounds based on monitoring the conversion between NADH and NAD^+ evidenced AXKO-0046 (**11**) (**Table 2**), an indole derivate, as a potent LDH-1 inhibitor (EC_{50} = 42 nM). Structural modifications, such as the addition of a methyl group to the benzylamine or cycloheptylamine groups, resulted in a substantial reduction in potency (Ec_{50} = 0.25 up to > 100 µM). Examination of the binding site revealed its location at the interface between two monomers, positioned differently from the previously described allosteric sites, approximately 20 Å away from the active site. Specifically, the indole ring is situated within a cavity formed by Gly-204, Asn-206, Gly-209, and Ser-211 (**Figure 12a**). Remarkably, the NH group of AXKO-0046 forms a hydrogen bond with the oxygen of Ser-203. The allosteric activity of the compound was elucidated by inducing changes in the active site loop of LDH-M. However, it did not exhibit cellular activity, indicating a need for several optimizations before enabling *in vivo* assessments.

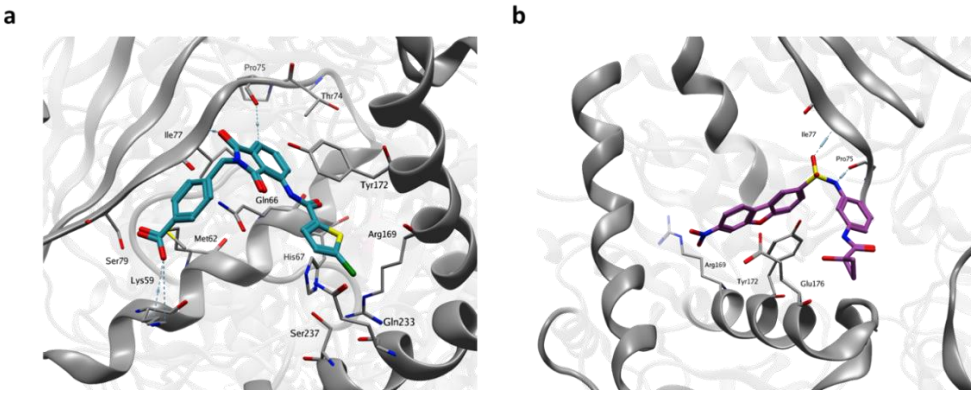

Figure 10. Co-crystallographic structures of LDH-5 allosteric inhibitors. The allosteric inhibitors bind in the same pocket but extend in two different directions. Displayed picture correspond to the LDH-5 subunit co-crystalized with (**a**) a phthalimide derivative (compound 9, PDB ID: 6DBU), which exhibits a stacking interaction with Tyr-172 and extends until Lys-59; and (**b**) a dibenzofuran derivative (compound 10, PDB ID: 6SBV) that also exhibits stacking interaction with Tyr-172 but extends until Ile-77 and Pro-75. Figure was generated using the MOE software.

Table. 2 Overview of LDH allosteric inhibitors: Structure, class, mechanisms of action and *in vitro*/*in cellulo* activity.

N°	Structure/ Sequence	Class	LDH-5 or/and (LDH-1) inhibition	Mechanism of action
8	**AQRMNTAFTP (FLCN-10)**	Linear peptide	$K_a \approx 1x10^8$ M^{-1} (N.D.)	Active site loop

9	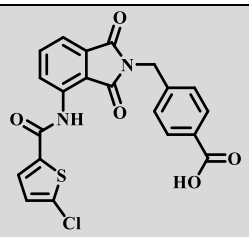	Small molecule	IC_{50} = 0.308 (N.D.) μM	Dimer-dimer interface (Site 2)
10	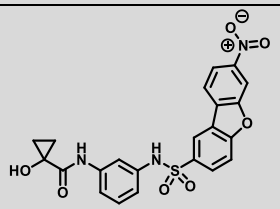	Small molecule	IC_{50} = 0.757 (N.D.) μM	Dimer-dimer interface (Site 2)
11	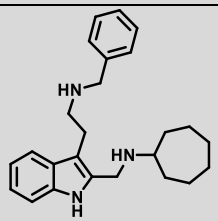	Small molecule	EC_{50} = N.D. (0.042) μM	Monomer-monomer interface
12	**QLIYNL**	Linear peptide	N.D.	*N*-terminal arm, dimer-dimer interface (Site1)
13	**LIYNLL**	Linear peptide	N.D.	*N*-terminal arm, dimer-dimer interface (Site1)
14	**IYNLLK**	Linear peptide	N.D.	*N*-terminal arm, dimer-dimer interface (Site1)
15	**CTLKCKLI linker: p-tetra fluorophenyl (macrocycle 7)**	Stapled peptide	K_D = 117 (380) μM LDH-Htr* K_D= 11 μM	*N*-terminal arm, dimer-dimer interface (Site1)

16	**LEDKLKGEMMDLQHGSLFLQTP (LP-22)**	Linear peptide	LDH-Htr K_D = 156 µM	Dimer-dimer interface (Site 2)
17	**GEMMDLQHGSLFLQTP (GP-16)**	Linear peptide	LDH-Htr K_D = 240 µM	Dimer-dimer interface (Site 2)
18	**CRRLCYRFWCFTVCRGR (cGmC9)**	β-hairpin peptide	IC_{50} = 2.5 (N.D.) µM	Dimer-dimer interface (β-sheet *N*-terminal arm)
19	**GCRrLCYRFWCFTVCrGr ([R/r]cGmC9)**	β-hairpin peptide	IC_{50} = 2.8 (N.D.) µM	Dimer-dimer interface (β-sheet *N*-terminal arm)

* LDH-Htr is a truncated LDH-H variant without the *N*-terminal arm. It will be further detailed in section 2.4.4 for its structural and functional implications.

2.4.4 Towards homomeric disruption

Over the past 20 years, targeting protein-protein interactions (PPIs) emerged as a new strategy for drug development [127, 128]. Most biological activities are regulated by protein complexes, controlled by PPIs [129]. Two main advantages account for this natural system: (1) an ordered oligomeric state where residues are hidden at interfaces increases protein stability, and (2) protein-protein interfaces are extensive, involving a much larger number of residues that are less conserved in general than enzyme active sites often sharing the same features in cofactor-dependent enzymes. Hence, directing attention towards these specific, less conserved sites holds promises for achieving the desired selectivity in targeting proteins [130]. Hence, compared to targeting substrate- and cofactor-binding sites, targeting protein-protein

interfaces could potentially lead to fewer selectivity problems and would thus generate fewer off-target side effects. Numerous biological processes, including neurodegenerative disorders and cancer, are governed by PPIs. Abrogation or irregularities in these interactions are closely linked to the onset of various diseases [131]. Homomeric interfaces represent potential allosteric sites, offering opportunities for protein inhibition and destabilization. Targeting these oligomeric interfaces can unveil novel approaches for addressing challenging targets, as observed upon disruption of the dimer-dimer active conformation of transcription factor signal transducer and activator of transcription 3 (STAT3) that inactivates the protein [132]. Additionally, disrupting homomeric interactions with a single inhibitor can result in the misfolding and degradation of the entire protein complex, presenting a favorable scenario compared to the 1:1 inhibition usually achieved through interaction with each active sites, if multiple are present [133]. This mode of action can lead to a substoichiometric effect, as one inhibitor has the potential to induce the degradation of several proteins. Paclitaxel, a widely recognized chemotherapeutic drug, perfectly illustrates this concept: it binds to β-tubulin, allosterically preventing its assembly at a low nanomolar concentration in a 1 inhibitor per 1,000 molecules of β-tubulin manner [134]. In the context of LDH inhibition, attaining a substoichiometric effect could serve as a strategy to address the challenge posed by the high cellular concentration (1-10 μM) of the enzyme [109].

Protein-protein interfaces tend to be larger than traditional receptor-ligand interfaces. With a contact surface ranging from 1,500 to 3,000 $Å^2$ predominantly dominated by hydrophobic interactions [129], it poses a challenge for inhibitors to cover this wide interaction area. This raises

concerns about unfavorable pharmacokinetics, including issues related to poor solubility and large molecular weights. A pivotal step in the process of developing inhibitors is the identification of "hotspots", *i.e.*, critical regions within a given protein-protein interface that play a key role in interaction stability. Presently, diverse strategies are deployed in the quest for identifying hits and leads against PPIs [128, 129].

Small molecules that function as protein inhibitors emerge as invaluable tools in modern drug discovery and therapeutic development. Their appeal lies in their straightforward development and suitability for oral administration, a crucial attribute [135]. This is particularly significant in the domain of PPIs, where binding sites are often challenging to access and are often characterized by limited spatial dimensions. Small molecules have surmounted this challenge by targeting the critical hotspots situated within the inner regions of protein-protein interfaces, thereby achieving inhibition of the protein itself [129]. However, peptides are also emerging as effective strategies for disrupting PPIs. Progress in identifying hotspots has enabled the design of sequences involved in interactions, rendering them highly specific binders [136].

While peptides face challenges in transitioning into drugs, the solutions described in the preceding paragraph could potentially overcome these hurdles. A striking illustration of the PPI inhibition strategy using two types of inhibitors can be found in the disruption of the MDM2/p53 complex, a complex frequently dysregulated in cancer, supporting abnormal cell proliferation [137]. Detailed examination using X-ray crystallography revealed critical residues that underpin the interactions between the α-helix of p53 and the deep hydrophobic pocket of MDM2 [137]. Roche [138]

optimized a pre-existing imidazole compound that showed inhibitory potency against MDM2/p53 by designing the small molecule RG7112 (IC_{50} = 18 nM), the first MDM2/p53 inhibitor to enter in clinical trials for advanced solid tumors [138]. Meanwhile, Chang *et al.* [139] successfully disrupted the interaction with peptides mimicking the α-helix residues of p53, reaching an IC_{50} of 0.9 nM with ATSP-7041 [139].

The forthcoming section presents an array of small molecules and peptides tailored to inhibit LDHs, focusing on the tetrameric site as their prime target. It includes earlier efforts by our team, where fundamental studies were conducted to identify and characterize oligomeric sites.

In 2019, Jafary F. *et al* [38] used computational methods to better characterize LDH-5 subunit interactions and to design peptides capable of disrupting the assembly process of tetramerization. Molecular dynamics simulations (MDS) were conducted to unveil the structural dynamics and interactions of different structural constructs (monomer, dimer, and tetramer) [38]. According to *in silico* data, subunits A-C and B-D (**Figure 10**) interact *via* *C*-terminal residues. Nevertheless, the critical interactions for the constitution of the tetramer depend on residues located at the *N*-terminal arm (residues 5-17) contacting 293, 297, 299 and 300-305 in the *C*-terminus of other subunits. As a strong confirmation of these analyses, removing the *N*-terminal arms of A-D dimers resulted in a more fluctuating structure compared to the native one, according to root mean square deviation (RMSD) and radius of gyration (R_{gyr}). Authors' conclusion is that this domain has a fundamental role in anchoring the dimers to maintain the correct tetrameric active form of LDH-5. Based on these results, a peptide library was designed to interact with this specific region. *In silico* studies confirmed QLIYNL (**12**),

LIYNLL (**13**) and IYNLLK (**14**) (**Table 2**) interacting with an appropriate binding position. Specifically, QLIYNL interacts with hydrophobic residues Ile-293, Ile-299, Leu-302, Val-303, and its side chain forms hydrogen bonds with Ser-300, Leu-302 and Lys-304. LIYNLL showed similar interactions with Ile-293, Ile-299, Leu-302 and Val-303, and same hydrogen bonds were achieved with the previous descripted residues (**Figure 11c**). IYNLLK has the same interaction pattern as the other peptides. A dynamic light scattering technique was used to validate their competency for disrupting the tetramer by competing with the *N*-terminal arm. Aggregation and solubility issues stopped further analyses but opened the door for further optimizations.

Following this work, Thabault *et al*. [30] from our team used a protein-protein disruption strategy to reveal a potential novel site for allosteric interaction with LDHs, which had the potential to disrupt LDH tetramers [30]. This study unraveled the epitope of the *N*-terminal domain, comprising 19 amino acids fundamental for dimer-dimer interactions (Site 1), as previously evidenced by F. Jafary *et al*. [38]. The first 8 amino acids corresponding to the α-helix of the arm proved to be the minimal interacting sequence with the other monomers. A single alanine substitution on this *N*-terminal sequence validated the hotspots of interactions. Investigations into the epitope and the hotspots led to the design and characterization of a peptide library derived from the highlighted *N*-terminal arm domain sequence. This discovery necessitated the development of a tool that could allow the evaluation of inhibitors against Site 1, leading to the design and production of a *N*-terminus-truncated version of LDH-H (LDH-Htr, **Figure 10**, see material and methods). This model was validated *via* enzymatic activity assays, showing a weaker activity compared to the tetrameric folded form (**Figure 11**). Size-

exclusion chromatography (SEC) confirmed the truncated protein to be in a native dimeric state with an experimental molecular weight (MW) of 73 kDa compared to full length LDH-H (LDH-Hfl) (MW = 155 kDa). All other analyses related to the validation of LDH-Htr are summarized in **Figure 11**. Designed peptide inhibitors included LB19, LB13 and LB8 (*not shown*) mimicking the first 19, 13 and 8 amino acids of the *N*-terminal arm and having interactions with LDH-Htr (K_D of 1.02 mM, 1.05 mM and 1.49 mM, respectively). LB8, the smallest designed peptide mimicking the last 8 amino acids of the *N*-terminal sequence, matched exactly the α-helix conformation of the arm. The mM K_D value of its binding affinity prompted for introducing a stapled structure to constrain linear LB8 in a more native α-helix. Among stapled peptides, macrocycle 7 (**15**) (**Table 2**, **Figure 12d**) stood out as the most potent one, confirmed by various biophysical assessments. Its binding affinity for LDH-1 and LDH-5 was measured *via* microscale thermophoresis (MST), with K_D values of 380 µM (CI95% of 315-457 µM) and 117 µM (CI95% of 94-144 µM), respectively. Different biophysical methods were used to demonstrate that this macrocycle competes with the *N*-terminal tetramerization domain of LDHs, ultimately inducing their destabilization and disruption of their tetrameric active forms. Identification of Site 1 and characterization of macrocycle 7 unveiled a pioneering strategy for targeting an allosteric site within the LDH family. This advancement holds significant promise for the development of novel compounds that could inhibit LDH activity by disrupting enzyme tetramerization states, providing valuable tools for further research in this field.

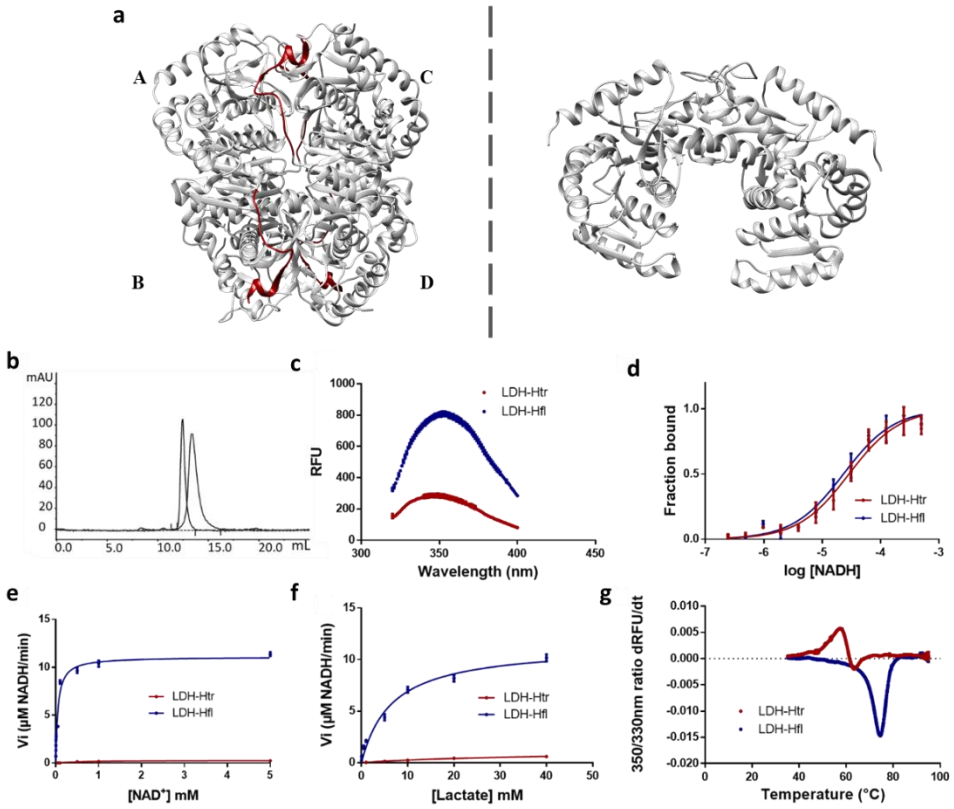

Figure 11. LDH-H truncated of its 19 *N*-terminal amino acids forms catalytically inactive dimers compared to full length LDH-H that forms catalytically active tetramers. (**a-g**) Comparison of full length (LDH-Hfl; blue) and truncated (LDH-Htr; red) LDH-H. (**a**) Crystallographic structures of LDH-1 (left) and LDH-Htr (right), A-D corresponding to the different monomers. The *N*-terminal arm is shown in red. Pictures were obtained using chimera software. (**b**) Overlay of size exclusion chromatograms of LDH-Htr (Rv = 12.45 mL, Experimental MW = 78 kDa) and LDH-Hfl (Rv = 13.35 mL, Experimental MW = 130 kDa). (**c**) Tryptophan fluorescence spectra of LDH-Htr (2.5 µM) and LDH-Hfl (2.5 µM). λ_{exc} = 286 nm (*n*

= 6). (**d**) Evaluation of the K_D for NADH using microscale thermophoresis at a 10 s "on time" (n = 3). (**e-f**) Kinetic evaluation of LDH-Htr (7.7 nM) and LDH-Hfl (13.5 nM) at various lactate (d) and NAD^+ (f) concentrations (n = 6). (**g**) Nano different scanning fluorimetry (NanoDSF) showing a melting temperature of 58°C for LDH-Htr (15 µM) and of 75°C for LDH-Hfl (15 µM) (n = 6). All data are from [30].

In a more recent investigation by our group, a second site involved in the LDH tetramerization process was identified using the Molecular Operating Environment software (MOE; Chemical Computing Group) [39]. This region seems to correlate with the binding site of the previously cited allosteric small-molecule inhibitors compounds 3 and 7 [125]. In agreement with this hypothesis, LDH-Htr underwent validation through MST, revealing its capability to self-interact at elevated concentrations. This observation suggested that dimer-dimer interactions involve a second site different from Site 1, the latter being absent in LDH-Htr. Mass photometry (MP), a technique for quantifying mass in solution using light scattering, confirmed an equilibrium between tetramer and dimer populations, which revealed that truncating the *N*-terminal arm does not totally hinder tetramer formation. In alignment with our work on Site 1, we aimed identifying peptide ligands specific to Site 2. A study explored interactions involving Site 2 and derived peptides like LP-22 (**16**) (**Table 2**, **Figure 12d**), which emulates the sequence of 22 amino acids within the α-helix conformation characterizing Site 2. Optimization of the minimal interacting sequence of LP-22 carried out *via* Water Logsy experiments led to the synthesis of GP-16 (**17**) (**Table 2**), obtained by eliminating the six terminal *N*-terminal residues. Both LP-22 and GP-16 were evaluated *via* MST and NanoDSF to characterize their affinity for LDH-M (EC_{50} =47 µM [32–68 µM] and EC_{50} = 262 µM [142–383 µM],

respectively). Collectively, these studies provided pharmacological resources to guide the future development of compounds modulating the oligomeric state of LDHs.

In similar approach, in 2020 Nadal-Bufi F. *et al.* [49] designed β-hairpin peptides capable of inhibiting LDH-5 activity that disrupted oligomerization by mimicking the β sheet of the interaction domain identified by our group as Site 1 [30, 49]. Challenges similar to those encountered in the pursuit of achieving a native-like structure, as illustrated with macrocycle 7 were also significant during the investigation of this peptide library. To reproduce the native β-hairpin conformation proved to be crucial for binding. Accordingly, Nadal-Bufi *et al.* selected Gomesine (Gm), an antimicrobial peptide possessing a β-hairpin structure and the capacity of penetrating cell membranes. Their rational design and computer-based strategies led to the discovery of peptides that successfully inhibited LDH-5 activity. Although the exact binding locations of these peptides were not reported, experiments using tryptophan fluorescence assays and SDS-PAGE confirmed their capability to disrupt tetramer formation. Among these peptides, cGmC9 (**18**) (**Table 2**, **Figure 12c**) turned out to be the most promising one (IC_{50} = 2.5 ± 0.3 μM). It underwent several competition assays against GNE-140, a small molecule competitive inhibitor of LDH-5, confirming inhibition. LDH-5 inhibition by cGmC9 was unaffected by changes in pyruvate concentration, suggesting a mechanism of action different from that of GNE-140 [49]. A follow-up work conducted by the same team optimized cGmC9 to reduce its cellular membrane toxicity [117]. The criteria behind the design were aiming to avoid cell membrane destabilization and were based on reducing the number of positively charged and/or hydrophobic residues to improve cell

penetration and increase peptide half-life. Among optimized peptides, [R/r]cGmC9 (**19**) (**Table 2, Figure12c**) showed a good inhibitory activity against LDH-5 (IC_{50} = 2.8 µM), similar to the precursor cGmC9 (IC_{50} = 2.5 µM); conversely the lower propensity of forming intramolecular hydrogen bonds in solutions makes it less rigid compared to the original analogue, displaying 50-fold lower membrane destabilization. Toxicity was measured using a resazurin assay [120] measuring metabolic activity *via* fluorescence intensity, reflecting cell viability. [R/r]cGmC9 did not show acute toxicity against healthy cells (IC_{50} > 64 µM) compared to the previous peptide library. Moreover, a study conducted to investigate its antiproliferative activity showed an important increase when cancer cells were treated under hypoxic compared to normoxic conditions. Validation revealed that [R/r]cGmC9 triggered reactive oxygen species (ROS) production, suggesting a potential link to the reduction of glycolysis expected from LDH-5 inhibition. Proteomic analyses provided further support for these findings, showing altered protein profiles in MDA-MB-231 cells treated with both GNE-140 and [R/r]cGmC9, indicating common changes in overall protein expression [120]. Specifically, proteins involved in glucose uptake and enzymes involved mitochondrial metabolic pathways were markedly upregulated after [R/r]cGmC9 treatment, aligning with the shift from glycolysis to OXPHOS and enhanced ROS production.

In summary, the array of LDHs inhibitors, with a notable emphasis on disrupting homomeric interactions, presents a promising approach to address the challenges in developing potent LDH inhibitors with potential implications in cancer and metabolic therapeutics.

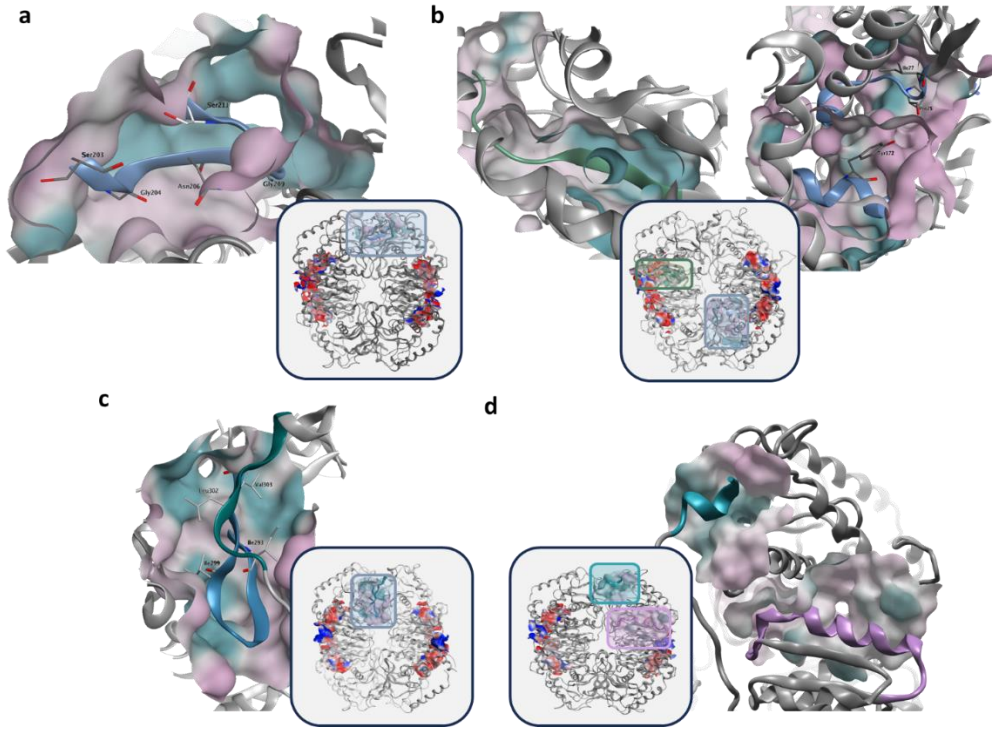

Figure 12. Allosteric and homomeric disruptor binding sites of LDH-1 and LDH-5: Mapping beyond the active site. Views of (**a-b**) LDH-1 (PDB ID: 1T2F) and LDH-5 (PDB ID: 1I10) allosteric inhibitors and (**c-d**) LDH-1 and LDH-5 homomeric disruptors. Pink and green surfaces for the binding sites represent polar and lipophilic regions, respectively. Red and blue surfaces for the active site represent polar and lipophilic regions, respectively. (**a**) Small molecule AXKO-0046 site of interaction (upper left, blue) with LDH-1 (bottom right). The main interacting residues are reported in the figure (Gly-204, Asn-206, Gly-209, Ser-211 and Ser-203). (**b**) Peptide FLCN-10 (top left) corresponds to the 91-99 amino-acid sequence of the *N*-terminal LDH-5 (central) catalytic loop. Compound 3 and Compound 7 binding sites (top right). Crucial residues for the interactions are shown (Tyr-172, Ile-77 and Pro-75). (**c**) Same binding site shared by peptides cGmC9, [R/r]cGmC9,

QLIYNL, LIYNLL and IYNLLK (top left) with tetrameric region of LDH-5 (bottom right). Residue interactions (green) among the three last peptides and the β-sheet (blue) are shown in the pocket (Ile-293, Ile-299, Leu-302 and Val-303). (**d**) Macrocycle 7 (blue), LP-22 and GP-16 (violet) interact at these two tetramer formation regions. Figure was generated using the MOE software.

3. Methods for targeting protein self-assembly

Developing PPI inhibitors requires the use of specific experimental tools to monitor protein self-association. In this chapter, we will describe classical and less classical techniques used for the identification and development of inhibitors targeting protein oligomeric interfaces. This discussion will focus on biophysical and biochemical techniques.

3.1 Applied techniques targeting protein self-assembly

3.1.1 Nano differential scanning fluorimetry

Differential scanning fluorimetry (DSF) is a powerful tool for drug screening [5, 127]. The technique measures the intrinsic fluorescence of a protein, particularly from tryptophan and tyrosine residues, as the protein is heated. When the protein unfolds, these residues become exposed to the solvent, resulting in a change in fluorescence intensity (**Figure 13**). This change is used to determine the melting temperature of the protein, which is a measure of its thermal stability. Nano-DSF is a modification of traditional DSF that allows for more sensitive and accurate measurements. It uses a nano-scale differential scanning fluorimeter that enables measurements on much smaller sample volumes (nanoliters), further allowing for the use of lower protein concentrations, typically in the nanomolar range. Nano-DSF is particularly

useful for studying protein-ligand interactions, as it allows for the detection of ligand-induced changes in protein stability by monitoring thermal stability of a protein in the presence of different ligand concentrations.

Homomeric disruptors often reduce the thermal stability of the target protein upon ligand titration, while ligand-induced multimerization can increase protein thermal stability [140, 141]. However, it is important to note that if observing a shift in the thermal denaturation profile confirms binding, it does not conclusively indicate stabilization or destabilization. Determining whether a binder stabilizes or destabilizes a protein requires further investigation.

3.1.2 Microscale thermophoresis

MST detects changes in the thermophoretic mobility of a fluorescently labeled protein upon ligand binding in solution [142] (**Figure 13**). It is important to note that MST is not limited to homomeric protein-protein interactions; it can also be used to study heteromeric interactions, as well as interactions with small molecules or peptides. Practically, the protein of interest is placed in capillaries and subjected to a temperature gradient created by an infrared (IR) Laser at a selected spot, which lead to a temperature increase. The fluorescently labeled protein moves from hot to colder regions, resulting in a time-dependent decrease in fluorescence. Upon ligand binding, the thermophoretic mobility of the protein can either increase or decrease, depending on the specific interaction. This change in mobility leads to concentration-dependent changes in its thermophoretic pattern. This change is converted in response units and fitted to a non-linear regression model to extract a dissociation constant, if any, which refers to the affinity of the ligand-protein binding interaction, not the dissociation of PPI. The observed

change of fluorescence is based on two distinct effects. On one hand, it is based on a temperature-related intensity change of the fluorescent probe, which can be affected by binding events. On the other hand, it is based on thermophoresis, the directed movement of particles in a microscopic temperature gradient. Any changes of the chemical microenvironment of the fluorescent probe and/or in the hydration shell of biomolecules result in a relative change of the fluorescence detected when a temperature gradient is applied and can be used to determine binding affinities. By measuring the extent of these changes across different ligand concentrations, MST can be used to determine binding affinities. MST allows measurement of interactions directly in solution without the need for protein immobilization on a surface. Of note, it is crucial for MST that the fluorescent labeling of the protein of interest maintains correct folding and high homogeneity. Of further note, MST has a significant limitation: it does not provide the means to measure the association rate constant (k_{on}) and the dissociation rate constant (k_{off}). This limitation arises because MST captures equilibrium states rather than the real-time kinetics of the binding process. MST indeed operates by detecting changes in the movement of fluorescently labeled molecules in response to a temperature gradient, which allows for the determination of K_D through analysis of the binding curve at equilibrium, but it does not track how quickly molecules associate or dissociate over time.

Fluorescent labeling of a protein while maintaining correct folding and high homogeneity is crucial. In this work, we evaluated a covalent labeling of LDH-Htr using Red fluorophores (Nanotemper) possessing a covalently linked reactive moiety allowing for a specific labeling of different functional groups of proteins. We tested the specificity of the labeling of cysteine

residues, lysine residues, and histidine tags. Cysteine labeling using the Red dye-MAL resulted in MST experiment, in a misfolded protein that did not bind to NADH, which revealed that cysteine thiol labeling likely disturbed the protein tertiary structure. Labeling of the *N*-terminal His-tag with Red tris-NTA resulted in a fluorescent protein able to interact with NADH. However, this labeling required a low protein concentration and was associated with protein instability, verifying its profile *via* NanoDSF. Labeling lysine residues using the Red NHS dye yielded a fluorescent LDH-Htr capable of interacting with NADH. Importantly, this labeling was performed at micromolar concentrations, and the covalently labeled protein was stable enough to be stored at -80°C. Consequently, we chose this labeling method for further MST experiments. For comparison, tetrameric LDH-1 and LDH-5 were also labeled using the Red-NHS fluorescent dye using standard procedures.

3.1.3 NMR STD

Saturation transfer difference (STD) nuclear magnetic resonance (NMR) is a technique used to study protein-ligand interactions in solution, providing valuable information about binding epitopes and affinity [5, 143, 144]. The experiment relies on a selective saturation of protein protons excitation achieved by an irradiation at the specific frequency of a nucleus of interest (**Figure 13**), which is then transferred to bound ligands through the nuclear Overhauser effect (NOE), resulting in a decrease in signal intensity in the 'on resonance' spectrum in case of binding. A control experiment must be performed, where the protein is not saturated, providing an 'off resonance' spectrum. The difference between the two spectra provides the final STD

spectrum. When a ligand bind to the protein of interest, the saturation is also transferred to the ligand, leading to a reduction in the intensity of ligand signals. Importantly, those ligand protons that are in closest contact with the macromolecule receive the most saturation. Therefore, their signals are reduced in intensity the most, allowing the binding epitope of the ligand to be mapped. Efficient spin diffusion and ligand accumulation in solution are necessary for observing differences between the reference and saturated spectra.

3.1.4 Mass photometry

Mass photometry (MP) is a label-free technique that enables high-resolution mass measurements of individual biomolecules in solution [145] (**Figure 13**). Applications are broad and diverse, including determining protein mass and stoichiometry, characterizing protein-ligand interactions, analyzing protein complexes and aggregates, and studying biomolecular conformational changes. In practice, biomolecules in a sample are passed over a glass surface. When illuminated with a beam of light, biomolecules induce changes in the intensity of both scattered and reflected light, which is influenced by their mass. The scattered light originates from the biomolecules themselves as they disrupt the path of the incident light. The reflected light, on the other hand, comes from the glass surface and the interface where the biomolecules are present. This reflected light is influenced by the presence and properties of the biomolecules on the surface. Larger molecules scatter more light compared to smaller ones. The changes in scattered light intensity are directly proportional to the mass of the biomolecule and are recorded in real-time. To calculate the mass of the proteins, standard reference compounds with known masses are used to create a calibration curve. MP offers several advantages.

Firstly, it is label-free, eliminating the need for fluorescent or radioactive labels. Secondly, it offers high sensitivity, being capable of detecting mass changes as small as a few kDa. Additionally, it provides single-molecule resolution, enabling the measurement of the mass of individual biomolecules.

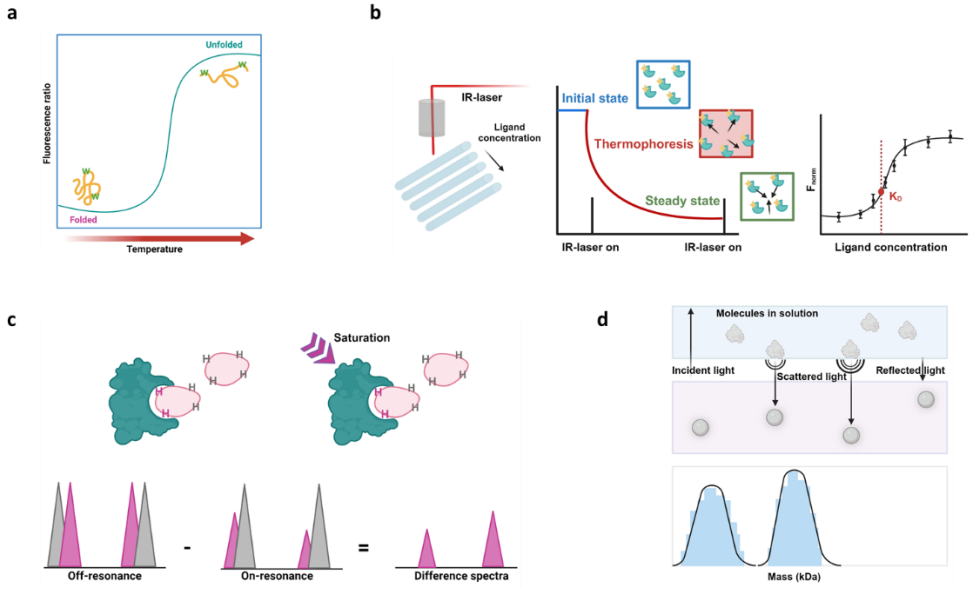

Figure 13. Biophysical techniques for analyzing molecular interactions. (**a**) Nano differential scanning fluorimetry (NanoDSF) measures the intrinsic fluorescence of proteins as a function of the temperature to determine their thermal stability. The graph illustrates a typical fluorescence ratio curve, showing the transition from a folded to an unfolded state. This transition can be impacted by the binding of a ligand altering protein stability. (**b**) Microscale thermophoresis (MST) measures binding affinities by tracking the movement of fluorescently labeled proteins placed in capillaries and subjected to a temperature gradient created by an infrared (IR) Laser. Initially, the proteins are uniformly distributed (initial state). Upon IR laser activation, they move due to thermophoresis (thermophoresis phase). This is followed by a steady state where the movement stabilizes. To test a potential binding, these measurements are made in the presence inf increasing concentrations of the tested compound. The resulting curve, plots the normalized fluorescence (F_{norm}) against ligand concentration. The K_D is determined at the inflection point, where the curve changes its slope most significantly. This point is highlighted with

a red marker. A vertical dashed line indicates the exact position of the K_D on the ligand concentration axis. (**c**) NMR-STD identifies binding interactions between ligands and proteins. It involves a saturation of the resonance of the protons of a protein using a specific radiofrequency pulse. The saturation is then transferred to the bound ligand. The difference spectrum, obtained by subtracting the off-resonance spectrum from the on-resonance spectrum, indicates the ligand regions in contact with the protein. (**d**) Mass photometry measures and quantifies single molecules in solution by analyzing the interference pattern of scattered and reflected light. The process includes providing an incident light hitting the sample, measuring the scattered and reflected light, and a subsequent analysis of the interference pattern. To convert the scattered light intensity to protein mass, standard reference compounds with known masses are used to create a calibration curve. The resulting mass distribution graph shows the molecular masses of the particles in solution. Figure adapted from [146-148].

3.1.5 SEC-MALS

SEC-MALS combines size exclusion chromatography with multi-angle light scattering detection [149]. This technique provides absolute molecular weight determination and oligomeric state analysis of proteins in solution. Size exclusion chromatography (SEC), also known as gel filtration chromatography, follows the migration of macromolecules through a column whose stationary phase is composed of inert polymeric porous beds. This method allows the measurement of the size of macromolecules and constitutes a direct probe to determine the oligomeric states of proteins in solutions. Multi-Angle Light Scattering (MALS) is a powerful method for determining the absolute molecular weight of macromolecules in solution (**Figure 14**). In SEC-MALS, as proteins elute from the SEC column, they pass through a flow cell where they are subjected to a beam of light at multiple angles. The scattering of light by the protein solution is measured, and the intensity of the scattered light at each angle is used to calculate the molecular

weight of the eluting protein. The intensity of the scattered light is directly proportional to the molecular weight of the protein, allowing for accurate determination of molecular weight. Unlike UV detection in traditional SEC, which provides only relative molecular weight information, SEC-MALS provides absolute molecular weight data, independent of protein concentration or elution volume.

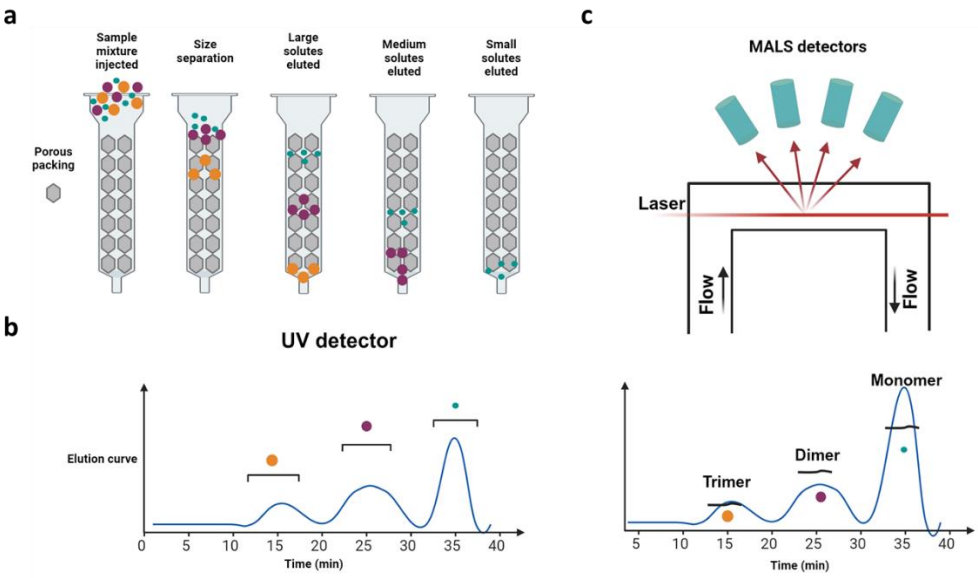

Figure 14. SEC-MALS setup and experiments. (**a**) Size exclusion chromatography with multi-angle light scattering (SEC-MALS) measurements begin with a sample mixture being injected into a column packed with porous material. As the sample flows through the column, solutes are separated based on their size. (**b**) As solutes elute from the column, they pass through a UV detector. The detector measures the absorbance of the eluting solutes, generating an elution curve that corresponds to the size and concentration of the solutes. The peaks in the elution curve represent different solute sizes. (**c**) Solutes pass through a MALS detector. A Laser beam is directed through the flow of eluted solutes, and light scattering is measured at multiple angles. The MALS detector produces an elution curve similar to the UV detector. Peaks in the curve correspond to different species such as monomers, dimers, and trimers.

3.1.6 Cellular engagement assay

Cellular engagement assay is a label-free method used to study drug-target engagement and protein-ligand interactions in complex biological systems, such as cells [150] (**Figure 15**). The technique relies on the principle that ligand binding stabilizes target proteins against thermal denaturation. In this assay, cells are subjected to a range of temperatures, causing proteins to denature and aggregate. However, when a ligand binds to its target protein, it stabilizes the protein, shifting its thermal denaturation curve to higher temperatures. After heat treatment, cells are lysed, and the soluble fraction is analyzed by immunoblotting or MS to quantify the remaining native protein. By comparing the levels of native protein in the presence and absence of a ligand, cellular target engagement can determine whether the ligand binds to the target protein in a cellular context. One of the key advantages of a cellular engagement assay is its ability to assess protein-ligand interactions in a physiologically relevant environment, providing insights into drug-target engagement under conditions that include the cellular milieu.

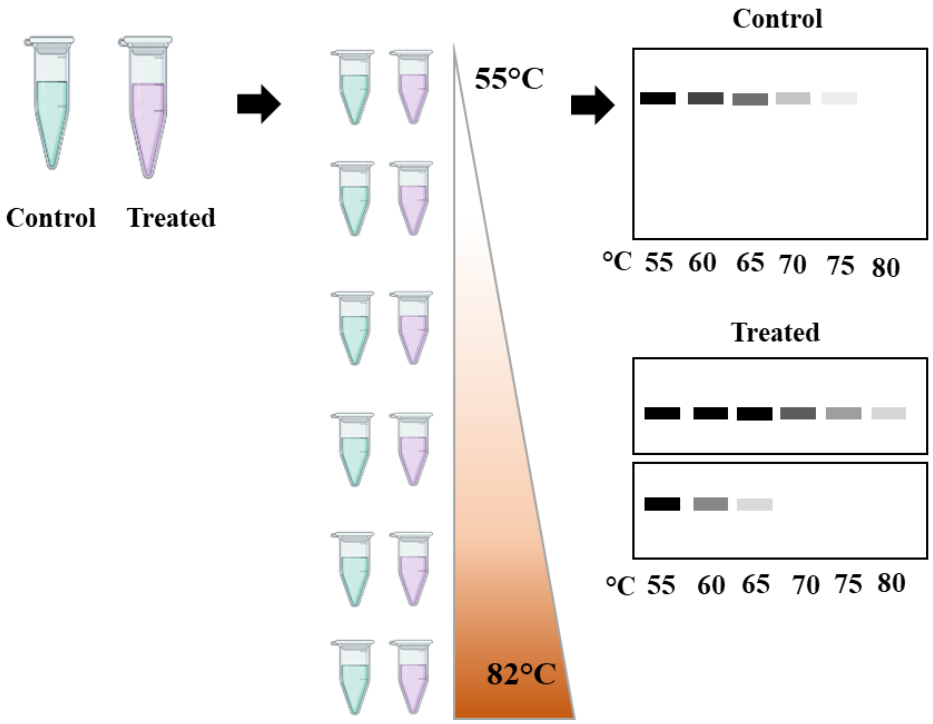

Figure 15. Cellular engagement assay overview. Protein samples (control and treated) are divided into multiple aliquots and subjected to different temperature treatments to induce thermal denaturation. After centrifugation, the soluble fractions from each temperature condition are analyzed by western blotting. The presence of a small molecule can cause a shift in the thermal stability of the target protein compared to when the small molecule is absent. This shift indicates binding between the small molecule and the target protein.

3.1.7 Isothermal titration calorimetry

Isothermal titration calorimetry (ITC) is a label-free technique that provides quantitative information about the binding affinity between biomolecules, such as proteins and ligands, by directly monitoring the heat released or absorbed during a binding event [151]. The principle of ITC involves titrating a solution containing one binding partner (*e.g.*, a protein) into a solution containing the other binding partner (*e.g.*, a ligand) while maintaining a

constant temperature. The ICT device thus comprises two thermally isolated cells containing the same buffer solution, with one cell holding the titrant/protein and the other the titrand/ligand in a more dilute solution. When small amounts of the titrant are injected into the titrand, heat is either absorbed or released depending on the nature of the binding interaction. The heat change is directly proportional to the amount of binding that occurs during each injection. A calorimeter measures these heat changes throughout the titration, and the data are then analyzed to determine the binding affinity, stoichiometry, and thermodynamic parameters of the interaction. Despite the advantages of ICT, the sensitivity of most calorimeters for monitoring protein association typically limits the technique to proteins with a dissociation constant in the μM range. Lower concentrations generate heat pulses that are more challenging to detect. However, ITC has proven to be useful for studying self-association, either for directly measuring the binding affinity between a disruptor and a protein interface or for monitoring homomeric association upon the addition of a protein disruptor.

3.1.8 Native polyacrylamide gel electrophoresis

Polyacrylamide gel electrophoresis (PAGE) is a widely used biochemical technique for assessing ligand-induced changes in protein oligomerization. PAGE can be conducted under native or denaturing conditions, with the latter often involving cross-linking. In native PAGE, protein complexes are separated in a polyacrylamide gel based on their electrophoretic mobility tha depends on their size, shape, and charge, with smaller proteins traveling more quickly than larger ones [152]. The process begins with the preparation of a polyacrylamide gel matrix, typically composed of a gradient of acrylamide concentrations to accommodate proteins of varying sizes. Protein samples,

prepared in native conditions without denaturing agents, are loaded into wells within the gel. Upon application of an electric field, proteins migrate through the gel matrix based on their size and charge. Following electrophoresis, proteins are visualized using staining methods such as Coomassie Brilliant Blue or silver staining. Alternatively, proteins can be transferred onto a membrane for immunodetection. Analysis of the resulting gel image allows for a quantification of protein bands, determination of molecular weights and assessment of changes in protein complex formation or composition. Native PAGE is versatile and can be applied across a broad range of concentrations, making it valuable for semi-quantitative studies of ligand-induced disruption of protein self-association [153].

3.1.9 Enzyme-linked immunosorbent assay (ELISA)

ELISA is a widely used technique for detecting and quantifying immunologic reactions. In this assay, one reaction component is bound to a solid phase, facilitating the separation of bound and free-labeled reactants. ELISA can quantify antigens or antibodies in a sample, depending on which component is bound to the solid phase. Traditionally used for antibody-antigen detection, ELISA has been adapted to investigate disruptors of protein oligomerization [154]. In this adapted approach, specific subunits of the protein complex are selectively labeled. The assay relies on detecting signal loss post-wash following disruptor addition, as disruption of a protein complex leads to a reduction in signal intensity. ELISA can detect either the absence of a particular subunit or of the complete protein complex. This method has proven to be effective in quantifying ligand-induced disruptions of protein complexes across various targets [154, 155]. However, it is critical to ensure

the stability of the protein complex under investigation to prevent significant subunit loss during control experiment wash steps.

3.1.10 Intrinsic fluorescence assays

Intrinsic tryptophan fluorescence (ITF) is a highly effective method for investigating protein oligomeric states [127, 156]. Tryptophan residues, due to their scarcity and the indole fluorophore high sensitivity to its surroundings, serve as valuable probes for monitoring protein oligomerization. Tryptophan residues are typically buried within the hydrophobic interfaces of homomeric complexes. Consequently, alterations in the quaternary state of a protein often result in significant changes of fluorescence intensity. This is because the tryptophan quantum yield decreases when tryptophan is exposed to a polar environment, such as when it is surrounded by water molecules. ITF is particularly useful for studying protein-protein and protein-small molecule interactions, providing valuable insights into binding affinity. Various proteins exhibit significant changes in their intrinsic fluorescence spectrum depending on their oligomerization state. ITF can therefore be effectively used to directly study interactions at oligomeric interfaces containing tryptophan residues or to monitor changes in the oligomeric state induced by inhibitors.

4. General context, preliminary work and objective

4.1 General context

Alterations of metabolic pathways are one of the strategies adopted by cancer cells to sustain anabolic growth and proliferation [157]. Such alterations were reported to affect lactate metabolism, allowing cancer cells to satisfy their bioenergetic needs and to survive in hostile environments. Lactate is playing an important role in processes such as invasiveness [3], angiogenesis [67] and autophagy [3], and is also involved in metabolic cooperativity among hypoxic and glycolytic cancer cells inside the tumor microenvironment [51].

In vitro and *in vivo* experiments demonstrated the active role of LDH-5 in promoting the migration and invasiveness of hepatocellular carcinoma (HCC) and RCC cells [91, 158]. Its overexpression in a large range of malignant cancer types makes it a metabolic predictor for unfavorable prognosis [159-161]. Comparatively *LDH-1* has been identified as a crucial gene for triple-negative breast cancer cell proliferation [94, 162] and a key contributor to lysosomal activity and autophagy in both oxidative and glycolytic cancer cells [3]. These studies, combined with the evidence of no noteworthy pathological clinical symptoms in individuals with LDH-1 or LDH-5 deficiency [1, 96, 163], make them appealing targets for anticancer therapy.

Quinoline 3-sulfonamides showed low micromolar potency against LDHs [109] (4, **Table 1**). However, crystallography established that binding occurs at the cofactor binding site. The highly polar characteristics and the

conservation of sequence and structure of the LDH catalytic site with other NAD^+/NADH-dependent enzymes make the production of selective inhibitors challenging [1, 107]. Recent studies brought interest on a novel class of pyrazol-based small molecules [111], with compound **63** (6, **Table 1**) having robust *in vitro* and *in cellulo* potency against LDHs. Nevertheless, the highly polar characteristic of the LDH active site brings, also for this class of inhibitors, the necessity of improvements of the ADME profile required for *in vivo* efficacy studies [109]. In this context, finding novel strategies to target LDHs were warranted.

Binders of allosteric sites of LDHs have been synthetized and evaluated [49, 120, 125, 126]. In 2020, A. Friberg *et al.* reported a phthalimide (10, **Table 2** and **Figure 10a**) and a dibenzofuran (11, **Table 2** and **Figure 10b**) derivative as inhibitors of LDH-5, with IC_{50} of 308 nM and 757 nM, respectively. Unfortunately, these compounds are not (yet) showing significant potency in more complex systems. Our laboratory and others have therefore decided to investigate a novel and innovative way to develop LDH inhibitors based on the disruption of protein oligomers. As many proteins express their biological activity in active complexes [164-166], targeting PPIs has become an attractive strategy for the development of novel drugs [127, 167, 168]. LDHs are active only as tetramers formed by dimer-dimer assembly [38, 169]. Hence, our proposed strategy is to prevent and/or disrupt tetramer formation by acting at the dimer-dimer oligomeric interface.

4.2 Preliminary work

This work is based on previous data obtained from the work of Thabault L. *et al.* [30] in a study on targeting an allosteric site of LDHs with the use of stapled peptides. With the aim of revealing new binding site(s) at the

oligomeric interface, they started from the observation of the importance of LDH *N*-terminal arms, which roles are to maintain a proper conformation holding together the four monomers, promoting the tetramer cohesion [38]. Because functional LDH enzymes are obligatorily tetramers, *N*-terminal arms are fundamental for their activities. Accordingly, the *N*-terminal arm (or *N*-terminal domain) of LDH-H was the starting point for the design of stapled peptides interfering with the tetramerization process. This approach was made possible by the identification of a first allosteric site involved in the tetramerization process (site 1) [38]. A truncated LDH construct lacking 19 amino acids of this site (LDH-Htr) was produced, and this tool allowed the development of promising stapled peptides, such as macrocycle 7 (5, **Table 2**). Following this strategy, a follow up work led to the identification of a novel tetramerization site (site 2), opening the doors to the development of new inhibitors [39]. LP-22 and GP-16 (6 and 7, respectively, **Table 2**) were characterize as oligomeric LDH disruptors acting at site 2.

The identification of site 1, site 2 and the characterization of macrocycle 7 and linear peptides LP-22 and GP-16 unveiled a pioneering strategy for targeting allosteric sites at the oligomeric interface in the LDH family. This advancement holds significant promises for the development of novel compounds that could disrupt LDH activity by targeting its tetramerization, providing valuable tools for further research in this field.

4.3 Objectives

Based on the above findings, I aimed to explore an additional path to inhibit LDH tetramerization. To this end **the objective** of this thesis work is **to identify small molecules capable of targeting LDH tetramerization domains to disrupt their oligomeric assembly process, block their**

activities and develop a novel class of LDH inhibitors. Of note, our approach aligns with a pan-inhibitor strategy that would target all LDH isoenzymes, underscoring the importance of validating our inhibitors across both glycolytic and oxidative cancer cells.

To accomplish this goal, we designed a strategy starting with an innovative screening process (**Figure 16**). We started with *in silico* screening evaluation, assessing a library of small molecules with a high chemical diversity for their potential interaction with LDHs. Selected compounds underwent a designed biophysical screening cascade, aimed to characterize and evaluate their binding *via* different biophysical methods, providing essential insights into their binding characteristics, affinities and SARs. Compounds were tested using three available models, LDH-H, LDH-M and the non-native LDH-Htr, used to validate their interactions at the tetrameric interface. To gain a deeper understanding of selected compound activities, we performed enzymatic assays and *in cellulo* tests, translating the characterized bindings into more intricate models. This evaluation aimed to provide strong evidence that the identification of small molecules with promising affinities and activities could constitute a new framework for the development of new LDH inhibitors with a novel mechanism of action, capable to overcome the historically challenging nature of targeting these enzymes.

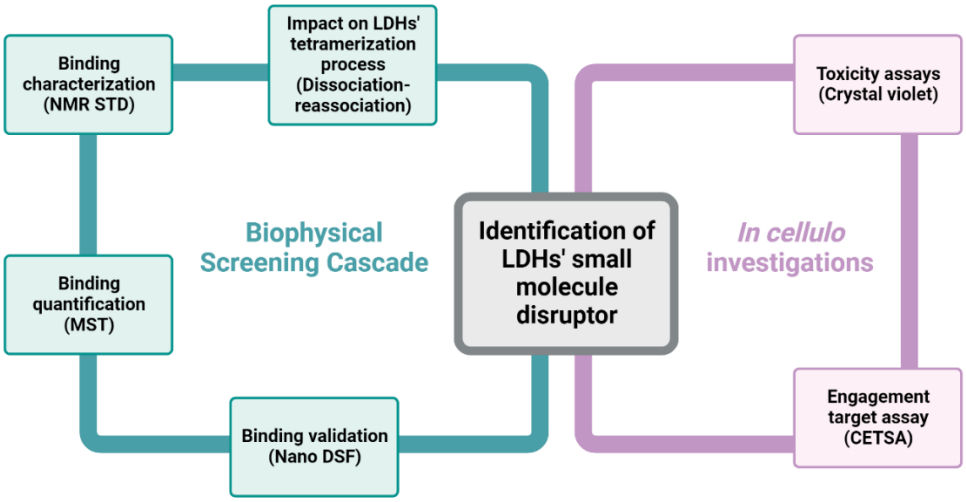

Figure 16. Key points of the discovery process. The schematic outlines the strategy to identify small molecule disruptors of LDHs. The left section (green) describes the biophysical processes that we used, starting with a binding validation of diverse small molecules, followed by biophysical characterization to assess binding properties and affinities. Compounds were tested on LDH-1, LDH-5, and non-native LDH-Htr models. The right section (pink) covers *in cellulo* investigation. The Figure was generated using Biorender.

The upcoming chapters will explore the detailed outcomes of the described objectives and strategies, utilizing the techniques outlined in Chapter 3. Some of the molecules identified through screening are FDA and EMA-approved drugs. Initially, these will be referred to as F2050 and F1787, and thereafter by their actual names, maprotiline (F2050) and triprolidine (F1787).

5. Results: Chapter 1

Discovery of Small Molecules Interacting at Lactate Dehydrogenases Tetrameric Interface Using A Biophysical Screening Cascade

This chapter is based on the following publication: Thabault L, Brustenga C, Savoyen P, Van Gysel M, Wouters J, Sonveaux P, Frederick R, Liberelle M. Discovery of small molecules interacting at lactate dehydrogenases tetrameric interface using a biophysical screening cascade. Eur. J. Med. Chem. 2022;230:114102.

Brustenga C and Thabault L shared the first position.

Graphical Abstract

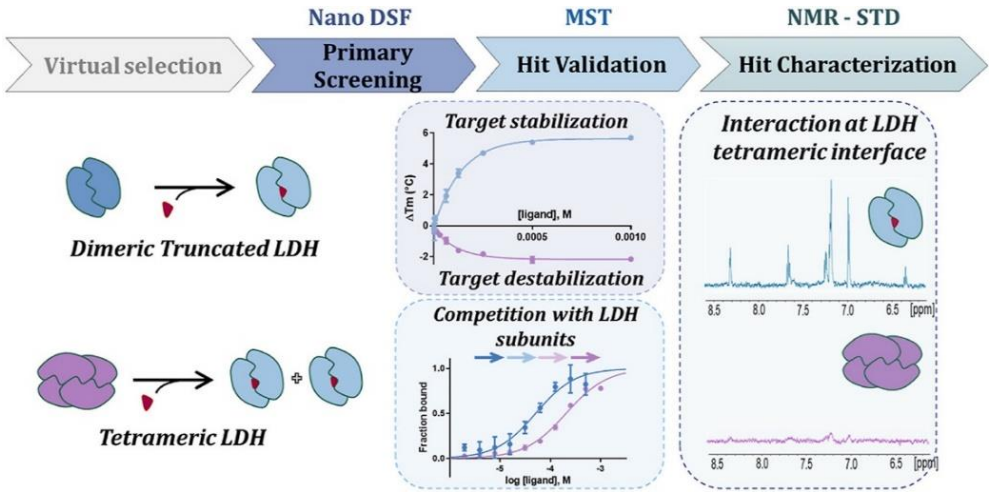

5.1 Introduction

In this chapter, we will describe the design and validation of a biophysical screening cascade to probe LDHs' oligomeric interface. The goal was to characterized a series of compounds as possible LDH' inhibitors with the innovative use of a variety of biophysical tools. We believed Nano differential scanning fluorimetry (Nano DSF) to be a promising technique to rely on as a primary screening step in order to probe proteins homomeric interfaces. Briefly, Nano DFS follows the denaturation profile of the protein of interest exposed under a temperature gradient, in the presence or absence of an inhibitor. Thermal stability is highly sensitive to protein oligomeric status, with a higher stability for the oligomeric order state conversely to the lower-ordered ones. In this context, ligands interacting at the oligomeric site will perturbate the order state, provoking a destabilization in terms of protein unfolding profile. Conversely the same ligand interacting with the solvent exposed area of the protein will lead to a stabilization of the low-order state. Following our belief, the tested compounds either had a destabilization, neutral or stabilization effect on our LDHs models.

What will be detailed in this chapter are all the methods that lead to the identifications of LDHs oligomeric state's binders.

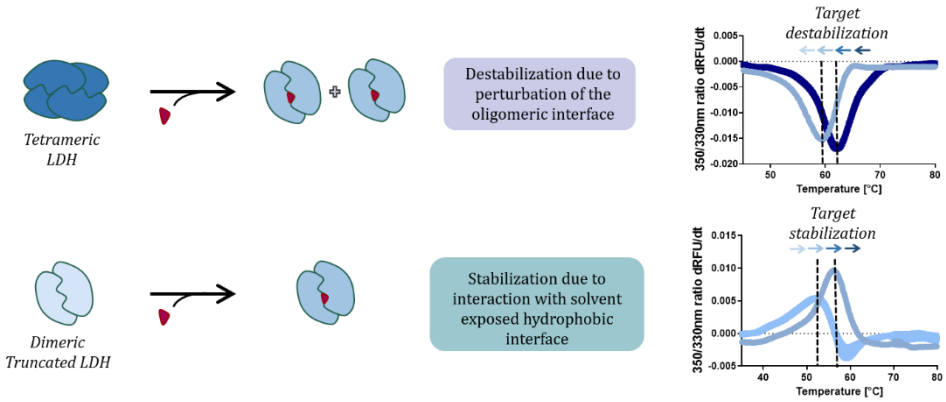

Figure 17: Compounds interacting at the LDH tetrameric interface destabilize tetrameric LDH while keeping a neutral or stabilizing effect on already dimeric LDH-Htr. The DSF profile displayed in the figure corresponds to compound F2050 that was identified in this study. This figure shows how compound F2050 impacts LDH tetramers and dimers. For tetrameric LDH, F2050 interacts at the oligomeric interface, destabilizing the tetramer and shifting the denaturation profile to lower temperatures. In contrast, for dimeric LDH-Htr, F2050 interacts with solvent-exposed hydrophobic areas, stabilizing the dimer and shifting the denaturation profile to higher temperatures. RFU: relative fluorescence unit.

5.2 Result and discussion

5.2.1 Primary screening using nanoDSF

A focused library was created from a Prestwick Drug-Fragment library using the Autodock Vina software for docking simulations [34]. In summary, we conducted three complementary docking studies on the apoLDH dimer (PDB ID: 1i0z, subunits B-D). The first study involved docking on the entire dimer without any area restrictions to explore the entire tetrameric interface. The other two studies focused on docking within the two tetramerization sites we had previously identified [18,19]. All docking results were analyzed together, and those with Vina scores higher than two-thirds of the initial library cutoff

and active-site binders were excluded. The final step involved a visual selection process, using docking results from the tetramerization sites to eliminate unreliable binders that did not show consistent binding poses across the different studies. Unique docking poses on alternative binding pockets at the interface were also considered. This virtual screening process yielded 29 virtual hits, which were then subjected to biophysical evaluation.

The first part of this biophysical screening relies on identifying compounds combining destabilizing properties on tetrameric LDH with a stabilizing or neutral effect on dimeric LDH-Htr. We set out to perform the primary screening assay using the nanoDSF technology, which monitors protein stability with low sample consumption. We evaluated a subset of 29 compounds preselected from a focused Prestwick library using nanoDSF against tetrameric LDH-1 (LDH-H4) and LDH-5 (LDH-M4) (**Figure 18**). As previously mentioned, we consider both LDH-1 and LDH-5 to be interchangeable for the probing of LDH tetrameric interface due to the high conservation of the dimer-dimer interface (Figure S1). However, the use of both LDH in this context adds an internal control to the screening to ensure that we select compounds with homogeneous profiles between both isozymes.

In parallel, we evaluated the same compounds for their stabilizing or neutral effect on dimeric LDH-Htr. This step also served as an internal control by eliminating either promiscuous binders that would stabilize unfolded fractions of the protein and chaotropic compounds that would be intrinsic destabilizers [170]. Of note, we performed this second step in parallel with the first screening on tetrameric LDHs for exemplification purpose. However,

to facilitate the screening procedure, this screening on dimeric LDH-Htr could be run only with "hits" compounds that can destabilize tetrameric LDH.

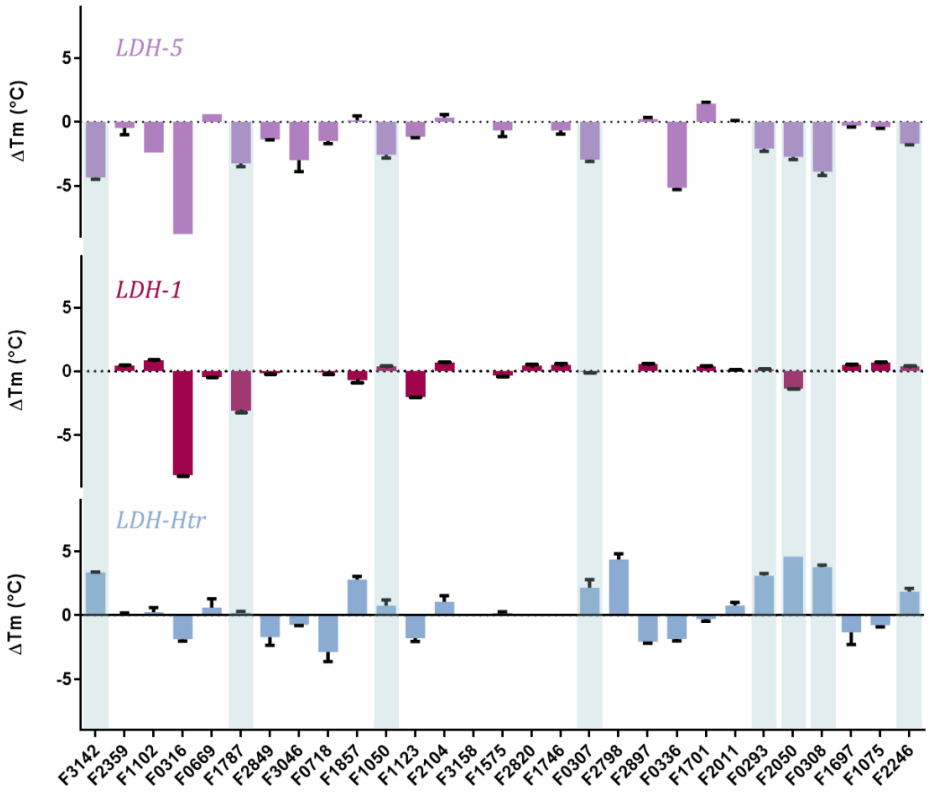

Figure 18. Primary screening using nanoDSF identifies 8 hits that can destabilize tetrameric LDHs and stabilize dimeric LDH-Htr. Top, thermal shifts of the different compounds screened at 1mM against tetrameric LDH-5 (25 µg/mL) (n = 3). Middle, thermal shifts of the different compounds screened at 1mM against tetrameric LDH-1 (25 µg/mL) (n = 3). Bottom, the thermal shift of the different compounds screened at 1mM against dimeric LDH-Htr (25 µg/mL) (n = 3). The blue vertical lines correspond to the hits that displayed a complementary profile and were selected for further investigation.

Following this primary screening on tetrameric LDHs, we identified 14 and 5 compounds that destabilized LDH-5 and LDH-1, respectively (**Figure 18**). As previously reported [30], the higher stability of LDH-1 compared to LDH-5 resulted in a lower sensibility to destabilization and, thus, to a lower hit rate. On the other hand, we identified 13 compounds displaying a stabilizing effect on dimeric LDH-Htr (**Figure 18**). By merging these results, we identified 8 compounds that combined a stabilizing or neutral effect on dimeric LDH-Htr with a destabilization of either tetrameric LDH-1, LDH-5 or both proteins. Among these 8 hits, we decided to discard 3 compounds from further evaluation due to their structure: Compound F0308 was excluded due to its estrogenic core, which can lead to unwanted hormonal interactions. Compounds F3142 and F0307 were excluded because their catechol moieties can be highly reactive, resulting in nonspecific binding. (Table S1) [171].

5.2.2 Hit validation

We next evaluated the ability of the five selected hits to interact with the LDH tetrameric interface using LDH-Htr. We monitored the interaction of each compound with LDH-Htr at 1 mM, using MST binding check experiments. The realization of this step was, in our case, optional due to the low number of hits. However, we set out to perform this first binding assessment to demonstrate our method scalability, as this step would become necessary for more extensive libraries. We evaluated the different hits at both 1.5 s and 20 s of MST on-time to account for ligands that would induce a change in the temperature-related intensity-change in fluorescence (TRIC) and the thermophoretic pattern of LDH-Htr. Interestingly, all five hits displayed an interaction at 1 mM with dimeric LDH-Htr (**Figure 19**).

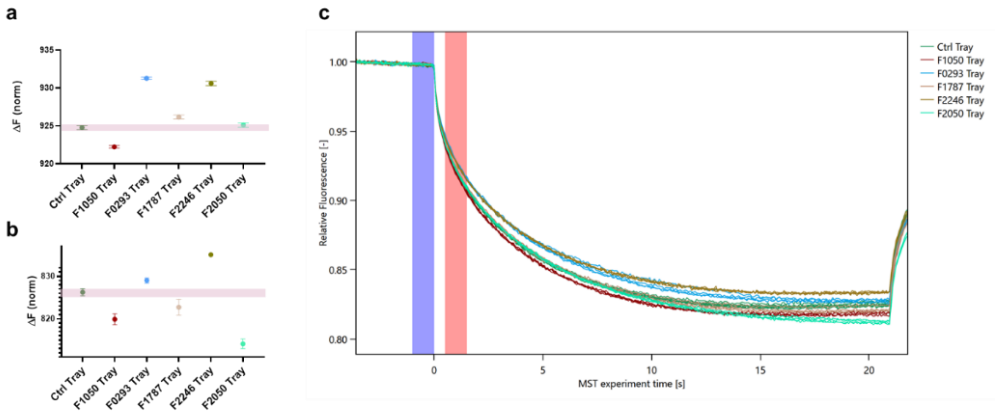

Figure 19. Binding check experiments using MST reveal that all five hits bind to LDH-Htr. a) Normalized variation in fluorescence (ΔF norm) at 1.5 s of MST time for the five identified hits compared to the control experiment (n = 4). b) Normalized variation in fluorescence (ΔF norm) at 20 s of MST time for the five identified hits compared to the control experiment (n = 4). c) MST traces of the different hits. The red and blue columns correspond to the MST on and off time used to extract the data to a).

Hits were then validated using saturation transfer difference NMR (STD) as an orthogonal biophysical technique. STD relies on the selective saturation of a target protein in solution. Upon binding, saturation is transferred from the protein to the ligand [172]. In accordance with MST, STD demonstrated a saturation transfer between dimeric LDH-Htr and the five different hits, thus validating these compounds for their interaction with dimeric LDH-Htr (Figures S2-S6).

To further characterize the five compounds, we measured their affinities for dimeric and tetrameric LDH. According to our model, compounds interacting at the LDH tetrameric interface should exhibit a weaker interaction with tetrameric LDH than with dimeric LDH-Htr. We expected

this weaker interaction to stem from a competition between the ligands and LDH native subunits for the LDH tetrameric interface. All 5 hits displayed a concentration-dependent interacting profile with dimeric LDH-Htr (**Table 3**). Strikingly, 3 hits exhibited a K_D in the µM range, with F1050 interacting in the high micromolar range (183 ± 56 µM) and F1787 and F2050 in the mid micromolar range (79 ± 37 µM and 37 ± 12 µM respectively). Compounds F0293 and F2246 interacted in the low millimolar range (Table 1, K_D's of 1.0 ± 0.5 mM and 0.9 ± 1.2 mM, respectively). All MST binding curves are displayed in Figures S7-S11.

Code	Structure	K_D (LDH-Htr)*	K_d (LDH-5)*	ΔTM dimeric LDH (°C)	ΔTM Tetrameric LDH-5 and LDH-1 (°C)	Binding (MST)	Binding (STD)**
1050	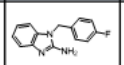	183 µM (+/- 56 µM)	324 µM (+/- 100 µM)	0.8 (+/- 0.9)	-2.6 (+/- 0.5) 0.4 (+/- 0.1)	Yes	Yes
0293	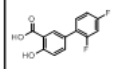	1.0 mM (+/- 0.5mM)	343 µM (+/- 100 µM)	3.1 (+/- 0.3)	-2.1 (+/- 0.3) 0.1 (+/- 0.1)	Yes	Yes
1787		79 µM (+/- 37 µM)	760 µM (+/- 357 µM)	0.2 (+/- 0.1)	-3.3 (+/- 0.4) -3.1 (+/- 0.2)	Yes	Yes
2050		37 µM (+/- 12 µM)	205 µM (+/- 40 µM)	4.6 (+/- 0.0)	-2.7 (+/- 0.4) -1.4 (+/- 0.1)	Yes	Yes
2246		0,9 mM (+/- 1.2 mM)	N.B	1.9 (+/- 0.5)	-1.7 (+/- 0.3) 0.4 (+/- 0.1)	Yes	Yes

Table 3. Characterization of the different hits identified
N.B: No binding up to 1 mM.
* MST profiles of the different hits are displayed in Figures S7-S11.
** STD spectra are displayed in Figures S2-S6.

Next, we evaluated these compounds against tetrameric LDHs to look for potential competitions with the native subunits for the tetrameric interface

that would result in weaker interactions. We assessed all 5 hits against tetrameric LDH-5 and LDH-1. All five hits that interacted with dimeric LDH-Htr demonstrated a concentration-dependent interaction with either tetrameric LDH-1, LDH-5 or both isozymes. Compounds F1050, F0293 and F2246 showed a similar or better interacting profile with LDH-1 [LDH-5] than with LDH-Htr, with K_D's of 48 µM [324 µM], 116 µM [343 µM] and 1.7 mM, respectively, suggesting that these compounds did not compete with LDH subunits for LDH tetrameric interface. Consistently, NMR STD revealed that these hits displayed a similar or higher saturation transfer against tetrameric LDH-1 than with dimeric LDH-Htr (Figures S2-4). Considering the high polarity and the structural homology with previously described ligands[173], we suspected that these compounds could interact with LDH active-site. However, upon further investigation, some of these compounds were already reported to have no activity inhibiting LDHs, and therefore, we discarded them from this study. On the other hand, compounds F1787 and F2050 showed a 5 to 10-fold decrease in their binding affinity for tetrameric LDHs (**Table 3** and **Figure 20a,b**), indicating a potential competition with LDH subunits for LDH tetrameric interface. In accordance with MST results, F2050 showed a 70% decay in saturation transfer to tetrameric LDH-1 in NMR STD (**Figure 20c**), while F1787 demonstrated only a very weak saturation transfer (**Figure 20d**). Overall, compounds F1787 and F2050 displayed a profile consistent with an interaction with the LDH tetrameric interface. These two compounds were the only hits that could destabilize both LDH-1 and LDH-5 while keeping a neutral or stabilizing effect on dimeric LDH-Htr. This result highlights the advantages of running

the screening on both LDH-1 and LDH-5 to eliminate promiscuous destabilizers.

5.2.3 Hit Characterization

We next characterized the ability of F2050 and F1787 to destabilize tetrameric LDHs. Interestingly, the two compounds displayed different destabilizing profiles, as assessed by nanoDSF (**Figure 20e,f**). Along with its K_D in the mid micromolar range, F2050 demonstrated a concentration-dependent ability to destabilize tetrameric LDH and to stabilize dimeric LDH-Htr (Figures 4e). These two events occurred around the same concentration range for LDH-Htr and LDH-5, suggesting that the same process was underlying stabilization and destabilization. However, F2050 could only destabilize tetrameric LDH-1 at higher concentrations (Figure S12a), consistent with this isozyme higher stability. Conversely, compound F1787 only destabilized tetrameric LDH at high concentrations (1 mM and above, Figures 4f and S12b-d), consistent with its weaker interaction with tetrameric LDH. Interestingly, F1787 induced a destabilizing conformational change that we could follow with nanoDSF. This conformational change corresponds to a shift of LDH fluorescent ratio upon denaturation, from a blue-shift (reduction of the 350/330 nm ratio) to a red-shift (elevation of the 350/330 nm ratio) (**Figure 20f**). Such pattern is coherent with a destabilization of LDH tetramer, as buried tryptophan residues tend to shift to longer wavelengths upon solvent exposure. Previously, we observed a similar destabilization of tetrameric LDH with a macrocyclic peptide (macrocycle 7) that competed with LDH *N*-terminal domain and disrupted tetrameric LDH, suggesting that compound F1787 could interact in the same fashion[30].

We also studied the ability of the two identified hits to prevent LDH tetrameric association. To do so, we relied on a biochemical assay recently described by Nadal-Bufi et al. on LDH-5 [49] Briefly, tetrameric LDH is dissociated to partially unfolded monomers in acidic conditions. Following denaturation, neutral pH is restored in the presence or absence of the studied compound, which allows for a slow reassociation of LDH in its native tetrameric structure. The protein then reassociated at room temperature, and its enzymatic activity, corresponding to the recovery of its proper quaternary structure, is followed afterwards. Interestingly, both compounds inhibited LDH activity at high concentrations under these conditions, with an IC_{50} of 970 µM (CI95% : [830 to 1277 µM]) for F2050 and 7.6 mM (CI95% : [4.4 to 12.0 mM]) for F1787 (**Figures 20g,h**). Conversely, neither F2050 nor F1787 could inhibit LDH activity without this pre-dissociative step (Figure S12e). These results are consistent with the destabilizing profiles of both compounds and their putative interaction at the LDH tetrameric interface. These interactions would not lead to any inhibition a priori, but would only weaken the strength of the tetrameric association, without significantly disturb the activity *in vitro*. Interestingly, F1787 and F2050 inhibited tetrameric LDH-5 at concentrations higher than their respective K_D assessed by MST. Recent reports of compounds interacting at proteins interfaces demonstrated similar differences between K_D and IC_{50} [49, 174]. We suspect that such a difference could result from cooperativity between LDH subunits that would reduce the efficacy of compounds interacting at the tetrameric interface.

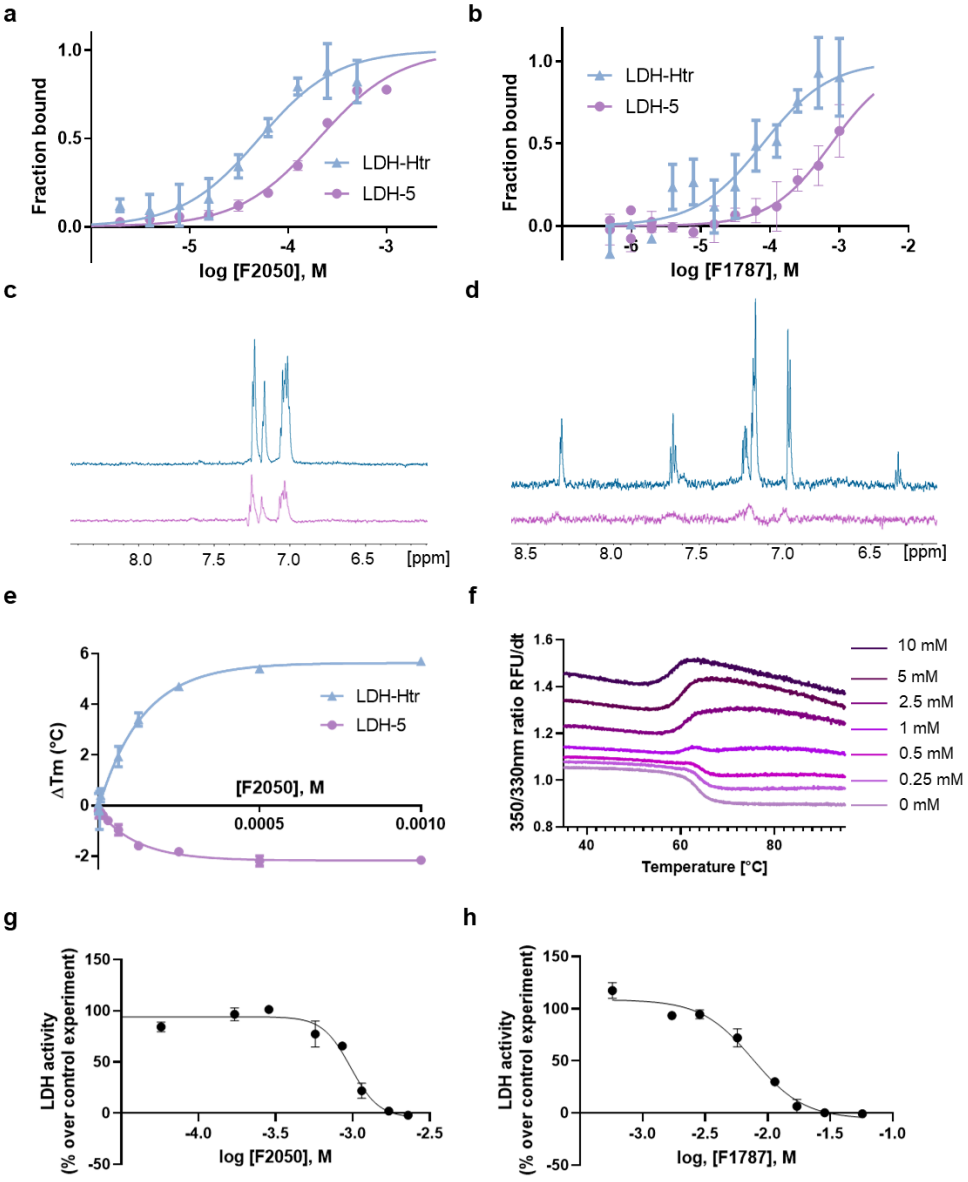

Figure 20. Hits F1787 and F2050 compete for the LDH tetrameric interface and destabilize the tetrameric proteins. a) MST binding curves of **F2050** with LDH-Htr (K_D = 37 µM ± 12 µM) and LDH-5 (K_D = 205 µM ± 40 µM) (n = 3). b) MST binding curves of **F1787** with LDH-Htr (K_D = 79 µM (± 12 µM) and LDH-5 (K_D = 760 µM (± 40 µM)) (n = 3). c) STD spectra of **F2050** (500 µM) with LDH-Htr (up,

15 µM) and LDH-1 (bottom, 15 µM) with 512 scans on and off-resonance. Both spectra have the same scale. d) STD spectra of **F1787** (500 µM) with LDH-Htr (up, 15 µM) and LDH-1 (bottom, 15 µM) with 512 scans on and off-resonance. Both spectra have the same scale. e) ΔTm (°C) of tetrameric LDH-5 (25 µg/mL) and dimeric LDH-Htr (25 µg/mL) as a function of **F2050** concentrations (n = 3). f) NanoDSF denaturation of tetrameric LDH-5 (25 µg/mL) with a gradient of **F1787** (from top to bottom : 10 mM, 5 mM, 2.5 mM, 1 mM, 500 µM, 250 µM and 0 µM) (n = 3). g) Inhibition of LDH-5 activity after renaturation upon exposure of increasing amount of **F2050** (IC_{50} = 970 µM [CI95% : 830 to 1277 µM]. h) Inhibition of LDH-5 activity after renaturation upon exposure of increasing amount of **F1787** (IC_{50} = 7.6 mM [CI95% : 4.4 to 12.0 mM].

We then set out to perform epitope mapping on **F1787** and **F2050** using NMR STD to guide future hit optimization (**Figure 21**). Of note, we apply the term epitope mapping here to describe the characterization of portions of the small molecule ligand, which are in contact with our target of interest (in this case LDH). Briefly, the signal intensity in NMR STD depends on the distance between a ligand proton and the protein. Protons close to the protein, and hence involved in the interaction, would display a high STD signal, while protons farther away would show little to no saturation transfer. This process allows one to identify the protons that make close contact with the protein and are thus important for the interaction. Consistent with the expected hydrophobic nature of the LDH tetrameric interface, epitope mapping analysis revealed a similar interaction pattern between **F1787** and **F2050**. According to NMR STD, the aromatic protons of both hits are the main contributors to the interaction with the LDH tetrameric interface. On the other hand, both **F1787** and **F2050** possess an aliphatic chain with a tertiary and secondary amine, respectively, that makes less interaction with LDH-Htr than the aromatic protons.

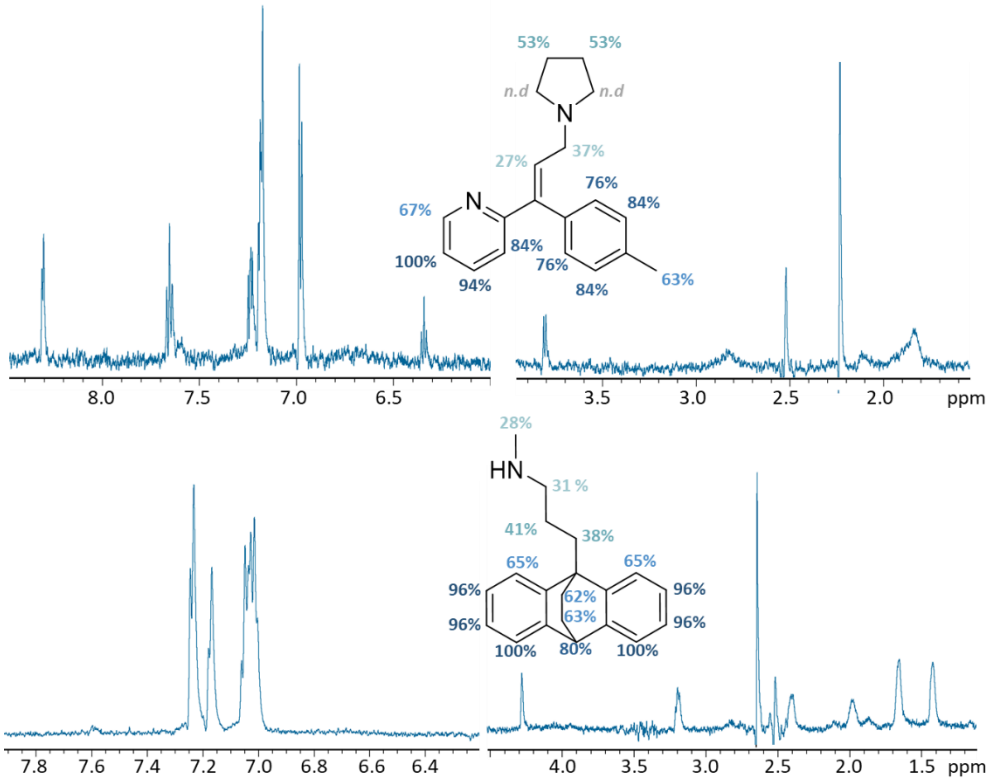

Figure 21. Epitope mapping reveals that F1787 and F2050 share a similar pattern of interaction with LDH-Htr. Top, NMR STD spectrum of **F1787** (500 µM) with LDH-Htr (15 µM). The aromatic region is displayed on the left, while the aliphatic region is on the right. Bottom, NMR STD spectrum of **F2050** (500 µM) with LDH-Htr (15 µM). The aromatic region is displayed on the left, while the aliphatic region is on the right. The different percentages correspond to the protons' relative signal intensity, compared to their intensity in ^{1}H NMR and normalized regarding the most interacting proton. Complete proton assignations were based on 2D NMR (**Figure S14** and **S15**) and previous reports.

Finally, we attempted to further characterize the two hits' biophysical profiles to precisely identify their site(s) of interaction and lay the ground for future optimization. To that end, we performed competition experiments with

the different peptidic probes that we had previously developed and that are selective for different binding sites at the tetrameric LDH interface[30, 39]. A competition with one of the two probes would mean that the compound and the probe share the same interaction site, which would facilitate the understanding of their structure-activity relationships (SARs). Hence, we performed competition experiments using NMR STD with macrocycle **7**, previously identified as competing with LDH *N*-terminal tetramerization domain [30]; and peptide **LP-22**, previously identified as interacting at a second site, buried at the core of LDH tetrameric interface [39]. Competition experiments with **LP-22** did not result in a diminution of STD intensity signals (Figure S13), meaning that the two hits do not compete with this peptide. However, when performing the competition experiments with macrocycle **7**, we noticed a substantial decay in the STD signal of **F1787** (~ 40 %, **Figure 22a**). This reduction in saturation transfer indicated a competition between the probe and the hit, suggesting that **F1787** shared the same site of interaction as macrocycle **7** and was hence a competitor of the LDH *N*-terminal domain. Conversely, **F2050** did not demonstrate any competition with either **7** or **F1787**, meaning that the two compounds do not share the same site of action. This result is in line with the different profile that **F2050** and **F1787** showed in both nanoDSF and MST, confirming that these two compounds, despite their structural similarity, do not share the same site of interaction. Based on these competition experiments, and on the epitope mapping, we provided a speculative binding mode for compound **F1787** at the LDH tetramerization site. Docking of **F1787** in the LDH tetramerization pocket showed several dockings poses congruent with epitope mapping experiments (**Figure 22b**), with the aromatic residues buried within

the lipophilic tetramerization site and the aliphatic amine exposed to the surrounding solvent.

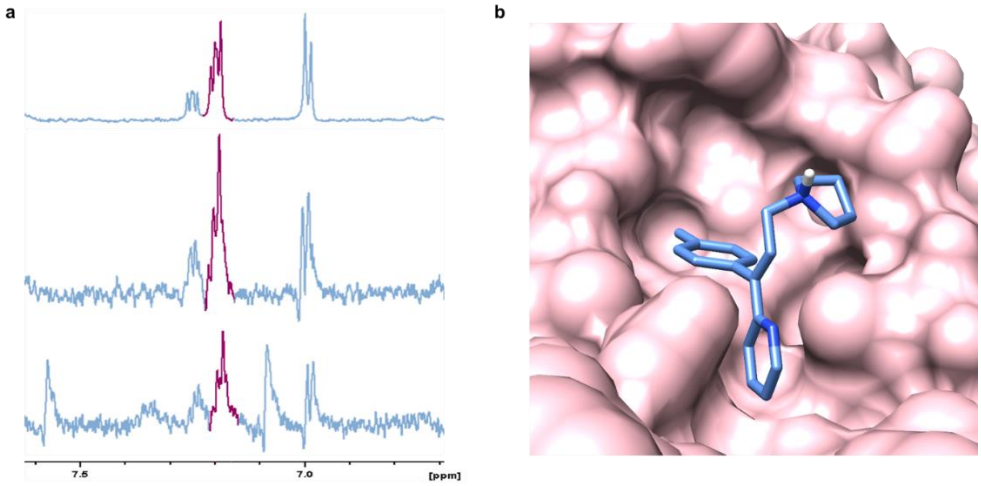

Figure 22. F1787 competes with macrocycle 7. a) Top. ^{1}H NMR spectrum of **F1787** (100 µM) with LDH-Htr (7.5 µM). Middle, ^{1}H NMR STD spectrum of **F1787** (100 µM) interacting with LDH-Htr (7.5 µM). Bottom, ^{1}H NMR STD spectrum of **F1787** (100 µM) and macrocycle **7** (1 mM) interacting with LDH-Htr (7.5 µM). The signals highlighted in purple correspond to aliphatic protons of **F1787** that show a ~ 40% decay in intensity upon macrocycle **7** addition. b) Proposed binding mode of F1787 with LDH tetramerization site. Best binding poses of **F1787** in LDH-H tetramerization site resulting from Auto dock Vina docking on the available crystallographic structure (PDB entry: 1I0Z, chain B, D, pictures made using UCSF Chimera).

Overall, hit characterization revealed that **F1787** interacted at the tetramerization site occupied by the LDH *N*-terminal domain. However, we could not identify the site of interaction of **F2050**, as this compound did not compete with any of the peptidic probes. Recent studies reported other

allosteric sites at the LDH-1 and LDH-5 tetrameric interface, highlighting the high druggability of this interface [125, 126]. We suggest that **F2050** might interact in one of these recently disclosed sites or elsewhere at the large and hydrophobic LDH tetrameric interface.

5.3 Preliminary conclusion

Targeting protein self-association is an emerging strategy that can provide different advantages over active site targeting. LDHs constitute attracting targets in cancer therapy that could benefit from alternative targeting approaches, such as the disruption of their oligomeric state. In the present work, we exemplify the concept of probing the LDH oligomeric interface using nanoDSF as a primary screening method, followed by MST and NMR STD for hit validation and characterization. We demonstrated that we could quickly and efficiently identify binders of the LDH tetrameric interface from a small initial subset of compounds. The apparent high hit rate (~ 6%) can be explained because this screening method probes the entire LDH tetrameric interface, which encloses multiple allosteric binding sites [30, 39, 125, 126]. The two hits identified in this work specifically target the LDH tetrameric interface and prevent its tetrameric association. Notably, Hit F2050 corresponds to maprotiline, an antidepressant, while Hit F1787 corresponds to triprolidine, an antihistaminic. They constitute promising starting points for further optimization. Interestingly, both hits were aromatic compounds and the structural similarity probably highlights the propensity of the hydrophobic LDH tetrameric interface to accommodate large and lipophilic molecules. These scaffolds contrast with LDH small and polar active sites and highlight the potential of this approach to identify more druggable

ligands. We anticipate this screening concept to be readily transposable to other obligatory homo-oligomers, pending that these targets can first be stabilized in a lower order oligomeric state.

Contribution in the paper:

My contributions to this work included conducting all the visual docking analysis and selection, performing all NanoDSF primary screening and stability assessments, and verifying and determining all the MST binding affinities.

5.4 Experimental section

5.4.1 General

All reagents were purchased from chemical suppliers and used without purification. The 29 compounds evaluated as potential hits were purchased from Prestwick and used without further purification. Structure conformity of F1787 and F2050 was confirmed using NMR. Hits F1787 and F2050 were repurchased from different suppliers and reevaluated with same results.

5.4.2 Virtual Screening and library selection

A focused library was designed from a Prestwick Drug-Fragment library through docking using the Auto dock Vina software [175]. Briefly, we relied on three complementary docking studies on the apoLDH dimer (PDB ID: 1i0z, subunits B-D). A primary docking study was performed on the dimer without area restriction to probe for the entire tetrameric interface. Two other docking studies were done by restricting the binding zone to the two tetramerization sites that we previously described.18,19 All docking poses

were processed together, and poses with Vina scores higher than -6.8, as well as active-site binders, were discarded, allowing a cutoff of two-third of the initial library. Visual selection was performed as the last step, using the docking focused on tetramerization sites as a comparison to eliminate non-reliable binders that did not display homogeneous binding poses between the different docking studies. Unique docking poses on alternative binding pockets at the interface were also considered. From this virtual screening, 29 virtual hits were selected and then processed towards biophysical evaluation.

5.4.3 Protein production

Production of LDH-1, LDH-5 and LDH-Htr was performed as described elsewhere.19 Briefly, sequences of hLDHA, hLDHB and hLDHBtr were inserted in a pET-28a expression vector using NdeI and Bpu1102I as restriction sites. Bacteria were grown in Terrific broth (TB) medium supplemented with 50 μg/mL kanamycin and 34 μg/mL chloramphenicol at 37 °C until an optical density of 0.8 was reached. Protein expression was induced by adding 1 mM isopropyl-β-D-1-thiogalactopyranoside (IPTG) at 20 °C for 20 h. Then, cells were collected by centrifugation at 5,000 rpm, 4 °C for 25 min. Pellets were suspended in a lysis buffer (Tris-HCl 50 mM, pH 8.5, MgCl2 10 mM, NaCl 300 mM, imidazole 5 mM, and glycerol 10%) and then disrupted by sonication, followed by centrifugation at 4 °C, 10 000 rpm for 30 min. The insoluble fraction was discarded, and 1 μL of β-mercaptoethanol was added per mL of soluble fraction. The purification of recombinant proteins was performed using 1 mL of His-trap FF-crude columns (GE Healthcare) according to the manufacturer's instructions.

5.4.4 NanoDSF

Solutions of proteins (LDH-1, LDH-5 or LDH-Htr) were evaluated on a Tycho NT.6 device (NanoTemper Technologies), at 25 µg/mL with and without 1 mM of compounds. Evaluations were run in a 50 mM sodium phosphate and 100 mM NaCl pH 7.6 buffer. According to standard manufacturer's procedures, samples were poured into capillaries and heated up to 95 °C in 3 min while following fluorescence emission at 330 and 350 nm. Melting temperatures were extracted from the derivative of the 350/330 nm fluorescence ratios upon increasing temperature.

5.4.5 Nuclear Magnetic Resonance

Human LDH-H (full length and truncated)-6His proteins for 1D NMR were expressed and purified from E. coli, as described above. All experiments were performed on a Bruker Ascend Avance III 600 MHz system equipped with a broadband cryoprobe (Bruker).

For STD NMR studies, samples were prepared in PBS containing 2% deuterated DMSO. The concentration of LDHs was ranging from 7.5 to 15 µM of monomer, depending on the experiment. Ligand binding was detected using a STD stddiffesgp.3 sequence with a 2 s saturation time. Water signal suppression was achieved using an excitation-sculpting scheme, and a 50 ms spinlock was used to suppress protein background signals. Experiments were performed at 277K to avoid protein degradation.

For epitope mapping experiments, 512 scans were collected on (0 ppm) and off-resonance (40 ppm) to yield a 32K point free induction decay (FID). STD spectra correspond to the difference of spectra between on and off-resonance experiments. Signal intensities in STD spectra were compared to reference

1H spectra in the same conditions to account for signal broadening due to protein addition.

For 2D experiments, F2050 was dissolved at 5 mM in a 50 mM phosphate buffer, pH 7.6, containing 100 mM NaCl, 90% D_2O and 10% DMSO-d6. F1787 was dissolved at 50 mM in a 50 mM phosphate buffer, pH 7.6, containing 100 mM NaCl and 100% D_2O. 2K time-domain points and 256 increments were applied for all the 2D spectra. Experiments were performed at 298K.

5.4.6 MST

MST measurements were performed on a Nanotemper Monolith NT.115 instrument (Nano-Temper Technologies) using Red-dye-NHS fluorescent labelling. LDH-5 and LDH-Htr purified to homogeneity were labelled with Monolith Red-dye-NHS second-generation labelling dye (Nanotemper Technologies), according to the supplied protocol. LDH-1, purified to homogeneity, was labelled using first generation labelling dye. Measurements were performed in 50 mM sodium phosphate, pH 7.6, and 100 mM NaCl containing 0.01% Tween-20 in standard-treated capillaries (Nano-Temper Technologies). The ligands (NADH and hits) were titrated in 1:1 dilution following manufacturer's recommendations. Experiments were performed in triplicates using 40% LED power, medium MST power, laser on-time 20 s, and laser off time 3 s. Hits were evaluated for their thermophoretic pattern, and K_D's were extracted from raw data at a 1.5 s to 20 s MST on time depending on the hit MST profile.

5.4.7 Denaturation assay

The experiments were performed with opaque 96-well plates using a Spectramax m2e spectrophotometer (Molecular Devices). The denaturation assay was adapted from a previous report.29 Active LDH-5 was diluted to 0.9 µM in 0.01 M phosphate buffer (pH 7.6), 1 mM EDTA, and 0.05% BSA (w/v). 500 µl of protein solution was incubated with 1mL of 0.1 M glycine buffer (pH 2.5) and 0.05% BSA (w/v) for 2 min. Afterwards, 30µl of the denaturated enzyme was added to 40 µL of 0.25 M phosphate buffer (pH 7.6), 1 mM EDTA, and 0.05% BSA containing different concentrations of the studied compounds. LDH-5 was then left at room temperature for 2h to allow tetrameric reassociation. After this incubation, 10 µL of LDH-5 + inhibitor sample were transferred into a 96- well microplate containing 90 µL of 0.25 M phosphate buffer (pH 7.6), 1 mM EDTA, and 0.05% BSA (w/v) per well. Finally, 20 µL of substrate buffer containing 18 mM pyruvate and 1.8 mM NADH was then added to the mix to initiate the enzymatic reaction. NADH consumption was followed over time by measuring the fluorescence emission intensity ($\lambda_{excitation}$ = 340 nm, $\lambda_{emission}$ = 460 nm).

5.5 Supporting information

**Here is a collection of the most illustrative and significative supporting figures. For more details [5].*

Table S1. Hits selected from the NanoDSF primary screening with their difference in melting temperature (ΔTM) on lactate dehydrogenases (LDHs). n.d. no transition detected in the presence of the hit.

Code	Structure	ΔTM dimeric LDH	ΔTM Tetrameric LDH-5 (LDH-1)
1050	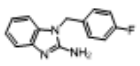	0.8 (+/- 0.9)	-2.6 (+/- 0.5) **0.4 (+/- 0.1)**
0293	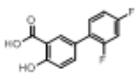	3.1 (+/- 0.3)	-2.1 (+/- 0.3) **0.1 (+/- 0.1)**
1787	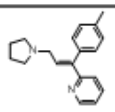	0.2 (+/- 0.1)	-3.3 (+/- 0.4) **-3.1 (+/- 0.2)**
2050	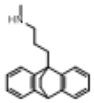	4.6 (+/- 0.0)	-2.7 (+/- 0.4) **-1.4 (+/- 0.1)**
2246	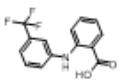	1.9 (+/- 0.5)	-1.7 (+/- 0.3) **0.4 (+/- 0.1)**
3142	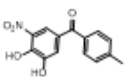	3.3 (+/- 0.1)	-4.4 (+/- 0.2) ***n.d***
307	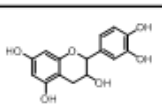	2.2 (+/- 1.1)	-3.0 (+/- 0.2) **0.0 (+/- 0.2)**
308	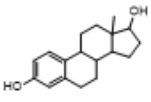	3.8 (+/- 0.3)	-3.9 (+/- 0.4) ***n.d***

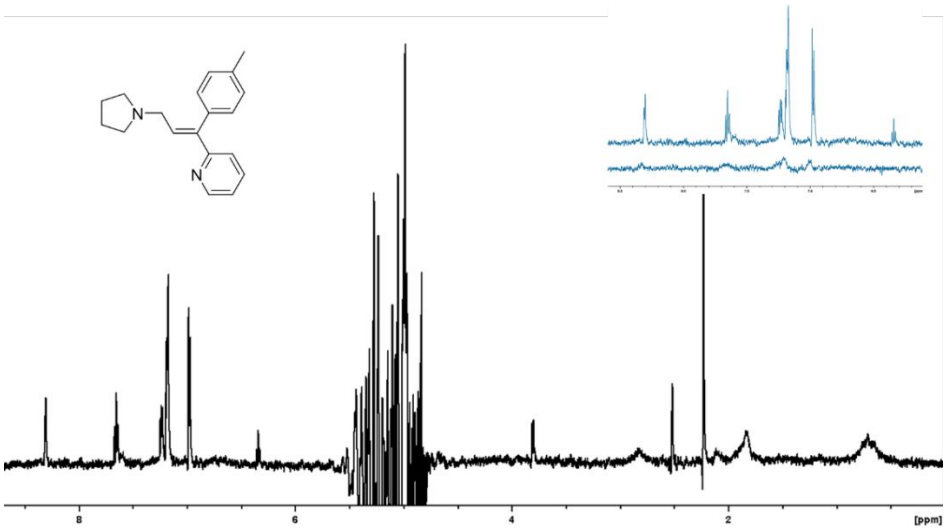

Figure S5. STD spectra of F1787 with LDH-Htr and LDH-1. The spectrum in black corresponds to the STD spectrum of **F1787** (500 µM) with LDH-Htr (15 µM) with 512 scans on and off-resonance. The spectra on the top right correspond to a close up of the aromatic region of the STD spectra of **F1787** with either LDH-Htr (15 µM, top) or LDH-1 (15 µM, bottom).

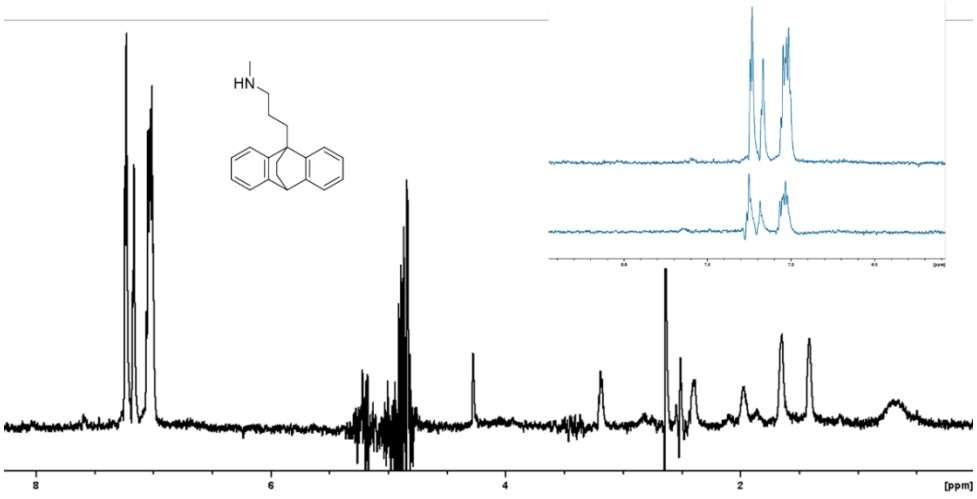

Figure S6. STD spectra of F2050 with LDH-Htr and LDH-1. The spectrum in black corresponds to the STD spectrum of **F2050** (500 µM) with LDH-Htr (15 µM) with 512 scans on and off-resonance. The spectra on the top right correspond to a

close up of the aromatic region of the STD spectra of **F2050** with either LDH-Htr (15 µM, top) or LDH-1 (15 µM, bottom).

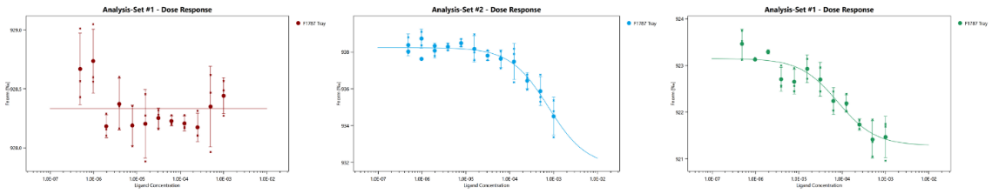

Figure S9. MST profile of F1787. Binding curves of **F1787** interacting with LDH-1 (red), LDH-5 (blue) and LDH-Htr (green). (*n = 3*)

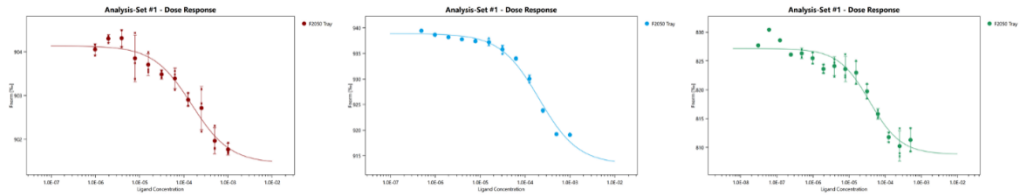

Figure S10. MST profile of F2050. Binding curves of **F2050** interacting with LDH-1 (red), LDH-5 (blue) and LDH-Htr (green). (*n = 3*)

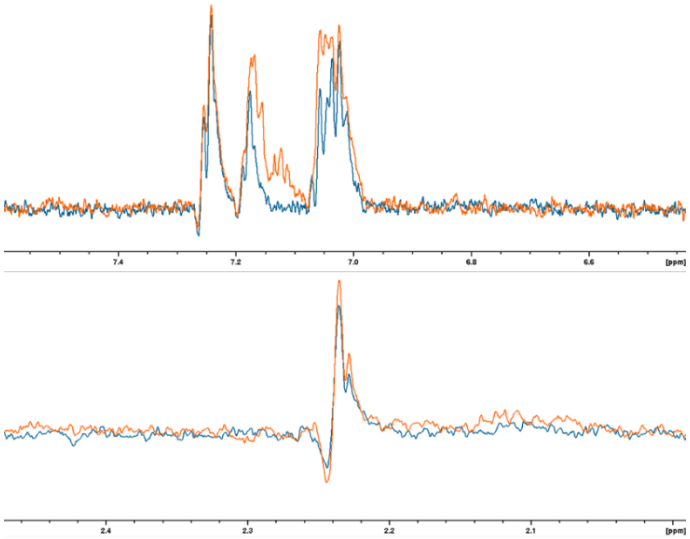

Figure S13. F1787 and F2050 do not compete with LP-22. Top, ^{1}H NMR STD spectrum of **F2050** interacting with LDH-Htr (10 µM), with (orange) or without (grey blue) **LP-22** (500 µM). Bottom, ^{1}H NMR STD spectrum of **F1787** interacting with LDH-Htr (10 µM), with (orange) or without (grey blue) **LP-22** (500 µM).

6. Results: Chapter 2

Exploring the therapeutic potential of Antidepressants and Antihistaminic: Targeting the oligomeric interface of Lactate Dehydrogenases

Graphical abstract

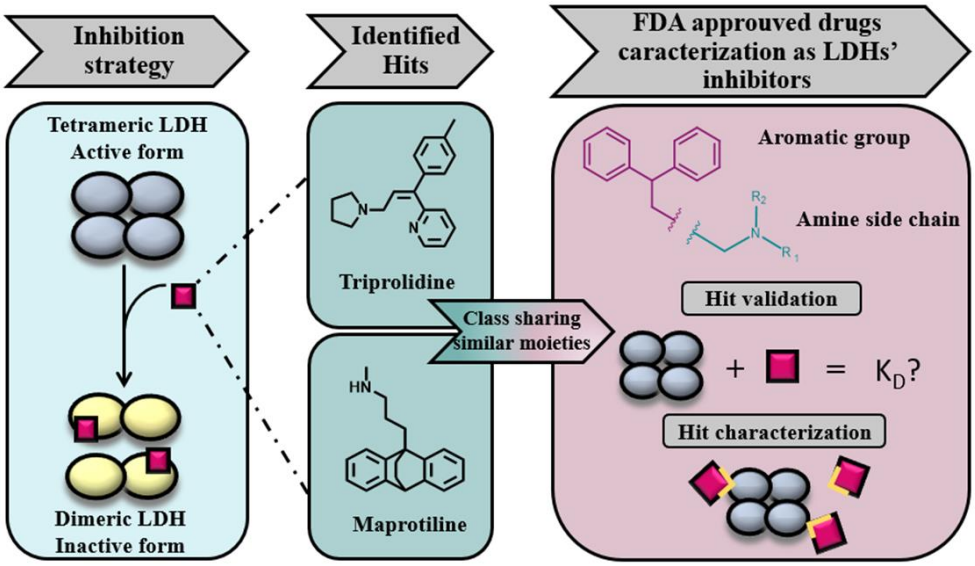

6.1 Introduction

LDHs are very attractive targets, notably in the field of cancer, and active-site directed inhibitors have therefore been searched during the last decade. Although very potent LDH inhibitors were identified, none entered clinical trials notably because of their non-optimum PK profile and lack of selectivity. New LDH inhibition strategies notably targeting LDH allosteric sites were

investigated and led to the identification of several allosteric inhibitors with promising properties [5, 30, 39] (**Figure 23**). Of note, our laboratory, along with others, pursued an innovative approach for LDH inhibition focusing on targeting LDH oligomeric state. Recognizing the importance of the LDH quaternary structure for proper LDH catalysis, our strategy seeks to prevent the formation of a functional tetramer or the disruption of the tetrameric state by targeting the dimer-dimer oligomeric interfaces. Hence, in previous works, we demonstrated that the LDH last 19 amino acids of the *N*-terminal end were crucial for LDH oligomerization. Removing these 19-Amino acids from the LDH sequence led to a truncated form of LDH, named LDH-Htr, that was shown to be properly folded, dimeric, but very weakly active. This dimeric form of LDH was used to identify very promising stapled peptides able to bind at the oligomeric interface and prevent, at least in part, the formation of an active LDH tetramer (**Figure 23**).

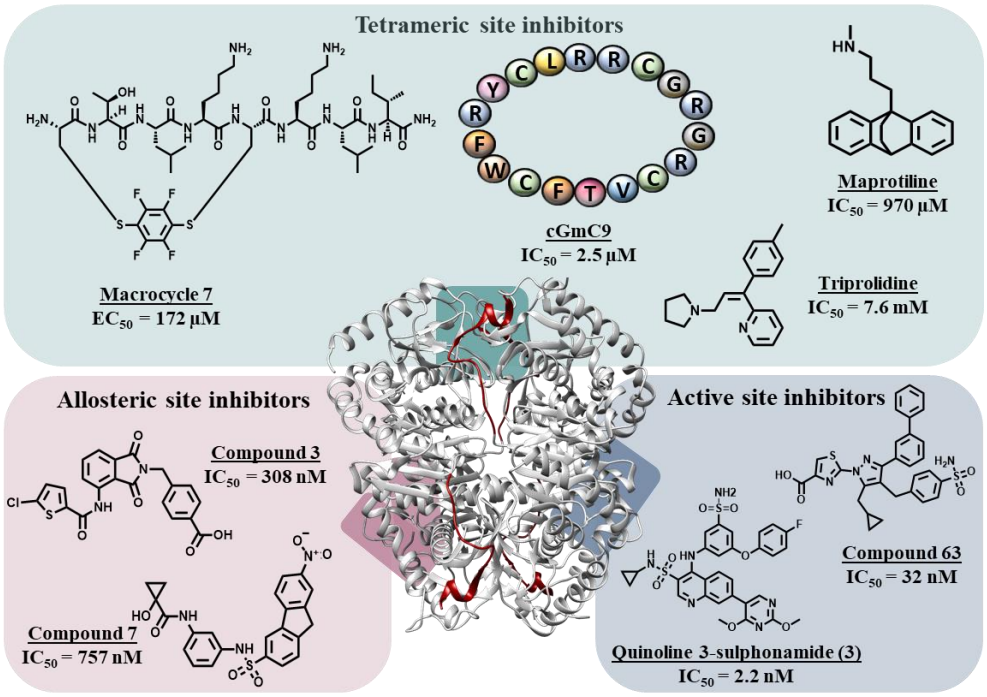

Figure 23. Small molecules and peptide interacting with LDHs. This figure illustrates various inhibitors targeting lactate dehydrogenases at different binding sites. The central image shows the LDH protein structure (PDB: 1t2f), highlighting different interaction sites. The upper green section presents tetrameric site inhibitors, including Macrocycle 7 (EC_{50} = 172 µM), cGmC9 (IC_{50} = 2.5 µM), Maprotiline (IC_{50} = 970 µM), and Triprolidine (IC_{50} = 7.6 mM), with the latter two being FDA-approved drugs. The pink section on the left displays allosteric site inhibitors, such as Compound 3 (IC_{50} = 308 nM) and Compound 7 (IC_{50} = 757 nM). The blue section on the right showcases active site inhibitors, featuring Compound 63 (IC_{50} = 32 nM) and Quinoline 3-sulphonamide (IC_{50} = 2.2 nM). Reported Hits (maprotiline and triprolidine) are two FDA approved drugs already characterized to target LDH at its oligomeric surface.

In our quest for LDH inhibitors targeting the oligomeric state of the enzyme, we identified two FDA approved drugs, namely the antidepressant maprotiline and the antihistaminic triprolidine [5] and demonstrated, using

biophysical experiments, that these two drugs were able to interact at the LDHs oligomeric interface (**Figure 23**). Interestingly, maprotiline, was shown, at least *in vitro*, to have antiproliferative properties on Burkitt lymphoma (BL) cell lines [176] whereas triprolidine was shown to induce cellular cell death in melanoma cancer cell lines [177]. Antidepressants and antihistaminic drugs are known for decades to reduce the risk of certain cancers through antineoplastic effects [176, 178-182]. For instance, fluoxetine was shown to exhibits promising anti-tumor effects in various cancers, including hepatocellular carcinoma (HCC), non-small cell lung cancer (NSCLC), colon cancer, and neuroblastoma[183]. It induces apoptosis in tumor cells through various mechanisms, including triggering ER stress and mitochondrial stress[184].

Based on these findings, we set out to investigate LDH inhibition by a series of antihistaminic and antidepressant drugs in more details.

6.2 Results and discussion

6.2.1 Elaboration of a focused library of antidepressant and antihistaminic drugs

A list of 21 drugs sharing the classical pharmacophoric features for antidepressant and antihistaminic drugs, namely the presence of an amine side chain linked to an aromatic ring structure [176], was assembled. It contains most of the Serotonin Reuptake Inhibitor (SSRI), Tricyclic (TCA) and atypical antidepressants, and H_1-antihistaminic drugs that are commercially available. These compounds were also selected because they have been previously shown to have antiproliferative/antineoplastic properties [176,

180, 185-187]. Was also considered norfluoxetine, the active metabolite of fluoxetine

From those 21 selected drugs, three of them, namely **escitalopram**, **dosulepine** and **ebastine** were discarded because of very low aqueous solubility profile that prevent their evaluation using biophysical techniques. The resulting 18 FDA approved drugs that will be investigated in this study are reported in **Figure 24**.

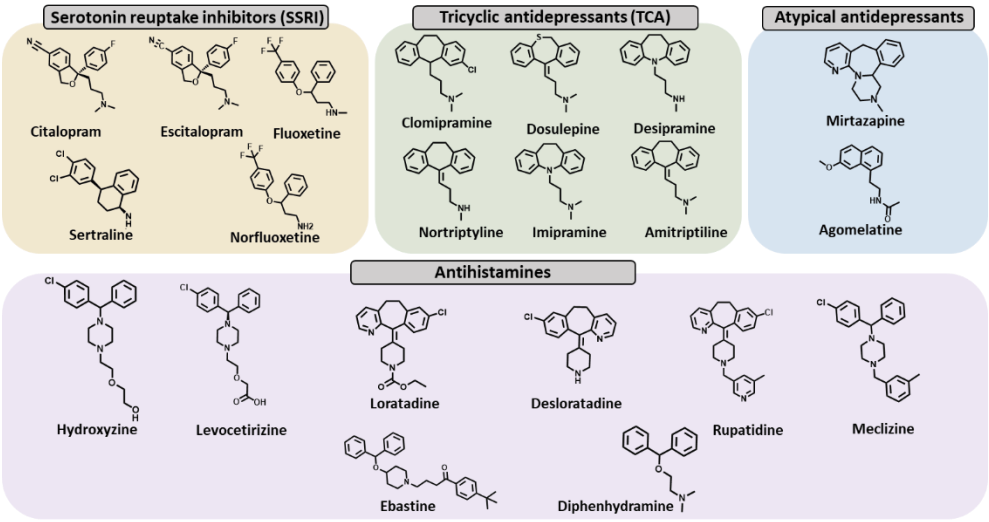

Figure 24. FDA Approved Drugs selected to be evaluated against LDHs. Selection of drugs among antidepressants (top) and antihistamines (bottom) to be screened against LDHs. Antidepressants are divided by pharmacological and structural classification. Selection was made based on their shared pharmacophore with previous Hits (Maprotiline and Triprolidine) and known antiproliferative activity against cancer cell lines.

6.2.2 Biophysical characterization

We first set out to investigate if, similarly to maprotiline and triprolidine, the selected antidepressants and antihistaminic drugs can bind LDH. To this end,

we initially preconized the use of nanoDSF to monitor the changes in LDH stability upon exposure with a compound as previously reported [5]. The experiments were undertaken using LDH-1, LDH-5 and LDH-Htr and the results are depicted on **Figure 25** and Table S2.

Strikingly, out of the 18 selected drugs, 14 drugs induced a stability change on all three LDH forms investigated with ΔTm in the same ranges to those observed with maprotiline and triprolidine. These data suggest a direct interaction between these 14 drugs and LDHs. Four drugs, citalopram, loratadine, mirtazapine and hydroxyzine did now reveal any interaction with LDH-Htr but only with LDH-1 and LDH-5. One drug, agomelatine, could not be analyzed by nanoDSF because of interferences in the nanoDSF experiment (signal saturation due to high brightness). It should be noted that, in nanoDSF, both stabilization (increase in ΔTm) or destabilization (decrease in ΔTm) can account for binding.

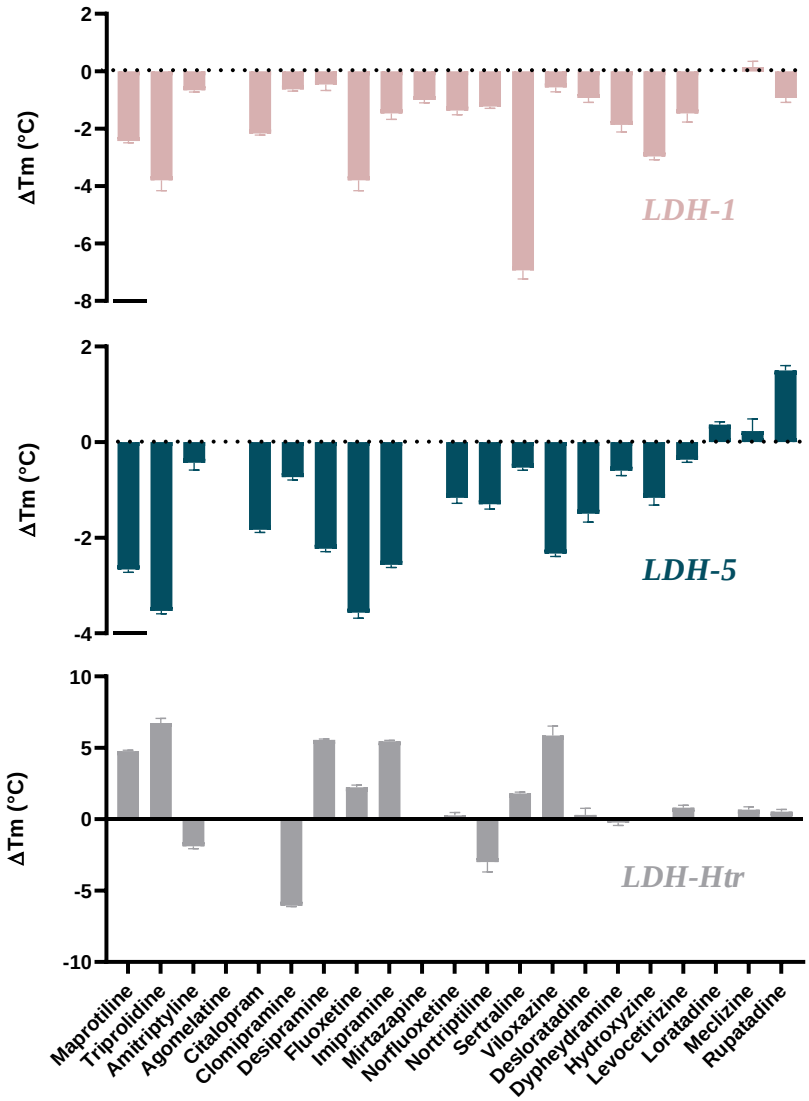

Figure 25. FDA approved drugs assessment through Nano DSF to detect an interaction against LDHs. Thermal shift of the screened compounds at 1 mM, 2% DMSO (*clomipramine, loratadine and sertraline 500 µM, rupatadine 250 µM due to solubility issue) against LDH-1 (pink), LDH-5 (blue) and LDH-Htr (grey) all proteins evaluated at 25 µg/mL.

To confirm the results obtained by nanoDSF, MST experiments was undertaken. Besides providing an orthogonal method to confirm the binding to LDHs, MST also gives access to equilibrium dissociation constants (K_D) values. All compounds were assayed at a range of concentrations from 0.5 mM to 2 mM and the results obtained can be found on Table 4.

Interestingly, compared to maprotiline (K_D (LDH-Htr) = 37 µM & K_D (LDH-5) = 205 µM) and triprolidine (K_D (LDH-Htr) = 79 µM & K_D (LDH-5) = 760 µM), some of the investigated compounds, such as clomipramine, fluoxetine, norfluoxetine, amitriptyline, sertraline and desloratadine, demonstrate better affinity for both LDH-Htr (K_D in the range 10-25 µM) and LDH-5 K_D in the range 20-70 µM (Table 4 and Figure S2-7).

Apart from mirtazapine, levocetirizine and rupatadine, all the other investigated compounds revealed some affinity to LDH-5, with agomelatine being the more affine drug to LDH-5 (K_D (LDH-5) = 6,5 µM). On LDH-1, the affinity is either very weak or no interaction was detected, in agreement with previous observations showing that LDH-1 is more stable (higher Tm) than LDH-5 and thus less susceptible to potential binders at the tetramerization interface [5, 30].

All MST binding curves are reported in Figure S3-8. In pursuit of additional characterization through orthogonal biophysical methods, all drugs that displayed a K_D higher than that of the parent hits maprotiline and triprolidine[5] were not further investigated.

Table 4. Characterization of the identified small molecules. Table reporting compound, Dissociation Constant (K_D) of identified small molecules against LDHs. N.B No binding up to 1 mM.

Compound	**K_D LDH-Htr (µM)[CI95%]**	**K_D LDH-5 (µM) [CI95%]**	**K_D LDH-1 (µM) [CI95%]**
Maprotiline	37 [25-49]	205 [165-245]	150 [105-148]
Triprolidine	79 [42-116]	760 [403-1117]	>1000
Amitriptyline	17 [8-39]	37 [25-64]	>1000
Agomelatine	514 [164-2769]	6 [2-16]	N.B.
Citalopram	98 [53-184]	101 [70-184]	N.B
Clomipramine	9 [5-16]	18 [12-25]	N.B
Desipramine	66 [41-106]	41 [30-62]	>1000
Fluoxetine	21 [12-32]	70 [58.1-88.7]	584 [280-1311]
Imipramine	53 [31-168]	22 [16-28]	182 [67-513]
Mirtazapine	N.B	N.B	N.B
Norfluoxetine	23 [12-47]	21 [15-29]	208 [71-601]
Nortriptyline	40 [16-172]	37 [27-50]	N.B
Sertraline	20 [14-38]	24 [15-37]	296 [54-786]
Desloratadine	19 [7-49]	32 [22-47]	N.B
Diphenhydramine	N.B	272 [175-436]	N.B
Hydroxyzine	N.B	624 [209-1672]	N.B
Levocetirizine	N.B	N.B	N.B
Loratadine	N.B	20 [15-27]	N.B
Meclizine	N.B	2 [0-7]	N.B
Rupatadine	N.B	>1000	N.B

The best binders were next investigated for their LDH inhibition properties. To this end, we relied on an *in vitro* biochemical enzyme assay which

involves quantification of NADH by fluorescence emission over time upon addition of pyruvate. Hence, to our surprise, none of the investigated drugs exhibited nor LDH-1 or LDH-5 inhibition (**Figure 26**). Hence, because the selected drugs were shown to bind LDH-Htr, and at least LDH-5, with K_D in the 10-30 µM range, LDH-5 inhibition was somehow expected. One hypothesis is that this still relatively weak binding affinity of the drugs cannot lead to LDH inhibition.

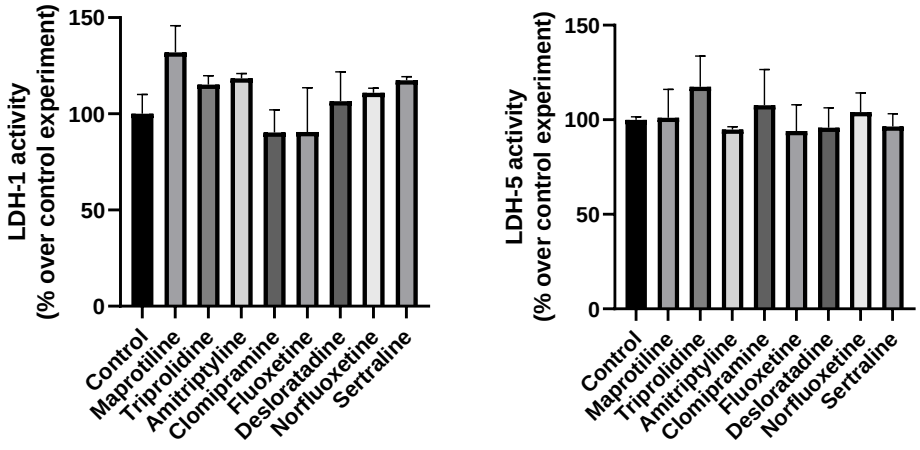

Figure 26. Impact of identified compounds on LDH activity: Lack of inhibition of LDH-1 and LDH-5. The figure illustrates the impact of identified compounds on the activity of lactate dehydrogenase (LDH) isoforms: LDH-1 activity upon exposure of identified compounds (1 mM), left. LDH-5 activity upon exposure of identified compounds (1 mM, 2.5% DMSO), right. *No statically different between the different compounds.*

At this stage, we reasoned that if the investigated compounds do not inhibit a preformed tetrameric LDH-5 probably because of a weak binding affinity at the tetramerization site, they could potentially interfere with the LDH self-assembly process. To verify this hypothesis, we set out to

investigate LDH inhibition by the selected drugs using a dissociation-association LDH assay inspired from the literature [5, 49]. Briefly, LDHs, under acidic conditions, (pH2.5) become partially dissociated and inactive but reassemble into functionally actives LDHs upon pH restoration (pH=7.4) (**Figure 27a,b**). LDHs activities are evaluated after this dissociation-reassociation step in the presence of absence of a tetramerization state inhibitor. Dose-response curves were generated for each selected drug and IC_{50}'s were deduced.

Remarkably, fluoxetine, norfluoxetine and sertraline demonstrated LDH-5 inhibition after a dissociation-reassociation step, with IC_{50}'s in the 300-500 µM (**Figure 27c**) range suggesting that these compounds could interfere with the self-assembly process of LDH-5, leading to LDH-5 inhibition. Because of solubility issues at high concentration a proper IC_{50} could not be determined for clomipramine and amitriptyline but the one can anticipate an IC_{50} in the same range of 100-1000 µM (**Figure 27c**). Desloratadine was found inactive in this assay. The compounds were also assessed against LDH-1 and similar trends were observed with inhibition data in the 100-1000 µM range (Figure S8).

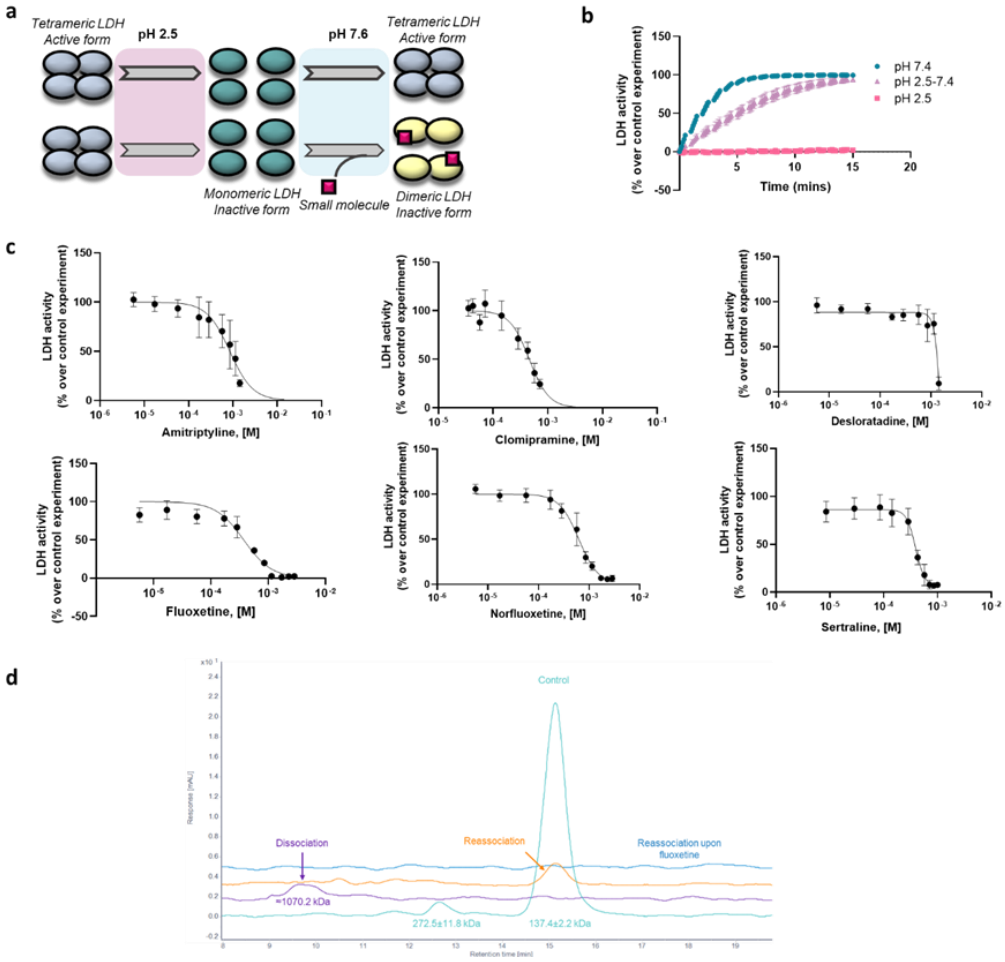

Figure 27. LDH-5 activity assay after denaturation/tetramer reconstitution and small molecules impact in this process. a) Schematic representation of the denaturation activity assay: Tetrameric structure of LDH is lost at acidic pH (pH 2.5) and restored in neutral pH (7.6). The presence of inhibitors affects protein reassociation. b) LDH-5 activity followed by NADH consumption (fluorescence intensity $\lambda_{excitation}$ = 340 nm, $\lambda_{emission}$ = 450 nm). The three curves show: "pH 7.4" LDH-5 under pH 7.4 condition, "pH 2.5-7.4" LDH-5 dissociated at pH 2.5 and reassociated at pH 7.4 and "pH 2.5" LDH-5 under pH 2.5 acidic condition . c) Inhibition curves of LDH-5 activity treated with dilution series of amitriptyline IC_{50} = 852 µM [CI95´% 737-974], clomipramine IC_{50} = 458.7 µM [CI95´% 423-496], desloratadine IC_{50} = 2.2 mM, fluoxetine IC_{50} = 374 µM [CI95´% 332-418],

norfluoxetine IC_{50} = 625 µM [CI95´% 585-687], sertraline IC_{50} = 392 µM [CI95´% 354-415], in 2.5% DMSO. d) Overlaid SEC traces of LDH-1 upon dissociation-reassociation assay: control sample (green), dissociation (purple), reassociation (orange), and reassociation upon fluoxetine (blue) with the assigned MW. ***d*** *shows unpublished data obtained by Dr. Magdalena Wierzbicka.*

To further validate the disruptive potential of fluoxetine obtained with our dissociation-association assay, we opted to utilize a complementary technique, namely, the Size Exclusion Chromatography with Multi-Angle Light Scattering (SEC-MALS). SEC-MALS is a robust and well-documented tool, based on size exclusion chromatography coupled with multi-angle light scattering, that enables the detection of the oligomeric state of a protein[149]. We applied this method to the samples obtained from the enzymatic assay following the dissociation process, both with and without treatment with fluoxetine. As anticipated, our results demonstrated that upon treatment with fluoxetine, the enzyme no longer refolds into an active tetramer, whereas without fluoxetine, the enzyme can be detected in its native folding (**Figure 27d**). This finding supports the hypothesis that fluoxetine interferes with LDH self-assembly, leading to inhibition of LDH activity. The SEC-MALS results provide direct structural insights into the mechanism by which fluoxetine disrupts LDH tetramerization, reinforcing its potential as a candidate for further investigation in the context of modulating LDH function.

6.2.4 Exploring binding interactions: Insights from structural analysis.

Having shown that fluoxetine, sertraline and clomipramine are able to inhibit LDHs activity through tetrameric disruption, we then wanted to assess if these compounds share the same binding site. Competition assays between fluoxetine and the two other molecules, using Nuclear Magnetic Resonance-Saturation transfer difference (NMR-STD), were therefore performed. As expected, due to their highly similar chemical scaffold and our previous bio-physical evaluations, the results demonstrated a decay in fluoxetine STD signal of approximately 40% for both molecules (**Figure 28a** and **b** respectively), indicating a clear competition for the same binding site. To strengthen our knowledges on the chemical interactions between our inhibitors and this specific binding site, NMR-STD was also used to perform an epitope mapping of fluoxetine. This technique reveals the specific regions of the molecule that interact most with LDH-1 (**Figure 28c**). Notably, aromatic protons and the methyl group of the secondary amine emerged as crucial contributors to the interaction by exhibiting an elevated saturation transfer. Altogether, these observations seem to be consistent with those of previous hits from the same class (i.e. maprotiline and triprolidine)[5].

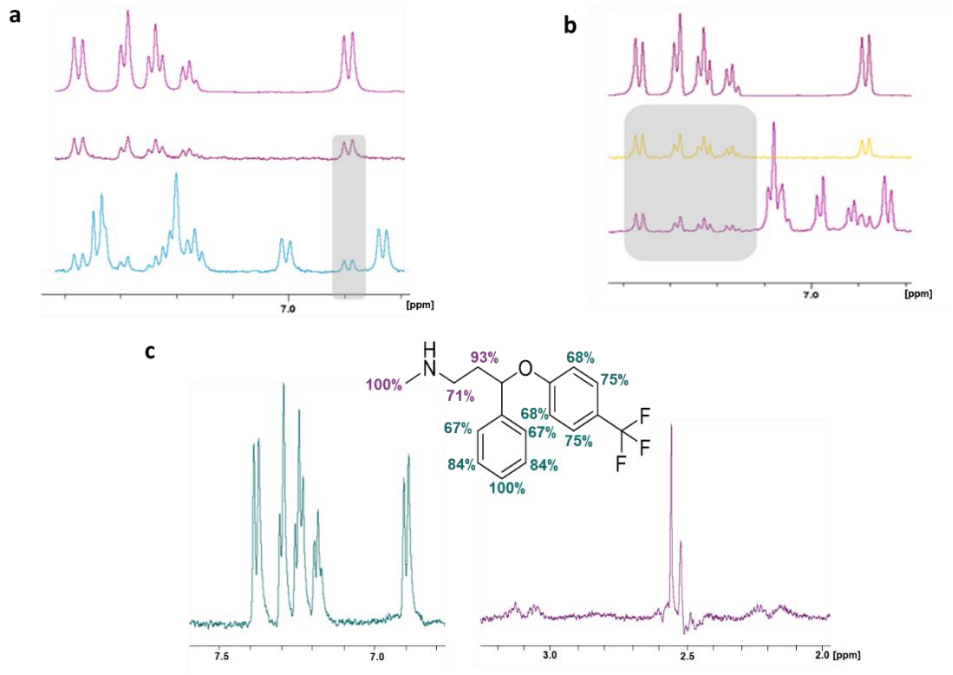

Figure 28. STD spectra of fluoxetine. a) Top, ^{1}H NMR spectrum of fluoxetine (300 µM) with LDH-1 (15 µM). Middle, ^{1}H NMR STD spectrum of fluoxetine (300 µM) interacting with LDH-1 (15 µM). Bottom, ^{1}H NMR STD spectrum of fluoxetine (300 µM) and sertraline (700 µM) interacting with LDH-1 (15 µM). The signals highlighted in gray correspond to aromatic protons of fluoxetine that show a ~40% decay in intensity upon sertraline addition. b) Top, ^{1}H NMR spectrum of fluoxetine (300µM) with LDH-1 (15 µM). Middle, ^{1}H NMR STD spectrum of fluoxetine (300 µM) interacting with LDH-1 (15 µM). Bottom, ^{1}H NMR STD spectrum of fluoxetine (300 µM) and clomipramine (700 µM) interacting with LDH-1 (15µM). The signals highlighted in gray correspond to aromatic protons of fluoxetine that show a ~40% decay in intensity upon clomipramine addition. Complete proton assignations were based on 2D NMR (Figure S14). c) NMR STD epitope mapping shows interactions between fluoxetine (500 µM) and LDH-Htr (15 µM). Left aromatic region (green), right aliphatic one (purple). Percentages represent protons' proper intensity signal normalized with the most interacting one, separately with the two different regions.

To finalize the full characterization of the binding mode of fluoxetine with LDH, we obtained cocrystal structures of LDH-1 with fluoxetine

(**Figure 29**). As expected from our dissociation/association assay, an examination of the ligand's conformations showed a binding of fluoxetine in close proximity to the tetrameric interface. Observed interactions include an hydrogen bond with His156, a salt bridge with Glu-13 residue situated on the *N*-terminal arm and a hydrogen bond with Val-11. Align with the interactions observed with NMR-STD, the terminal amine appears crucial for the interactions. The discrepancy between the aromatic part's interaction with LDH-1 in NMR-STD and the co-crystal structure can be explained by the dynamic nature of NMR-STD when co-crystal structures represent static interactions in a crystalline state. However, the crystal evidence confirms fluoxetine interaction around the tetrameric interface area, reinforcing its significance in our findings. It is worth noting that protein crystals failed to form in the absence of NADH, underscoring the significance of its presence in the co-crystallization process.

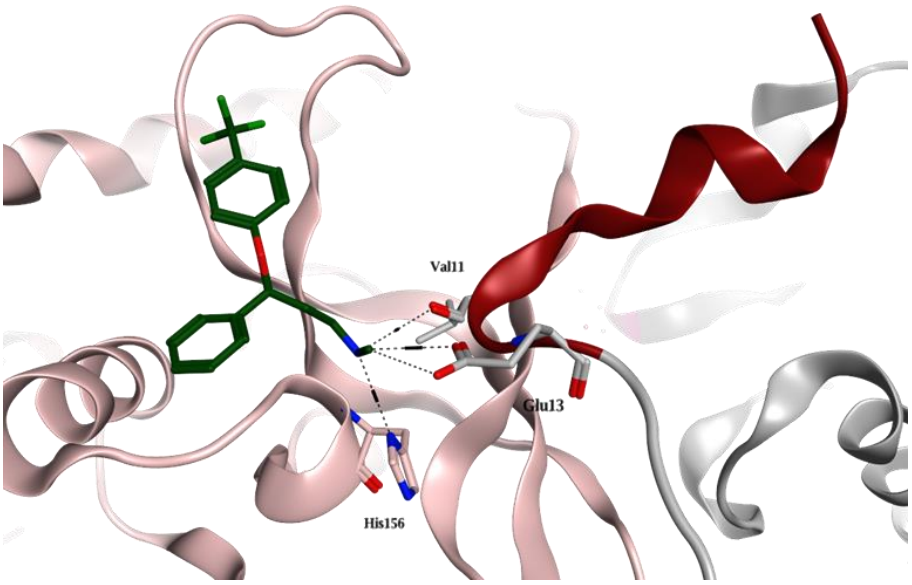

Figure 29. Characterization of fluoxetine interactions with LDH-1 via co-crystallization studies (PDB: 8S88). fluoxetine is located at the tetrameric interface between two subunits, and forms a salt bridge and hydrogen bonds with several residues including His156 and Glu-13, Val-11 which are located at the *N*-terminal arm, involved in the tetramerization process. Chain 4 is in light pink, chain 3 is in gray (*N*-ter 13AA in dark red). fluoxetine co-crystallize conformation is in green. Residues involved in the interaction with fluoxetine are shown. Figure was generated using the MOE software.

To better understand the discrepancy between the binding with LDH-1 and LDH-5, we decided to performed SAR *in silico* analysis through a series of docking simulations. Based on the previously obtained crystal structure, we used the molecular operating environment (MOE chemgroup) to dock fluoxetine on both LDH-1 and LDH-5, guided by the binding site observed in the co-crystallographic structure. Docking on LDH-1 was identical to the co-crystal structure, in addition to a pi-cation consistent with the binding trajectory observed in the co-crystal structure, which confirmed our *in silico*

model (Figure S9). Fluoxetine showed a higher score of ΔG = -5.78 Kcal/mol for LDH-5 and' LDH-1 having ΔG =-4,88 Kcal/mol (See Materials and Methods; Figure S10). The higher score for LDH-5 reflects the higher number of formed interactions (Hydrogen bonds with Glu14, Asn297, Lys131; CH-π Asn129; Pi-cation Arg156). This data provides structural basis for understanding the obtained biophysical results.

6.2.3 Cellular target engagement profiling of selected compound in Cancer Cell

As previously reported, fluoxetine and other compounds based on the same pharmacophore have demonstrated antineoplastic effects. Consistent with the reported IC_{50} range in the literature in antiproliferative assays against various cancer cell lines, our findings fall within the 15-25 µM range following 24 hours of treatment. Specifically, fluoxetine (HCT116 10.2 µM; SiHa 19.64 µM; MDA231 24.09 µM) (Figure S11).

To further analyze if the antiproliferative effect was partially due to LDH cellular inhibition, we set out to investigate LDH target engagement using cellular thermal shift assays in tumor cells, using fluoxetine as an example. In our assays[161], HCT116 cell lines were treated with fluoxetine at a concentration of 15 µM. The data obtained revealed that, compared to a melting temperature for LDH of around 64.7°C in cells, the melting temperature for LDH rises to 66.8°C upon treatment with fluoxetine, that is a ΔTm of 2.1°C (**Figure 30**). This increase in melting temperature of LDH-H, suggests that fluoxetine effectively bind LDH in cells.

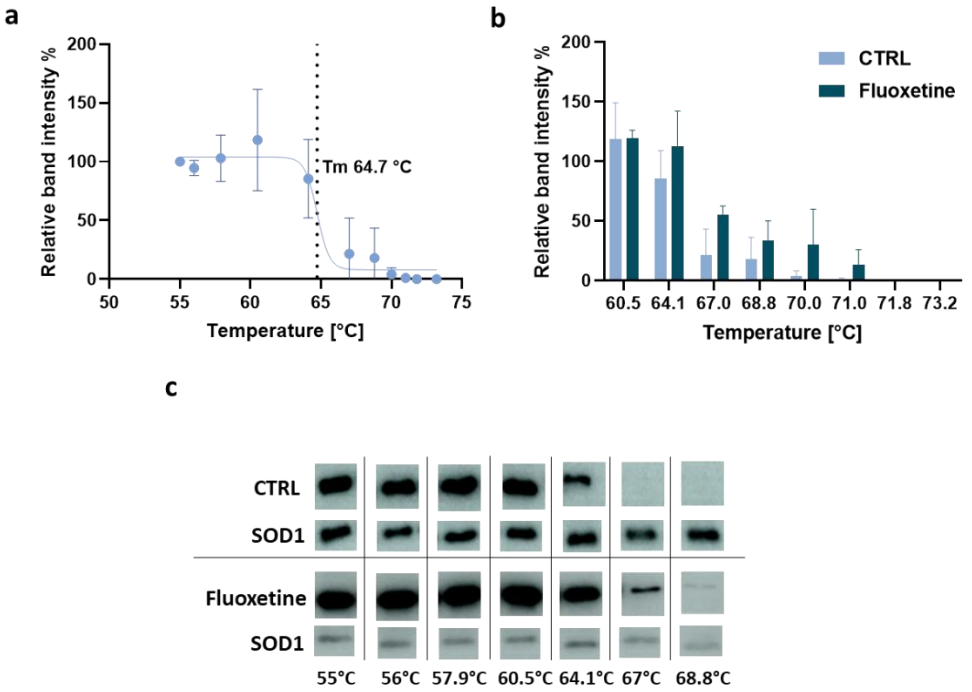

Figure 30. Cellular target engagement reveals the stabilization of fluoxetine, delineated as a function of the temperature applied during the heat treatment of HCT116 cells. Quantification was measured by Western blot band intensity. Data are provided as the average and standard error of mean (S.E.M.) from two independent experiments. a) Relative band intensity analysis was performed in the control (CTRL) assay, resulting in a Tm value of 64.73°C. b) Comparative analysis between control and treated samples, highlighting the specific temperature ranges where the fluoxetine-induced stabilization of LDH-1 occurs (Tm= 69.03°C). c) Western blot quantification of LDH-1 in HCT116 cell line treated with or without fluoxetine (15 µM, 0.2% DMSO).

6.3 Preliminary conclusion

In recent years, lactate dehydrogenases have garnered significant attention as potential targets in understanding cancer-related metabolic adaptations. However, LDHs possess a challenging-target active site, which lead to

obstacles in inhibitors development. To solve this challenge, previous works have unveiled an allosteric site at the oligomeric interface of the protein. Targeting this specific site has the potential to impact on LDH's tetrameric structure, therefore on the activity itself. With this work we aimed to identify small molecules able to bind the oligomeric state as a potential therapeutic target. We conducted a biophysical cascade, evaluating analogues of previously identified compounds belonging to the antidepressant and antihistaminic classes against LDHs isoforms. Among these compounds, we were able to identify fluoxetine and sertraline exhibiting notable affinity for LDHs and the ability to modulate protein's activity. These findings were confirmed by co-crystallization studies, *in silico* and NMR STD which provides structural insights into their bindings. Furthermore, we confirmed that fluoxetine binds to LDH-1 in cells using a cellular engagement assay. Collectively, this research not only expands our understanding of LDH's allosteric interactions but also displayed promising optimizations for future drug development. The study highlights the potential for repurposing existing compounds, previous structural modifications, for innovative therapeutic interventions in the context of cancer treatment and metabolic adaptations.

Contribution in the paper:

I conducted all NanoDSF, MST binding affinities, NMRSTD, enzymatic assays, dissociation/reassociation assays, cell viability assays, and cell engagement assays.

6.4 Experimental section

6.4.1 General

All reagents were purchased from chemical suppliers and used without purification. Structure conformity of fluoxetine was confirmed using NMR.

6.4.2 Protein production

Production of LDH-1, LDH-5 and LDH-Htr was performed from a previously described procedure [30]. Briefly, hLDHA, hLDHB, and hLDHBtr sequences were inserted into a pET-28a expression vector using NdeI and Bpu1102I restriction sites. Bacteria were cultured in Terrific broth (TB) medium with 50 µg/mL kanamycin and 34 µg/mL chloramphenicol at 37 °C until reaching an optical density of 0.8. Protein expression was induced with 1 mM isopropyl-β-D-1-thiogalactopyranoside (IPTG) at 20 °C for 20 hours. Cells were collected by centrifugation (5,000 rpm, 4°C for 25 min), suspended in lysis buffer (Tris-HCl 50 mM, pH 8.5, MgCl2 10 mM, NaCl 300 mM, imidazole 5 mM, and glycerol 10%), and sonicated. After centrifugation (4 °C, 10 000 rpm for 30 min), the soluble fraction was collected, 1 µL/mL of β-mercaptoethanol was added to the soluble fraction and recombinant proteins were purified using His-trap FF-crude columns following the manufacturer's instructions. Bradford method was used to measured protein concentration with Biorad Protein Assay Kit. Protein quality was assessed using sulfate−polyacrylamide gel electrophoresis (SDS−PAGE) with Coomassie brilliant blue as a staining agent.

6.4.3 Nano DSF

Nano DSF assays were performed as previously described [5]. Briefly, protein solutions (LDH-1, LDH-5, or LDH-Htr) were analyzed using a Tycho

NT.6 instrument (NanoTemper Technologies) at a concentration of 25 µg/mL, both with and without the addition of compounds in a range from 1 mM to 250 µM. The assessments were conducted in a buffer consisting of 50 mM sodium phosphate and 100 mM NaCl at pH 7.6. Following standard protocols, samples were loaded into capillaries and subjected to a temperature increase up to 95°C over 3 minutes, with fluorescence emission at 330 and 350 nm monitored. Melting temperatures were determined from the derivative of the fluorescence ratios (350/330 nm) as the temperature increased.

6.4.4 MST

MST measurements were performed as previously described [5]. Briefly, Nanotemper Monolith NT.115 instrument (Nano-Temper Technologies) was used to performed the assays. LDH-1, LDH-5 and LDH-Htr were labeled with the Monolith RED-NHS 2nd generation labeling dye according to manufacturer's instructions (Nanotemper Technologies). Measurements were performed in 50 mM sodium phosphate, pH 7.6, and 100 mM NaCl containing 0.01% Tween-20 in standard-treated capillaries (Nano- Temper Technologies) and in premium-treated capillaries. The ligands (NADH and compounds) were titrated in 1:1 dilution following manufacturer's recommendations. Experiments were performed in triplicates using 40% LED power, medium MST power, laser on-time 20 s, and laser off time 3 s. Compounds were evaluated for their thermophoretic pattern, and K_D were extracted from raw data at a 1.5 s-20 s MST on time depending on the compound MST profile.

6.4.5 enzymatic assay

The experiment was performed in 96-well plates using a Spectramax m2e spectrophotometer (Molecular Devices). Proteins were diluted to 1 µM in 0.01 M phosphate buffer (pH 7.6), 1 mM EDTA, and 0.05% BSA (w/v). 500 µl of protein solution was incubated with 1 mL of 0.25 M phosphate buffer (pH 7.6), 1 mM EDTA, and 0.05% BSA and 0.05% BSA (w/v) for 2 min. Afterwards, 30µl of the unfolded enzyme was added to 40 µL of 0.25 M phosphate buffer (pH 7.6), 1 mM EDTA, and 0.05% BSA containing different concentrations of the compounds. After 2h incubation room temperature, 10 µL of LDH-5 + inhibitor sample were transferred into Corning black polystyrene 96- well microplate containing 90 µL of 0.25 M phosphate buffer (pH 7.6), 1 mM EDTA, and 0.05% BSA (w/v) per well. Finally, 20 µL of substrate buffer containing 18 mM pyruvate and 1.8 mM NADH, for a final concentration of 3 mM pyruvate and 0.3 mM NADH, was then added to the mix to initiate the enzymatic reaction. NADH consumption was followed over time by measuring the fluorescence emission intensity ($\lambda_{excitation}$ = 340 nm, $\lambda_{emission}$ = 460 nm). To calculate the inhibitory activity of each compounds, the fluorescence emission intensity of the samples was compared directly to a positive control without inhibitors before reaching the plateau phase of the reaction.

6.4.6 Dissociation-reassociation assay

Dissociation-reassociation assays were performed as previously described [5, 49]. Briefly, the experiments were performed with opaque 96-well plates using a Spectramax m2e spectrophotometer (Molecular Devices). Proteins were diluted to 0.9 µM in 0.01 M phosphate buffer (pH 7.6), 1 mM EDTA, and 0.05% BSA (w/v). 500 µl of protein solution was incubated with 1mL of

0.1 M glycine buffer (pH 2.5) and 0.05% BSA (w/v) for 2 min. Afterwards, 30µl of the unfolded enzyme was added to 40 µL of 0.25 M phosphate buffer (pH 7.6), 1 mM EDTA, and 0.05% BSA containing different concentrations of the compounds. After 2h incubation room temperature, 10 µL of LDH-5 + inhibitor sample were transferred into a Corning black polystyrene 96- well microplate, containing 90 µL of 0.25 M phosphate buffer (pH 7.6), 1 mM EDTA, and 0.05% BSA (w/v) per well. Finally, 20 µL of substrate buffer containing 18 mM pyruvate and 1.8 mM NADH was then added to the mix to initiate the enzymatic reaction. NADH consumption was followed over time by measuring the fluorescence emission intensity ($\lambda_{excitation}$ = 340 nm, $\lambda_{emission}$ = 460 nm). To calculate the inhibitory activity of each compounds, the fluorescence emission intensity of the samples was compared directly to a positive control without inhibitors before reaching the plateau phase of the reaction.

6.4.7 NMR STD

NMR STD experiments were assessed as previously described [5]. Briefly, the experiments were conducted on a Bruker Ascend Avance III 600 MHz system equipped with a broadband cryoprobe. samples were prepared in PBS containing 2% deuterated DMSO, with LDHs concentrations ranging from 7.5 to 15 µM of monomer, depending on the experiment. Ligand binding was probed using a STD stddiffesgp.3 sequence with a 2 s saturation time. Water signal suppression utilized an excitation-sculpting scheme, and a 50 ms spinlock suppressed protein background signals. Experiments were carried out at 277 K to prevent protein degradation.

6.4.8 Co-crystallographic studies

LDH-H used for crystallization was produced and purified on a similar way than described in the previous section. The LDH-H sequence was cloned into a bacterial overexpression vector pET-24a (+) (Genscript) with NdeI and XhoI as restriction sites. The crystallization was performed using the sitting-drop vapor-diffusion method using the crystallization screening kit JCSG-plus^{TM} MD1-37 (Molecular Dimensions). The protein was concentrated at 9 mg.mL^{-1} in Tris buffer (50 mM Tris-HCl pH 7.6, 150 mM NaCl, 5% (v/v) glycerol), and incubated with NADH (disodium salt) and oxamic acid (3:1) for at least one hour on ice. Crystals were obtained after 10 days in 0.2 M lithium sulfate, 0.1 M sodium acetate pH 4.5 and 50% (v/v) PEG 400. Crystals were then flash-frozen in liquid nitrogen. Data collection was performed at Soleil synchrotron (Gif-sur-Yvette, France) on PROXIMA-1 beamLine at 100 K, using a Dectris EIGER X 16M detector at a single wavelength of 0.97857 Å. Data were processed with *XDS[188]* and the structure was solved by molecular replacement with Phaser[189] with a monomer of LDH-H (PDB entry: 1I0Z) [190]. Model building and refinement were performed with Phenix [191] and Coot [192]. Ligands in the structure were added using *eLBOW*.

6.4.9 *In silico* study

Docking simulations were conducted using the Molecular Operating Environment 2022 (MOE; ChemGroup) [193] employing the AMBER10 forcefield. Initially, the protein structure was prepared using MOE's quick prep protocol with (Din = 1, Dout = 80) for reaction-field electrostatics and a flat bottom tether (10.0 kcal/mol, 0.25 Å). The 2D structure of fluoxetine was imported as SMILES, and its energy was minimized. Subsequently, a

conformational search resulted in 65 conformations and was performed using default conditions, modified as follows: MM iteration limit of 1000 and planar systems as rigid bodies. Due to the structural similarity between LDHA and LDHB, the binding site was defined using the crystallographic structure of LDHB (PDB: 1X1X). Docking was executed using the Conformation import application on both LDHB (PDB: 1X1X) and LDHA (PDB: 1i10). The Triangle Matcher protocol was employed to generate 1000 poses, which were subsequently scored using the London dG scoring function. Following placement, energy minimization was achieved using the induced fit protocol, allowing sidechain movement with modified default parameters: tethering of 2Å, rigid planar systems, and 1000 iterations. Final refinement and scoring were conducted through the GBVI/WSA dG (Generalized-Born Volume Integral/Weighted Surface Area). The best structures were reported.

6.4.10 Cellular toxicity assays

SiHa cervix carcinoma cells and HCT116 colon cancer cell were routinely cultured in DMEM supplemented with 10% FBS and antibiotics. For the cytotoxicity assay, cells were seeded at a density of 5 x 103 cells/wells in DMEM media. Media were then aspirated and cells were incubated in fresh DMEM media containing 10 mM lactate, drugs at (1-100 µM) concentrations or vehicle (DMSO). Cells were grown for 24 h at 37°C before washing the cell with PBS and add staining crystal violet solution (0.25% Crystal violet dye, 20% methanol, ddH_2O qsq 100mL) 100 µl each well for 40min, finally washing with water. Add the lysing solution (100 µl 20% acetic acid in ddH_2O), 20 min agitation rt and measurement the optical density at 570 nm with an absorbance plate reader.

6.4.11 Cellular engagement assay

Cellular thermal shift assay was assessed as described in [150]. Briefly, 30 µl of DMSO (CTRL) and fluoxetine (15 µl) were added to 15 mL of 2 million/mL HCT116 cell line in DMEM (10% FBS, antibiotics, 10 mM lactate). After 1 h incubation rt into separate T75 flasks, centrifugation (300 g, 3 min at rt) to pellet the cells and discard the culture medium. Resuspension of the pellet with 15mL PBS and centrifuge (300 g, 3 min at room temperature). To the pellet add 1 mL PBS supplemented with protease inhibitors and distributed 100 µl of the resuspended cells into PCR tubes. Aliquots were heated individually into different endpoints (55-73.2°C). tubes were incubated 3min rt and then Snap-freeze in liquid nitrogen. The cells were Freeze-thaw the cells five times using liquid nitrogen and a thermal cycler or heating block set at 27 °C. The soluble fraction was separated by centrifugation (20,000 g, 20 min at 4°C) and protein concentration was quantified for each tube. Determination of protein concentration was carried out using Nano drop. Protein was denaturated by boiling, resolved by sodium dodecyl sulfate–polyacrylamide gel electrophoresis and transferred to 2-lm nitrocellulose membranes using a semi-dry Transblot Turbo system. After saturation of the membrane with 20% milk, membranes were probed with primary antibodies against LDHB Rabbit mAb (1:500). Primary antibodies were detected with antirabbit (1:5,000). The protein bands were detected by chemiluminescence using ECL Lumina Forte (Millipore) and a chemiluminescence detector Amersham imager-600.

6.5 Supporting information

Table S1. ΔTM values of selected compounds against LDH-Htr, LDH-5 and LDH-1. *N.D no transition detected.

Compound	ΔTM LDH-Htr (°C) [SD]	ΔTM LDH-5 (°C) [SD]	ΔTM LDH-1 (°C) [SD]
Amitriptyline	-1.9 [±0.173]	-0.4 [±0.15]	-0.6 [±0.05]
Agomelatine	N.D	N.D	N.D
Citalopram	N.D	-1.8 [±0.05]	-2.1 [±0.05]
Clomipramine	-6 [±0.05]	-0.7 [±0.05]	-0.6 [±0.05]
Desipramine	5.5 [±0.07]	-2.2 [±0.05]	-0.4 [±0.2]
fluoxetine	2.2 [±0.15]	-3.5 [±0.11]	-3.8 [±0.36]
Imipramine	5.4 [±0.05]	-2.5 [±0.05]	-1.4 [±0.2]
Mirtazapine	N.D	N.D	-1 [±0.1]
Norfluoxetine	0.2 [±0.2]	-1.1 [±0.11]	-1.3 [±0.15]
Nortriptyline	-3 [±0.7]	-1.3 [±0.1]	-1.2 [±0.05]
Sertraline	1.8 [±0.1]	-0.5 [±0.05]	-6.9 [±0.3]
Viloxazine	5.8 [±0.65]	-2.3 [±0.05]	-0.5 [±0.15]

Desloratadine	0.3 [±0.45]	-1.5 [±0.17]	-0.9 [±0.15]
Diphenhydramine	-0.2 [±0.2]	-0.6 [±0.1]	-1.8 [±0.25]
Hydroxyzine	N.D	-1.1 [±0.15]	-2.9 [±0.11]
Levocetirizine	0.8 [±0.17]	-0.3 [±0.05]	-1.46 [±0.3]
Loratadine	N.D	0.3 [±0.05]	N.D
Meclizine	0.6 [±0.2]	0.2 [±0.25]	0.1 [±0.2]
Rupatadine	0.5 [±0.15]	1.5 [±0.1]	-0.9 [±0.15]

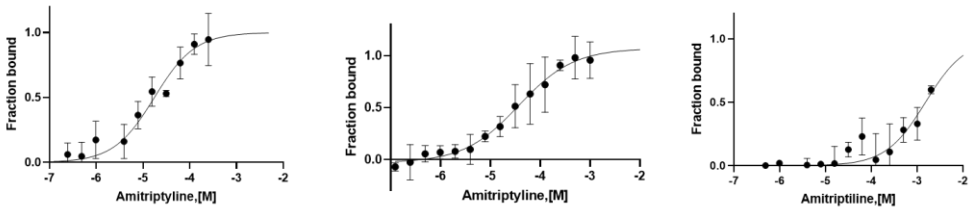

Figure S2. MST profile of Amitriptyline. Binding curves of **Amitriptyline** interacting with LDH-Htr (left), LDH-5 (center) and LDH-1 (right). (n = 3)

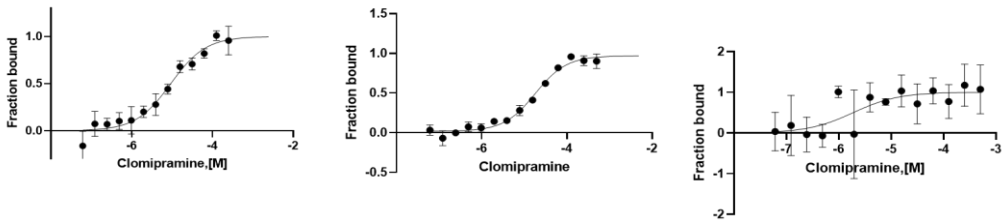

Figure S3. MST profile of Clomipramine. Binding curves of **Clomipramine** interacting with LDH-Htr (left), LDH-5 (center) and LDH-1 (right). (n = 3)

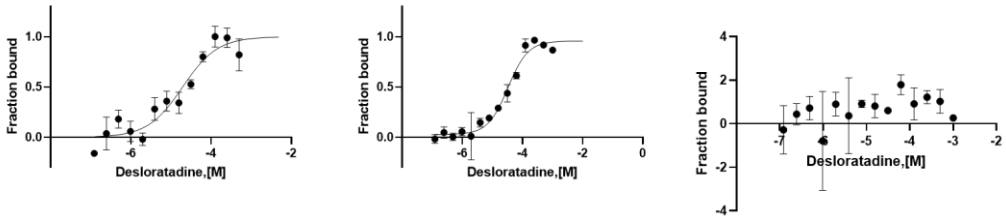

Figure S4. MST profile of Desloratadine. Binding curves of **Desloratadine** interacting with LDH-Htr (left), LDH-5 (center) and LDH-1 (right). (n = 3)

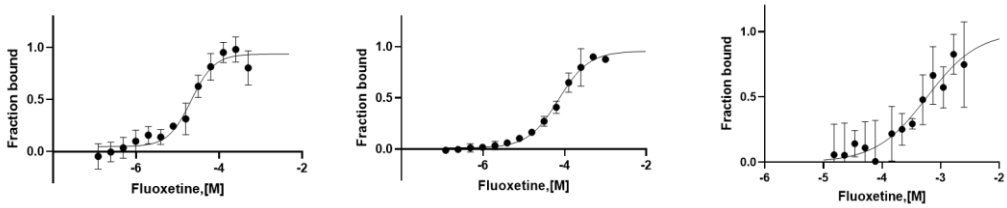

Figure S5. MST profile of fluoxetine. Binding curves of **fluoxetine** interacting with LDH-Htr (left), LDH-5 (center) and LDH-1 (right). (n = 3)

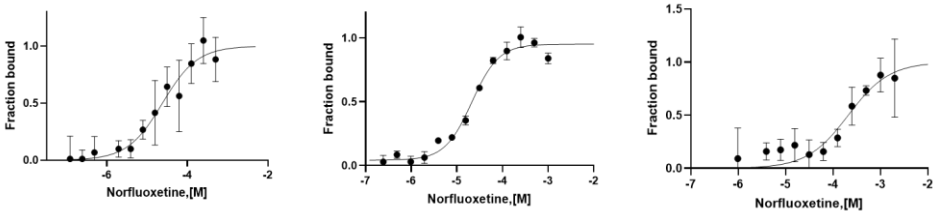

Figure S6. MST profile of Norfluoxetine. Binding curves of **Norfluoxetine** interacting with LDH-Htr (left), LDH-5 (center) and LDH-1 (right). (n = 3)

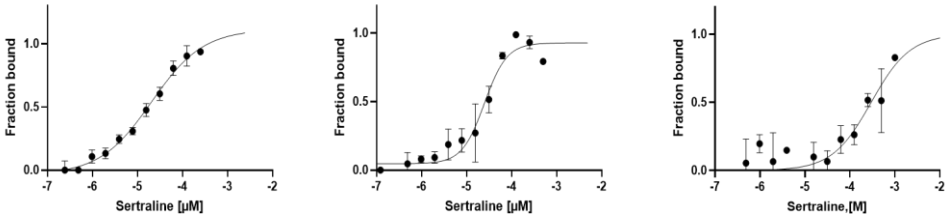

Figure S7. MST profile of Sertraline. Binding curves of **Sertraline** interacting with LDH-Htr (left), LDH-5 (center) and LDH-1 (right). (n = 3)

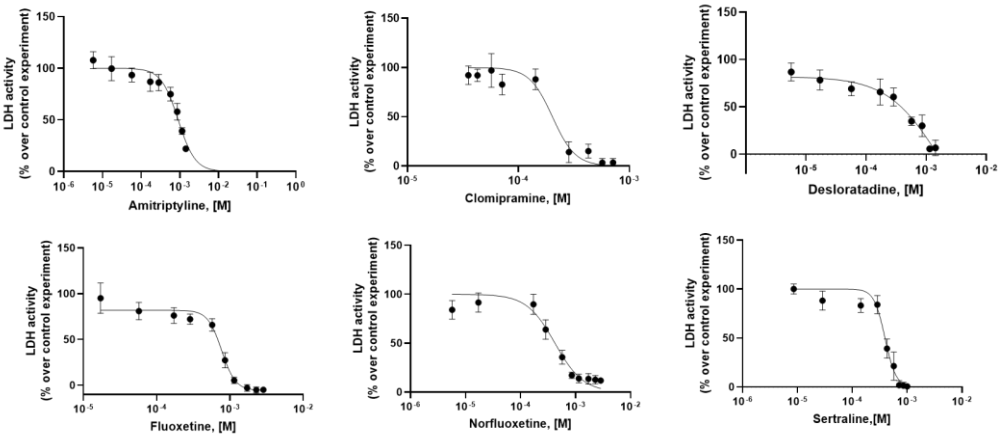

Figure S8. LDH-1 activity assay after denaturation/tetramer reconstitution and small molecules impact in this process. a) Inhibition curves of LDH-1 activity treated with dilution series of amitriptyline IC_{50} = 906 µM [CI95´% 844-969], clomipramine IC_{50} = 203 µM [CI95´% 183-222], desloratadine IC_{50} = 1.6 Mm [CI95´% 889-4236], fluoxetine IC_{50} = 769 µM [CI95´% 683-813], norfluoxetine IC_{50} = 421 µM [CI95´% 384-461] and sertraline IC_{50} = 393 µM [CI95´% 370-417].

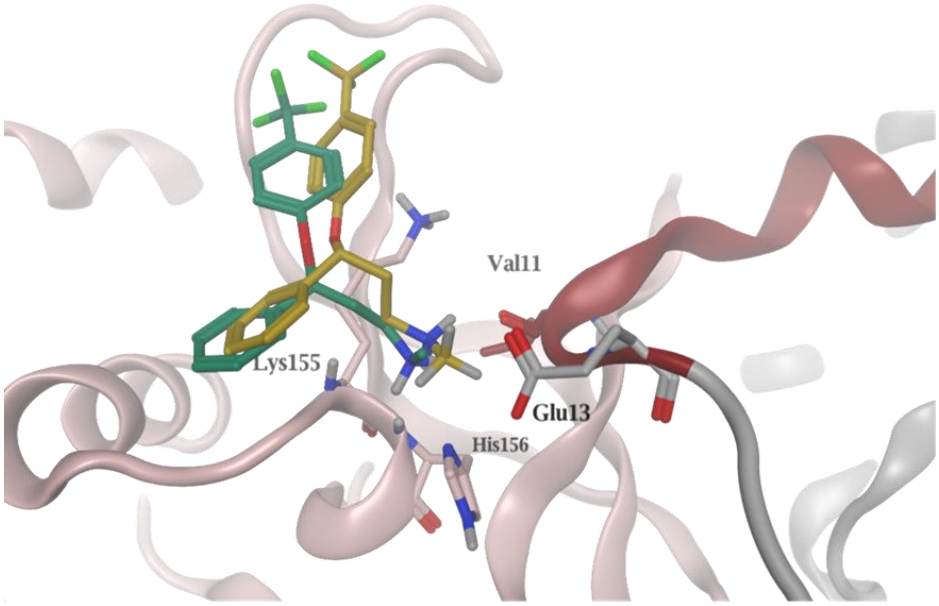

Figure S9. Validation of the docking model. LDH-1 Superimposition of fluoxetine docked structure in yellow and crystallographic structure in green Chain 3 is in gray (dark red = *N*-ter 13AA), chain 4 is in light pink. Figure was generated using the MOE software.

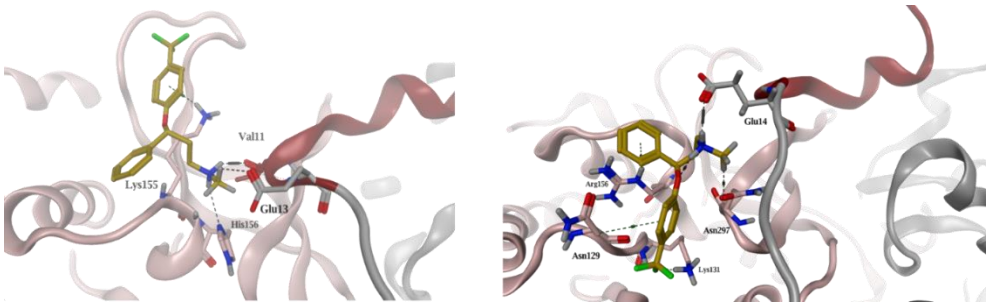

Figure S10. Validation of the docking model. LDH-1 (left) and LDH-5 (right) fluoxetine docked structure in yellow Chain 3 is in gray (dark red = *N*-ter 13AA), chain 4 is in light pink. H bonds in dark gray Pi-H interactions in green – bond strengths are illustrated with cylinders. LDH-1: dG (GBVI/WS)=-4,88. LDH-5: dG (GBVI/WS)= -5,78. Figure was generated using the MOE software.

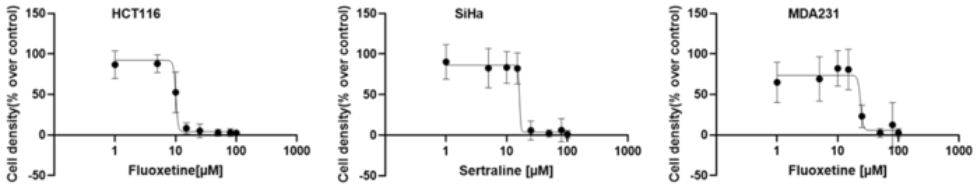

Figure S11. Dose-Response Curve of fluoxetine on Cell Viability. The x-axis represents increasing concentrations of fluoxetine and Sertraline, while the y-axis depicts the relative cell viability (%). IC_{50} Values of fluoxetine HCT116 10.2 µM; SiHa 19.64 µM; MDA231 24.09 µM. Cell were seeded at a density of 5 x 103 cells/wells and incubated with various ligand concentrations (1-100 µM, 0.2% DMSO) for 24h. Each point represents the mean of three independent experiments.

7. General discussion and perspectives

7.1 Major outcomes of the thesis

The main objective of this PhD thesis was to identify original small molecules acting as homomeric binders of LDHs, hence inhibiting protein activity by impacting is native active tetrameric structure. As major outcomes, we designed an innovative screening method consisting in using different biophysical tools to probe the LDH tetrameric interface. This strategy led to the identification of different hits (**Figure 31**) with confirmed binding to LDHs in classes of FDA-approved antidepressant and antihistaminic drugs.

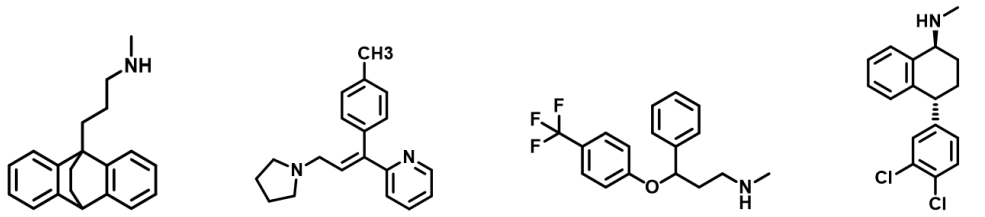

Maprotiline ***K_D 37 µM*** ***IC_{50} 970 µM***

Triprolidine ***K_D 79 µM*** ***IC_{50} 7.9 mM***

Fluoxetine ***K_D 21 µM*** ***IC_{50} 447 µM***

Sertraline ***K_D 20 µM*** ***IC_{50} 335µM***

Figure 31. Identified inhibitors of LDHs.

LDHs play critical roles in cancer development, making them appealing targets for therapy [1-3]. Challenges in targeting LDHs stem from their polar active site shared with other dehydrogenases and their high cellular expression levels, which hinder effective *in vivo* inhibition. LDH activities are strictly linked with a correct subunit association where dimers are anchored *via* specific interaction sites. These structural features initially

supported our willingness to target the oligomeric state as a novel pathway to develop LDH inhibitors. The most promising hits were effective *in cellulo*, suggesting the possibility of yielding long-term clinical outcomes.

Targeting PPIs offers numerous advantages, presenting promising solutions for inhibiting targets that were previously considered difficult to address [30, 39, 127]. LDHs are among these: identifying an orthosteric PPI site holds the potential for better drug-like features compared to active-site inhibitors, with improved ADME profiles and selectivity towards other NAD(H)-dependent enzymes [1, 127]. Previous work conducted by our laboratory identified site 1 (residues 1-19) and site 2 (55-77) participating in the oligomerization process of LDHs, and identified stapled peptides specifically targeting these sites [30, 39]. This structural elucidation not only contributed to our comprehension of the molecular determinants governing the LDH tetrameric interface, but it also provided essential pharmacological tools for the prospective development of compounds in the future. It allowed for substoichiometry inhibition, which addresses the challenge of a high LDH cellular concentration [109, 127]. Comparatively, traditional inhibitors, despite often demonstrating nanomolar affinity, struggle to surpass the millimolar threshold for *in cellulo* inhibition.

As major outcome of the present work, we designed a cascade of biophysical methods to efficiently identify LDH binders from a diverse chemical subset [5]. The use of NanoDSF, MST and NMR STD was instrumental for the characterization of five compounds inducing changes in LDH denaturation profiles. Particularly noteworthy were maprotiline and triprolidine, FDA-approved antidepressant and antihistaminic drugs, respectively, sharing a similar pharmacophore and demonstrating promising

competition with native LDH subunits for the tetrameric interface. The observed structural similarity likely underscores the hydrophobic LDH tetrameric interface capacity to accommodate large and lipophilic molecules. This stands in stark contrast to LDH small and polar active sites, emphasizing the potential of our approach to uncover more druggable ligands. Notably, certain antidepressant and antihistaminic dugs are associated with a reduced cancer risk and antineoplastic effects [179, 181, 182]. Building on these observations, we further characterized a series of FDA-approved drugs among these two classes to elucidate their cancer-related mechanisms and to validate LDHs as potential primary targets. In-depth analyses demonstrated the impact of these drugs on the LDH tetramerization process. Particularly promising, an *in cellulo* target engagement assay with antidepressant fluoxetine provided compelling evidence of binding with LDH-1 in human HCT116 colon cancer cells. The successful co-crystallization of fluoxetine bound to LDH-1 confirmed predicted binding at the tetrameric interface. A summary of this workflow is shown in **Figure 32**. Overall, our research unveiled a novel pathway for LDH inhibition, presenting exciting possibilities for designing more effective and specific therapeutic interventions. It also opens avenues for potential modifications of FDA-approved drugs, enabling the creation of a new library of molecules targeting the LDH tetramerization site.

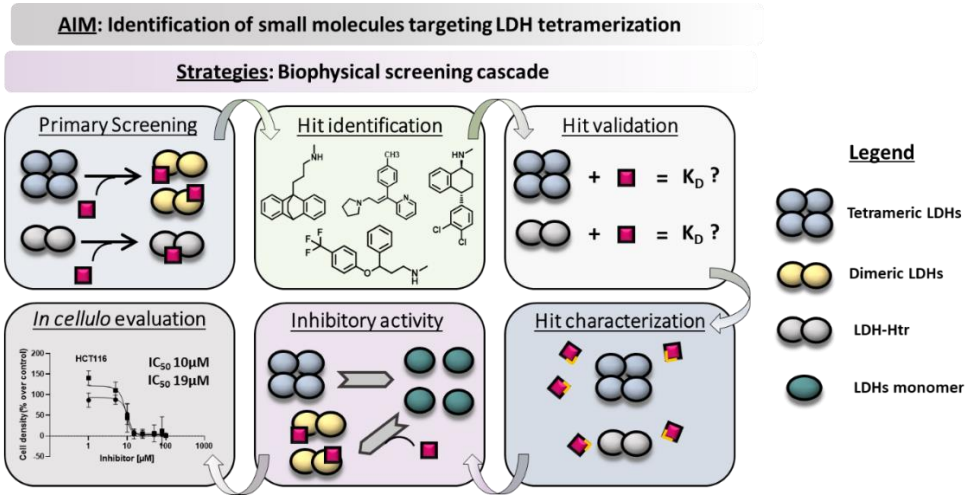

Figure 32. Overview of the thesis workflow. We began by conducting a biophysical screening, employing a range of methods to analyze molecular interactions. Promising candidates from this screening were then subjected to *in vitro* inhibition assays to evaluate their potential to inhibit LDHs. Those showing potential, advanced to *in cellulo* assessment, where their efficacy and specificity within cells were examined.

Among the findings presented in this work, the primary achievement is the validation of the strategy of targeting the oligomeric folding of LDH proteins, a concept previously conceptualized in our laboratory. As mentioned in the introduction of the thesis [38, 49], various research groups are now pursuing the identification of this new class of LDH inhibitors. With our contribution, we are introducing innovative methodologies, techniques, and workflows to advance toward the same objective. This groundbreaking approach holds great potential in overcoming traditionally considered challenging features of this protein, offering exciting prospects for the future development of drug discovery.

7.2 Challenges in the quest for LDHs inhibition

The study and development of novel LDH inhibitors was not a straightforward process, and the current thesis project ended with some unresolved questions. This section aims to give an overview on the complexities and challenges associated with this pursuit, and offers an examination of potential solutions and insights.

7.2.1 Probing disruption: Assessing the influence of identified Hits on LDH activity and structure

It was a requirement of our project to not only demonstrate binding to and inhibition of LDHs, but also to study the binding site of the compounds to confirm that their mechanism of action was *via* tetramer disruption. This task was particularly challenging due to the scarcity and complexity of techniques that allow measurements of this nature (see Chapter 3). We addressed binding location with various techniques and the use of a previously engineered LDH-Htr construct [30], observing binding of the identified compounds at the tetrameric interface, in line with our expectations. Co-crystallization studies further showed that the binding of fluoxetine occurred at the location of the *N*-terminal arm. To fulfill our primary aim, a question was addressed: Can binding at the tetrameric interface exert enough potency to compete with the native *N*-terminal arm, impacting the folding of tetrameric LDH and disrupting it into lower oligomeric populations? Classical enzymatic assays were conducted to confirm this inhibitory potential. However, as shown in **Figure 33** and in the results section, there was no inhibitory activity of the tested drugs against the native tetrameric forms of LDHs, contradictory to the LDH destabilization profiles induced by the compounds in NanoDSF. This observation may be explained by the possibility that these molecules do not

entirely inhibit LDH folding, as indicated by crystallization studies. Instead, they would engage in interactions that weaken the tetramer. In fact, they could interact with LDH during the folding process that follows translation in cells, primarily impeding the formation of protein quaternary structure and, consequently, inhibiting its function.

To address this hypothesis, we used an enzymatic assay previously described by Nadal-Bufi *et al.* [49, 193], which involves denaturing tetrameric LDHs to partially unfolded monomers in acidic conditions. Following denaturation, neutral pH was restored in the presence or absence of the studied compounds, allowing the reassociation of LDH in its native tetrameric structure. After incubation, the protein was allowed to renature at room temperature, and its enzymatic activity, corresponding to the recovery of its proper quaternary structure, was monitored. Using this technique, all identified hits exhibited inhibitory activities against LDHs. It confirmed our hypothesis of folding inhibition by the compounds, but not that they impacted LDH oligomeric states. We therefore further tested whether the molecules were able to break tetramers. This is why we used fluoxetine against purified LDH-5 as an example to repeat the dissociation-reassociation assay in the presence of a cross-linker glutaraldehyde (GTA) in the reassociation steps, followed by SDS-PAGE. The gel revealed the presence of two different populations (dimers and tetramers), indicating that fluoxetine can inhibit tetramer oligomerization, leading to dimers. An analogous experiment conducted on SDS-PAGE gel but without the dissociation-reassociation step and using Bis(sulfosuccinimidyl) suberate **(**BS3) as a cross-linker yielded surprising results: fluoxetine (2.2 mM) was strong enough to disrupt native LDH-1 tetramers (**Figure 33**). This observation contrasted with the previous

one that a dissociation-reassociation step was necessary for fluoxetine to inhibit LDH activity. Unlike GTA, which can create longer and more flexible cross-links due to its ability to react at multiple sites, BS3 forms shorter, more rigid links because of its defined spacer arm. Although they have different reactivities, both crosslinkers not only react with primary amines in lysine residues, but could also react with the secondary amine of fluoxetine, limiting its availability to react with the protein. At least two strategies could be proposed to address the issue. First, fluoxetine could be tested with an unrelated oligomeric protein. If fluoxetine does not react with the crosslinker, then it should impact oligomerization. Second, a native gel could be used to bypass the need for a cross-linker.

To further explore this issue, we are currently collaborating with Professor Joris Messens at Vrije Universiteit Brussel (VUB) for Mass Photometry (MP), a method enabling label-free single molecule detection and mass measurement in solution through light scattering [194] (see Section 3.1.4). We used MP to study LDH and LDH-Htr enzymes in the presence of tested ligands, which was never done before to our knowledge to study inhibitors. Regrettably, the results obtained with fluoxetine and LDH-5 exhibited inconsistencies. This lack of reproducibility was likely linked to the limited solubility of fluoxetine, leading to its precipitation. This underscores the importance of addressing solubility challenges when using MP for inhibitor studies in solution.

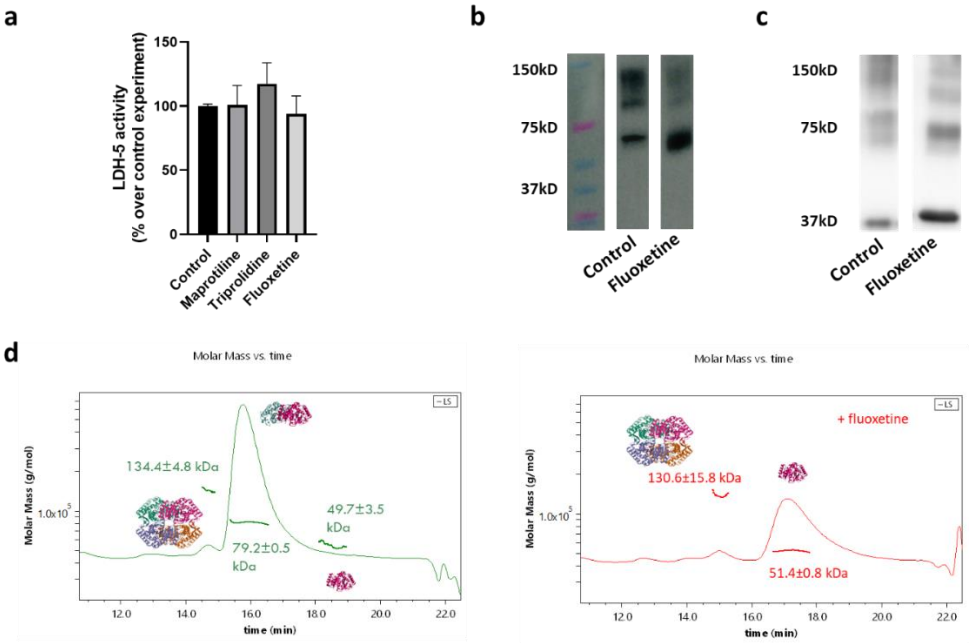

Figure 33. Validation Strategies: Assessing the influence of identified compounds on LDH structures and populations. (**a**) LDH-5 activity upon exposure to maprotiline (1 mM), triprolidine (1 mM) or fluoxetine (2.2 mM). Untreated LDH-5 was used as control (n = 3). (**b**) SDS-PAGE of pH-induced dissociated (glycine buffer 2.5 pH, 2 min) and reassociated (PBS buffer 7.6 pH, 2 h) LDH-5 (1.3 µM) treated with fluoxetine (2.2 mM). After treatment, samples were cross-linked with glutaraldehyde 0.5% to covalently bind interacting LDH-5 subunits. (**c**) SDS-PAGE of LDH-1 (1 µM) with fluoxetine (0.62 mM). After treatment, samples were cross-linked with BS3 (0.33 mM). (**d**) SEC-UV-MALS-dRI performed with LDH-1 L7A (25 µM) and fluoxetine (1 mM). The mobile phase was 50 mM Na-PB, 200 mM Arginine and 5% MeCN at pH 7.6 for BioResolve and 25 Na-PB, 100 mM Arginine for Xbridge columns. Abbreviations: Vi, initial velocity; RFU, relative fluorescence unit. (***c*** *shows unpublished data obtained by Perrine Savoyen and* ***d*** *by Magdalena Wierzbicka in our lab*).

Another collaboration with Professor Marian Fillet of the University of Liège was initiated to use size-exclusion chromatography with multi-angle

light scattering (SEC-MALS). SEC-MALS separates biomolecules by size and measures their absolute molecular weight, providing precise insights on their size distribution and molecular weight in solution [149] (see Section 3.1.5). An interesting observation was made by Dr. Magdalena Wierzbicka from Professor Fillet laboratory using LDH-H L7A and LDH-H L71A, *i.e.*, LDH-H mutants lacking crucial residues at Site 1 and Site 2, respectively: the dimeric form of LDH-H L7A, but not LDH-H L71A, dissociated to monomers when treated with fluoxetine (*unpublished data*). This suggested that fluoxetine has specificity for Site 1, as previously anticipated in co-crystallization studies and by biophysical characterization. The next step, which already started, is to replicate the dissociation-reassociation assays and running the proteins on SEC-MAL to evidence different oligomeric LDH populations.

7.2.2 Is the anti-proliferative effect of our LDH inhibitors in cancer cells LDH-dependent?

A critical aspect in concluding this project is the observed antiproliferative effects of the identified hits in the complex context of cancer cells, which we attributed to their binding to LDHs. In parallel with our *in vitro* investigations, a cellular engagement assay was used to confirm binding. Yet, a pivotal and unanswered question persists: do the antiproliferative effects on cancer cells indeed result from a binding of the identified hits with LDHs? An intriguing possibility is that hits, seemingly inert against the purified native protein *in vitro*, might have a pronounced impact *in cellulo*. It is important to recognize that, within cells, a delicate equilibrium exists among various LDH populations. An LDH-binding agent could potentially disrupt this

equilibrium, hindering tetramer formation and, consequentially, inhibiting LDH activities.

In summary, the journey of this PhD thesis encountered challenges in inhibiting LDH activities by focusing on the tetramerization domain as a target. The compounds that we identified exhibited binding to the proteins, confirming interaction at the designated sites. In my opinion, the observation that binding influences protein folding, subsequently impacting their activities *in vitro*, is a significant achievement. The remaining question is whether this interaction results in protein disruption. Nonetheless, *via* an innovative workflow, we established a proof of concept for LDH inhibition, highlighting hits that structurally impact the targeted site. This sets the stage for the development of more potent inhibitors in the future. Next section explores the perspectives and potential implications of our findings.

7.3 Perspectives

Overall, this work opens the door for selective LDH inhibition, which in medium to long term could be converted in the market. The realization of this potential involves implementing numerous optimizations and conducting additional essential experiments. Several perspectives are outlined to guide the future trajectory of this work.

7.3.1 Probing metabolic shift unveiling the impact of LDH inhibition.

To further enhance the narrative, after having confirmed that certain FDA-approved drugs act as LDH binders, it is compelling to investigate their impact on cellular metabolism. Indeed, previous sections of this thesis have underscored the role that LDHs play in several metabolic pathways that are

crucial for both physiological and cancer cell sustenance. Inhibiting LDHs is thus expected to alter the production of intermediates and metabolites in these metabolic pathways.

Of particular interest in this context is the maintenance of the ratio $NADH/NAD^+$, a parameter influencing various cellular processes and critical for cancer cells proliferation and survival [52, 195-197]. Lactate biosynthesis by LDHs serves for the regeneration of NAD^+ to maintain glycolysis at a high rate in hypoxic and proliferating cancer cells. Given this tight correlation between LDH activity and the $NADH/NAD^+$ ratio, it is now warranted to document the effects of LDH inhibitors. In pursuit of this objective, the $NAD^+/NADH$ ratio must be determined in different malignant and non-malignant cell lines subjected to treatment with our identified hits. For what concerns cancer cells, model selection has to be strategic, representing the oxidative population, for example the previously used HCT116 human colon cancer cell line, and the glycolytic population, represented, *e.g.*, by MDA-MB-231 triple negative breast cancer cells [198]. We anticipate distinct responses based on metabolic preferences. Inhibiting LDH-5, prevalent in glycolytic cancer cells, is expected to disrupt NAD^+ oxidation, leading to an increase in the $NADH/NAD^+$ ratio. Conversely, inhibiting LDH-1, more abundant in oxidative cancer cells, is likely to decrease the $NADH/NAD^+$ ratio [3].

Importantly, our approach aligns with a pan-LDH isoform inhibitor strategy. With this aim, the use of spheroids could be valuable for validating pan-LDH inhibitors across both glycolysis and OXPHOS in cancer cells, as they closely mimic tumor architecture and microenvironments, offering a physiologically model for studying drug responses [199]. LDH inhibitors

could disrupt the balance between oxidative and hypoxic cells within spheroids, leading to alterations in survival, proliferation, growth, and invasion.

To gain more insights into the metabolic alterations resulting from LDH inhibition by the inhibitors that we identified, comprehensive approaches, such as metabolomics and U-^{13}C-glucose tracer studies, can be used [200]. These methodologies have already demonstrated their efficacy in elucidating the impact of LDH inhibition on cellular metabolism, providing information on the dynamic metabolic shifts occurring across cancer cell populations [201, 202]. For example, Dutta P. *et al*. [201] showed that LDH-5 inhibitor FX11 decreased the conversion of ^{13}C-pyruvate to lactate, indicating that ^{13}C-pyruvate reduction to lactate could serve as a biomarker of LDH-5 inhibition. Incorporating ^{13}C-labeled lactate uptake and metabolomics could offer further insights into LDH-1 inhibition in oxidative cancer cells. It could be interesting to effectively track metabolites like lactate and pyruvate directly impacted by LDHs activities. Metabolites like alanine and serine, intricately connected to glycolysis, act as sensitive indicators for disruptions in these metabolic pathways [25, 203]. Additionally, an assessment of TCA cycle intermediates, such as citrate, isocitrate and malate, would provide insights into the repercussions of LDH inhibition on mitochondrial metabolism. These metabolites could collectively serve as robust markers, facilitating a comprehensive validation of LDH inhibition and offering broader insights into the intricate network of pathways that could be affected by the therapeutic intervention.

7.3.2 Optimization of fluoxetine for a novel library of small molecules inhibitors

Fluoxetine, primarily known as an antidepressant, exhibits binding affinity not only to its intended targets, serotonin transporters (SERTs), but also demonstrates non-specific interactions with LDHs. Given the risk of unintended side effects associated with non-selective binding to various targets, a perspective lies is to strategically modify fluoxetine and the other identified inhibitors to create novel molecules that would not only be more specific, but also more effective against LDHs. For that aim, I believe that exploiting the crystallographic structure obtained from the co-crystallization study is key to visualize the interactions between fluoxetine and LDH-H. A Van der Waals surface analysis (**Figure 34**) already proved to be valuable in dissecting atomic-level details of binding interactions. By examining fluoxetine surroundings, we identified steric hindrance, located binding pockets, and evaluated the overall compatibility between fluoxetine and LDH-1. The highlighted pockets in **Figure 34**, characterized by lipophilic and hydrophilic features, suggest opportunities for structural enhancements. One conceivable modification involves the branching of an ethyl or propyl chain, to optimize binding within the yellow-highlighted pocket in the figure. This modification could be coupled to an elongation of the existing aliphatic chain, aiming to minimize the distance between the secondary amine and Glu-13 of the *N*-terminal arm. Finally, to better occupy the hydrophilic environment highlighted by the "green pocket", the addition of a polar group could be considered, extending the chain containing the CF_3 group. These proposed modifications are poised to refine the interaction profile and enhance the binding affinity of fluoxetine with LDH-1.

Fluoxetine exhibits an octanol-water partition coefficient (LogP) value around 3.9 to 4.2 and demonstrates moderate solubility in water (14 mg/mL at room temperature). The proposed chemical modifications, such as adding an ethyl or propyl chain and a polar -OH group, have been assessed using the ChemDraw software. Despite these structural enhancements, the predicted LogP values consistently remain around 3.8 to 3.9. While a primary objective is to enhance the affinity between fluoxetine and LDH-H, these modifications could also positively impact solubility.

This analysis ensures that any chemical adjustments to fluoxetine maintain its solubility characteristics, ensuring effective drug delivery and therapeutic efficacy in (pre)clinical settings. In my opinion, such approach is very relevant for the development of novel molecules that can exert a more targeted and potent antineoplastic effect against LDHs.

It is important to note that several drugs of our selected library, particularly those with cationic amphiphilic properties, have the potential to induce phospholipidosis [204, 205]. It can be detected using various biophysical and imaging techniques, such as electron microscopy, fluorescence-based methods and MS, which can collectively help to quantify lipid changes within cells. Considering the well-established safety profiles and therapeutic windows of many antidepressant and antihistaminic drugs, we could consider future *de novo* designs within these molecule classes while effectively addressing phospholipidosis-related risks in novel applications.

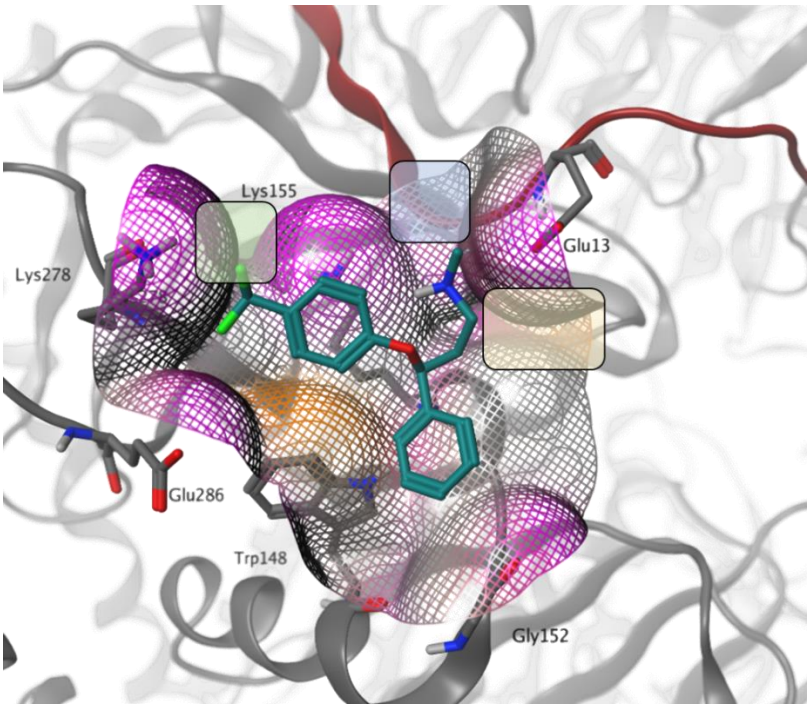

Figure 34. Van der Waals mapping of LDH-1: Insights from fluoxetine co-crystallization revealing potential chemical modification pockets for enhanced interactions. The LDH-H Van der Waals surface was generated within 4.5 Å around the ligand using the MOE software. Colors represent the degree of lipophilicity (orange, white and magenta correspond to lipophilic, neutral and hydrophilic surfaces, respectively). The pockets, where modification of fluoxetine can occur, are highlighted by green, blue and yellow rectangles. Reported are the main residues for the interactions with fluoxetine (Glu-13, Lys-155, Lys-278, Glu-286, Trp-148 and Gly-152).

7.3.3 Unlocking synergy: Development of dual inhibitors for enhanced LDH targeting

Several new allosteric or homomeric inhibitors of LDHs have been discovered, including some by our team [30, 39, 49, 121, 125, 126]. All must be optimized. Allosteric inhibitors induce conformational changes, while

homomeric disruptors interfere with the assembly of subunits, collectively leading to a more potent and synergistic inhibition of LDH activity. Having already some of these inhibitors and others being commercially available, we could use biophysical methods, such as NanoDSF, MST and NMR STD, to compare their potencies and study possible synergistic effects against LDHs. Preliminary results have been produced by Dr. Nadal-Bufi in our lab (**Figure 35**), who exemplified a synergic effect between fluoxetine and cGmC9 to inhibit LDH-5. Both compounds are homomeric inhibitors, and they have close binding sites at the dimer interface. The figure illustrates the noteworthy observation of the proximity of the binding sites of the two inhibitors. In the conducted test, the protein was first dissociated in an acidic pH and then reassociated in slightly basic pH after treatment with the inhibitors individually or combined. The results clearly indicate a synergistic effect, as evidenced by a lowered IC_{50} compared to individual treatments. Pursuing this insight, the design of a novel compound capable of interacting simultaneously with both sites holds the potential for increased specificity against LDHs and a significant enhancement of the affinity for the protein. This prospect is not distant, as our lab is well-equipped with the necessary methods for synthesizing, characterizing, and evaluating such compounds. To further elucidate the impact of the new molecule, I propose to couple *in vitro* and *in cellulo* evaluations with SEC-MALS, offering a comprehensive analysis of its effect on LDH tetramers. Expanding on the "dual inhibitor" concept, consideration can be given to Site 1 and Site 2 inhibitors, given their close proximity. Using peptide-peptide or small molecule-peptide as inhibitors may bring a substantial increase in affinity.

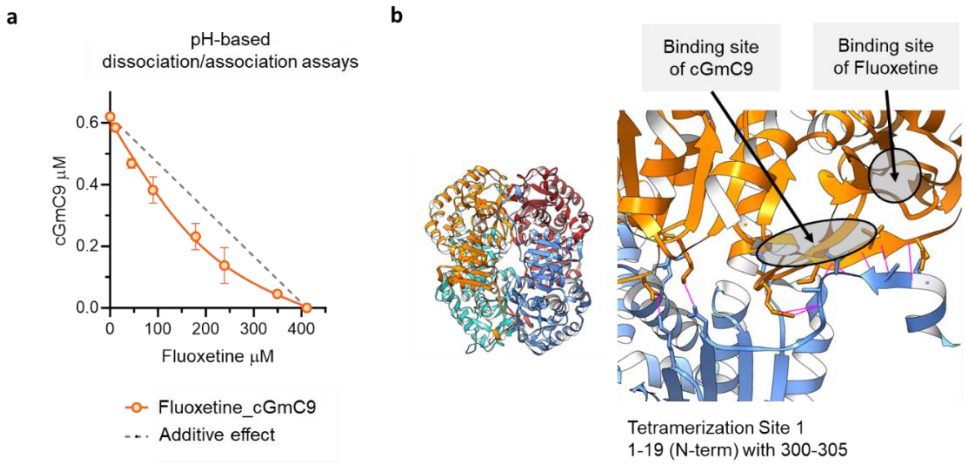

Figure 35. Synergistic inhibition of LDH-5 by Fluoxetine and cGmC9: preliminary data (a) Concentration of each compound required to achieve 50% of activity (IC_{50}) in pH-based dissociation/association assays (orange). The grey dotted line represents the expected concentrations of both inhibitors if they would interact with a mere additive effect, while the orange line shows the observed synergistic effect with a lower IC_{50}. (**b**) General view of the tetrameric structure of LDH-1 (left) and close-up view of the dimer:dimer interface (right). The binding sites of cGmC9 and fluoxetine are shown in grey circles. *Figure and data from Ferran Nadal-Bufi (unpublished).*

Additionally, we recently obtained co-crystal structures of LDH-1 with triprolidine, revealing its binding in a region similar to that of fluoxetine, although the exact positions and interactions differ (**Figure 36**). The triprolidine co-crystal shows binding at the tetrameric interface, involving hydrogen bonds with Met280 and Asn305. This binding region is crucial for enzyme tetramerization, suggesting that triprolidine can significantly impact the structural and functional properties of LDH-1.

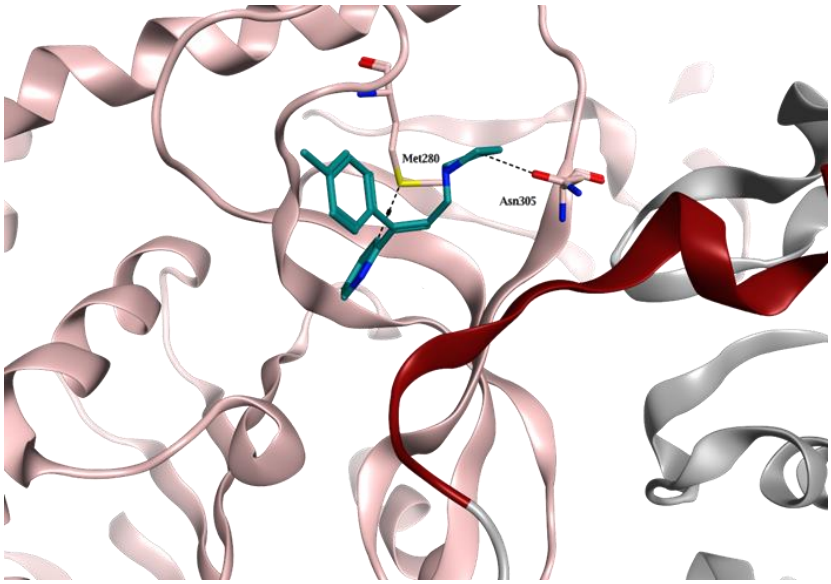

Figure 36. Co-crystal structure of LDH-1 with triprolidine at the tetrameric interface. The co-crystal structure of LDH-1 bound to triprolidine (light blue) reveals its binding at the tetrameric region. Triprolidine forms hydrogen bonds with Met-280 and Asn-305, marked by black dashed lines. Chain 4 is depicted in light pink, chain 3 in gray, and the *N*-terminal arm is highlighted in red. Crystallization was performed using the sitting-drop vapor-diffusion method with the JCSG-plus MD1-37 crystallization screening kit. Crystals were flash-frozen in liquid nitrogen, and data collection was performed at the Soleil synchrotron. Data were processed with XDS, and the structure was solved by molecular replacement with Phaser using a monomer of LDH-H (PDB entry: 1I0Z). Model building and refinement were performed with Phenix and Coot, with ligands added using eLBOW.

Comparatively to triprolidine, fluoxetine forms hydrogen bonds with His156 and a salt bridge with Glu-13. Moreover, competition experiments with macrocycle 7, which mimics the *N*-terminal arm of LDH-1, showed a substantial reduction in the saturation transfer difference (STD) signal of triprolidine (~ 40%, **Figure 18a**). This reduction confirmed the competitive binding of triprolidine at the same site as macrocycle 7, further validating the

significance of this region. Given these insights, there is a promising potential for designing a dual inhibitor that targets both the fluoxetine and triprolidine-binding sites. This approach could result in increased specificity and affinity for LDH-1.

7.3.4 Mimicking the *N*-Terminal arm: insights from foldamer design

Foldamers, known for mimicking the folding capabilities of peptidic structures, offer a potential solution to address the ADME challenges and protease susceptibility of peptides [206]. In our laboratory, a foldamer structure has recently been designed to emulate the α-helix conformation of the *N*-terminal arm of LDH-H, incorporating essential residues (Leu-3, Leu-7, and Ile-8) involved in interactions at the tetrameric interface, in positions i, i+4, and i+5, respectively. A benzodiazepine O-alkylated oligobenzamide (DO-03-63) (**Figure 37**) was synthesized with this objective and assessed using MST binding check and MST binding affinity, revealing a promising K_D of approximately 300 µM against LDH-Htr (*unpublished data*). These encouraging results pave the way for the synthesis of a foldamer library, allowing for amino acid residue substitutions. The potential substitution of the three fundamental residues presents an opportunity to evaluate their interactions with LDHs in the *N*-terminal arm region.

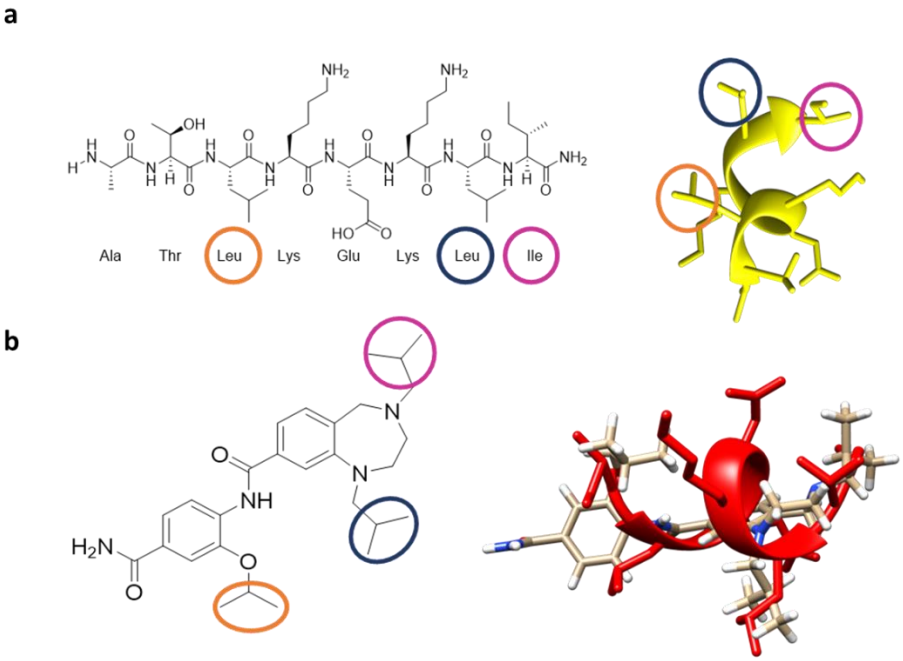

Figure 37. Towards a peptidomimetic approach: design of the foldamer. (**a**) On the left, the figure depicts the 8 amino acid *N*-terminal LDH-B arm sequence. Leu, Leu and Ile were found to be the fundamental residues for the interaction at the tetrameric interface. The draw is based on the α-helix conformation fold with the i, i+4, i+5 positions occupied by those residues. (Leu, Leu and Ile in orange, blue and magenta, respectively). An *in silico* representation of the foldamer showing the α-helix conformation is proposed on the right. (**b**) Representation of DO-03-63 (*left*). The benzodiazepine O-alkylated oligobenzamide constrains the structure in an α-helix fold maintaining the desired residues in native LDH-B *N*-terminal arm positions. On the right, a 3D alignment of the molecule with the *N*-terminal arm (residues 1 to 8) of LDH-H (PDB:1i0z) shows hotspot side chains. Pictures were generated using UCSF Chimera.

Among the perspectives that I listed, priority lies in validating the metabolic impact of the identified compounds on cellular metabolism, upon LDH inhibition. This needs evaluation through comparison with nonmalignant cell lines to elucidate their specific effects on cancer cells.

Furthermore, the potential for chemical modifications of the compounds holds promises for developing a new library of drugs based on the identified pharmacophore, offering exciting avenues for further investigation. While exploring the development of a peptidomimetic molecule as a homotetrameric disruptor presents an innovative strategy, progress requires chemical modifications to enhance solubility and affinity to the target protein.

In conclusion, through the insights gained in probing the homomeric interface of LDHs, we have opened a small yet significant door for further exploration in this field, contributing to the advancement of anticancer research with the aim to ultimately impact patient outcomes.

8. References

1. Fiume, L., et al., *Inhibition of lactate dehydrogenase activity as an approach to cancer therapy.* Future Med Chem, 2014. **6**(4): p. 429-45.
2. Claps, G., et al., *The multiple roles of LDH in cancer.* Nat Rev Clin Oncol, 2022. **19**(12): p. 749-762.
3. Brisson, L., et al., *Lactate Dehydrogenase B Controls Lysosome Activity and Autophagy in Cancer.* Cancer Cell, 2016. **30**(3): p. 418-431.
4. Granchi, C. and F. Minutolo, *Anticancer agents that counteract tumor glycolysis.* ChemMedChem, 2012. **7**(8): p. 1318-50.
5. Thabault, L., et al., *Discovery of small molecules interacting at lactate dehydrogenases tetrameric interface using a biophysical screening cascade.* Eur J Med Chem, 2022. **230**: p. 114102.
6. Danhier, P., et al., *Cancer metabolism in space and time: Beyond the Warburg effect.* Biochim Biophys Acta Bioenerg, 2017. **1858**(8): p. 556-572.
7. Vander Heiden, M.G., L.C. Cantley, and C.B. Thompson, *Understanding the Warburg effect: the metabolic requirements of cell proliferation.* Science, 2009. **324**(5930): p. 1029-33.
8. Semenza, G.L., *Hypoxia-inducible factor 1: oxygen homeostasis and disease pathophysiology.* Trends Mol Med, 2001. **7**(8): p. 345-50.
9. Stubbs, M. and J.R. Griffiths, *The altered metabolism of tumors: HIF-1 and its role in the Warburg effect.* Adv Enzyme Regul, 2010. **50**(1): p. 44-55.
10. Jensen, M.M. and A. Kjaer, *Monitoring of anti-cancer treatment with (18)F-FDG and (18)F-FLT PET: a comprehensive review of pre-clinical studies.* Am J Nucl Med Mol Imaging, 2015. **5**(5): p. 431-56.
11. Chalhoub, N. and S.J. Baker, *PTEN and the PI3-kinase pathway in cancer.* Annu Rev Pathol, 2009. **4**: p. 127-50.
12. Bartrons, R., et al., *Fructose 2,6-Bisphosphate in Cancer Cell Metabolism.* Front Oncol, 2018. **8**: p. 331.
13. Gottlob, K., et al., *Inhibition of early apoptotic events by Akt/PKB is dependent on the first committed step of glycolysis and mitochondrial hexokinase.* Genes Dev, 2001. **15**(11): p. 1406-18.

14. Deprez, J., et al., *Phosphorylation and activation of heart 6-phosphofructo-2-kinase by protein kinase B and other protein kinases of the insulin signaling cascades.* J Biol Chem, 1997. **272**(28): p. 17269-75.
15. Osthus, R.C., et al., *Deregulation of glucose transporter 1 and glycolytic gene expression by c-Myc.* J Biol Chem, 2000. **275**(29): p. 21797-800.
16. Wieman, H.L., J.A. Wofford, and J.C. Rathmell, *Cytokine stimulation promotes glucose uptake via phosphatidylinositol-3 kinase/Akt regulation of Glut1 activity and trafficking.* Mol Biol Cell, 2007. **18**(4): p. 1437-46.
17. Yu, M., et al., *The prognostic value of GLUT1 in cancers: a systematic review and meta-analysis.* Oncotarget, 2017. **8**(26): p. 43356-43367.
18. Stanton, R.C., *Glucose-6-phosphate dehydrogenase, NADPH, and cell survival.* IUBMB Life, 2012. **64**(5): p. 362-9.
19. Wang, C., et al., *Identification of transaldolase as a novel serum biomarker for hepatocellular carcinoma metastasis using xenografted mouse model and clinic samples.* Cancer Lett, 2011. **313**(2): p. 154-66.
20. Xu, X., et al., *Transketolase-like protein 1 (TKTL1) is required for rapid cell growth and full viability of human tumor cells.* Int J Cancer, 2009. **124**(6): p. 1330-7.
21. de Queiroz, R.M., et al., *Hexosamine Biosynthetic Pathway and Glycosylation Regulate Cell Migration in Melanoma Cells.* Front Oncol, 2019. **9**: p. 116.
22. Akella, N.M., L. Ciraku, and M.J. Reginato, *Fueling the fire: emerging role of the hexosamine biosynthetic pathway in cancer.* BMC Biol, 2019. **17**(1): p. 52.
23. Pavlova, N.N. and C.B. Thompson, *The Emerging Hallmarks of Cancer Metabolism.* Cell Metab, 2016. **23**(1): p. 27-47.
24. Snell, K., Y. Natsumeda, and G. Weber, *The modulation of serine metabolism in hepatoma 3924A during different phases of cellular proliferation in culture.* Biochem J, 1987. **245**(2): p. 609-12.
25. Mattaini, K.R., M.R. Sullivan, and M.G. Vander Heiden, *The importance of serine metabolism in cancer.* J Cell Biol, 2016. **214**(3): p. 249-57.

26. Feron, O., *Pyruvate into lactate and back: from the Warburg effect to symbiotic energy fuel exchange in cancer cells.* Radiother Oncol, 2009. **92**(3): p. 329-33.
27. Stine, Z.E., et al., *Targeting cancer metabolism in the era of precision oncology.* Nat Rev Drug Discov, 2022. **21**(2): p. 141-162.
28. DeBerardinis, R.J., et al., *Beyond aerobic glycolysis: transformed cells can engage in glutamine metabolism that exceeds the requirement for protein and nucleotide synthesis.* Proc Natl Acad Sci U S A, 2007. **104**(49): p. 19345-50.
29. Semenza, G.L., et al., *Hypoxia response elements in the aldolase A, enolase 1, and lactate dehydrogenase A gene promoters contain essential binding sites for hypoxia-inducible factor 1.* J Biol Chem, 1996. **271**(51): p. 32529-37.
30. Thabault, L., et al., *Interrogating the Lactate Dehydrogenase Tetramerization Site Using (Stapled) Peptides.* J Med Chem, 2020. **63**(9): p. 4628-4643.
31. Rao, S.T. and M.G. Rossmann, *Comparison of super-secondary structures in proteins.* J Mol Biol, 1973. **76**(2): p. 241-56.
32. Granchi, C., et al., *Inhibitors of lactate dehydrogenase isoforms and their therapeutic potentials.* Curr Med Chem, 2010. **17**(7): p. 672-97.
33. Read, J.A., et al., *Structural basis for altered activity of M- and H-isozyme forms of human lactate dehydrogenase.* Proteins, 2001. **43**(2): p. 175-85.
34. Quistorff, B. and N. Grunnet, *The isoenzyme pattern of LDH does not play a physiological role; except perhaps during fast transitions in energy metabolism.* Aging (Albany NY), 2011. **3**(5): p. 457-60.
35. Swiderek, K. and P. Paneth, *Differences and similarities in binding of pyruvate and L-lactate in the active site of M4 and H4 isoforms of human lactate dehydrogenase.* Arch Biochem Biophys, 2011. **505**(1): p. 33-41.
36. Hewitt, C.O., et al., *A general method for relieving substrate inhibition in lactate dehydrogenases.* Protein Eng, 1999. **12**(6): p. 491-6.
37. Zdralevic, M., et al., *Double genetic disruption of lactate dehydrogenases A and B is required to ablate the "Warburg effect" restricting tumor growth to oxidative metabolism.* J Biol Chem, 2018. **293**(41): p. 15947-15961.

38. Jafary, F., et al., *Novel Peptide Inhibitors for Lactate Dehydrogenase A (LDHA): A Survey to Inhibit LDHA Activity via Disruption of Protein-Protein Interaction.* Sci Rep, 2019. **9**(1): p. 4686.
39. Thabault, L., et al., *Discovery of a novel lactate dehydrogenase tetramerization domain using epitope mapping and peptides.* J Biol Chem, 2021. **296**: p. 100422.
40. Van Hall, G., *Lactate as a fuel for mitochondrial respiration.* Acta Physiol Scand, 2000. **168**(4): p. 643-56.
41. Gertz, E.W., et al., *Myocardial substrate utilization during exercise in humans. Dual carbon-labeled carbohydrate isotope experiments.* J Clin Invest, 1988. **82**(6): p. 2017-25.
42. Lane, A.N., T.W.M. Fan, and R.M. Higashi, *Metabolic acidosis and the importance of balanced equations.* Metabolomics, 2009. **5**(2): p. 163-165.
43. Lee, S.H. and J.R. Griffiths, *How and Why Are Cancers Acidic? Carbonic Anhydrase IX and the Homeostatic Control of Tumour Extracellular pH.* Cancers (Basel), 2020. **12**(6): p. 1616.
44. Adams, M.J., et al., *Structure of lactate dehydrogenase at 2-8 A resolution.* Nature, 1970. **227**(5263): p. 1098-103.
45. Opitz, U., et al., *Proteolytic dimers of porcine muscle lactate dehydrogenase: characterization, folding, and reconstitution of the truncated and nicked polypeptide chain.* Biochemistry, 1987. **26**(5): p. 1399-406.
46. Zheng, Y., et al., *Effects of N-terminal deletion mutation on rabbit muscle lactate dehydrogenase.* Biochemistry (Mosc), 2004. **69**(4): p. 401-6.
47. Yuan, C., H. Hu, and G. Xu, *Single amino-acid substitution in the N-terminal arm altered the tetramer stability of rat muscle lactate dehydrogenase A.* Sci China C Life Sci, 2001. **44**(6): p. 576-84.
48. Schmidt, R.K. and J.E. Gready, *Molecular Dynamics Simulations of L-Lactate Dehydrogenase: Conformation of a Mobile Loop and Influence of the Tetrameric Protein Environment.* Molecular modeling annual, 1999. **5**(9): p. 153-168.
49. Nadal-Bufi, F., et al., *Designed beta-Hairpins Inhibit LDH5 Oligomerization and Enzymatic Activity.* J Med Chem, 2021. **64**(7): p. 3767-3779.
50. Madeira, F., et al., *Search and sequence analysis tools services from EMBL-EBI in 2022.* Nucleic Acids Res, 2022. **50**(W1): p. W276-W279.

51. Sonveaux, P., et al., *Targeting lactate-fueled respiration selectively kills hypoxic tumor cells in mice.* J Clin Invest, 2008. **118**(12): p. 3930-42.
52. Chiarugi, A., et al., *The NAD metabolome--a key determinant of cancer cell biology.* Nat Rev Cancer, 2012. **12**(11): p. 741-52.
53. Fan, J., et al., *Tyrosine phosphorylation of lactate dehydrogenase A is important for NADH/NAD(+) redox homeostasis in cancer cells.* Mol Cell Biol, 2011. **31**(24): p. 4938-50.
54. Puri, S. and K. Juvale, *Monocarboxylate transporter 1 and 4 inhibitors as potential therapeutics for treating solid tumours: A review with structure-activity relationship insights.* Eur J Med Chem, 2020. **199**: p. 112393.
55. Andres, V., J. Carreras, and R. Cusso, *Regulation of muscle phosphofructokinase by physiological concentrations of bisphosphorylated hexoses: effect of alkalinization.* Biochem Biophys Res Commun, 1990. **172**(1): p. 328-34.
56. Marchiq, I. and J. Pouyssegur, *Hypoxia, cancer metabolism and the therapeutic benefit of targeting lactate/H(+) symporters.* J Mol Med (Berl), 2016. **94**(2): p. 155-71.
57. Walenta, S., T. Schroeder, and W. Mueller-Klieser, *Lactate in solid malignant tumors: potential basis of a metabolic classification in clinical oncology.* Curr Med Chem, 2004. **11**(16): p. 2195-204.
58. White, E., *Deconvoluting the context-dependent role for autophagy in cancer.* Nat Rev Cancer, 2012. **12**(6): p. 401-10.
59. Pamarthy, S., et al., *The curious case of vacuolar ATPase: regulation of signaling pathways.* Mol Cancer, 2018. **17**(1): p. 41.
60. Urbanska, K. and A. Orzechowski, *Unappreciated Role of LDHA and LDHB to Control Apoptosis and Autophagy in Tumor Cells.* Int J Mol Sci, 2019. **20**(9): p. 2085.
61. Ko, Y.H., et al., *Glutamine fuels a vicious cycle of autophagy in the tumor stroma and oxidative mitochondrial metabolism in epithelial cancer cells: implications for preventing chemotherapy resistance.* Cancer Biol Ther, 2011. **12**(12): p. 1085-97.
62. Perez-Escuredo, J., et al., *Monocarboxylate transporters in the brain and in cancer.* Biochim Biophys Acta, 2016. **1863**(10): p. 2481-97.
63. Liu, Z.L., et al., *Angiogenic signaling pathways and anti-angiogenic therapy for cancer.* Signal Transduct Target Ther, 2023. **8**(1): p. 198.
64. Nishida, N., et al., *Angiogenesis in cancer.* Vasc Health Risk Manag, 2006. **2**(3): p. 213-9.

65. Lu, H., et al., *Reversible inactivation of HIF-1 prolyl hydroxylases allows cell metabolism to control basal HIF-1.* J Biol Chem, 2005. **280**(51): p. 41928-39.
66. Polet, F. and O. Feron, *Endothelial cell metabolism and tumour angiogenesis: glucose and glutamine as essential fuels and lactate as the driving force.* J Intern Med, 2013. **273**(2): p. 156-65.
67. Vegran, F., et al., *Lactate influx through the endothelial cell monocarboxylate transporter MCT1 supports an NF-kappaB/IL-8 pathway that drives tumor angiogenesis.* Cancer Res, 2011. **71**(7): p. 2550-60.
68. Sonveaux, P., et al., *Targeting the lactate transporter MCT1 in endothelial cells inhibits lactate-induced HIF-1 activation and tumor angiogenesis.* PLoS One, 2012. **7**(3): p. e33418.
69. Dhup, S., et al., *Multiple biological activities of lactic acid in cancer: influences on tumor growth, angiogenesis and metastasis.* Curr Pharm Des, 2012. **18**(10): p. 1319-30.
70. Gatenby, R.A., et al., *Acid-mediated tumor invasion: a multidisciplinary study.* Cancer Res, 2006. **66**(10): p. 5216-23.
71. Stubbs, M., et al., *Causes and consequences of tumour acidity and implications for treatment.* Mol Med Today, 2000. **6**(1): p. 15-9.
72. Estrella, V., et al., *Acidity generated by the tumor microenvironment drives local invasion.* Cancer Res, 2013. **73**(5): p. 1524-35.
73. Rozhin, J., et al., *Pericellular pH affects distribution and secretion of cathepsin B in malignant cells.* Cancer Res, 1994. **54**(24): p. 6517-25.
74. Chen, A.N., et al., *Lactylation, a Novel Metabolic Reprogramming Code: Current Status and Prospects.* Front Immunol, 2021. **12**: p. 688910.
75. Latham, T., et al., *Lactate, a product of glycolytic metabolism, inhibits histone deacetylase activity and promotes changes in gene expression.* Nucleic Acids Res, 2012. **40**(11): p. 4794-803.
76. Colegio, O.R., et al., *Functional polarization of tumour-associated macrophages by tumour-derived lactic acid.* Nature, 2014. **513**(7519): p. 559-63.
77. Reckzeh, E.S., et al., *Inhibition of Glucose Transporters and Glutaminase Synergistically Impairs Tumor Cell Growth.* Cell Chem Biol, 2019. **26**(9): p. 1214-1228 e25.
78. Siebeneicher, H., et al., *Identification and Optimization of the First Highly Selective GLUT1 Inhibitor BAY-876.* ChemMedChem, 2016. **11**(20): p. 2261-2271.

79. Lin, H., et al., *Discovery of a Novel 2,6-Disubstituted Glucosamine Series of Potent and Selective Hexokinase 2 Inhibitors.* ACS Med Chem Lett, 2016. **7**(3): p. 217-22.
80. Rathod, B., et al., *Tumor pyruvate kinase M2 modulators: a comprehensive account of activators and inhibitors as anticancer agents.* RSC Med Chem, 2021. **12**(7): p. 1121-1141.
81. Prakasam, G., et al., *Posttranslational Modifications of Pyruvate Kinase M2: Tweaks that Benefit Cancer.* Front Oncol, 2018. **8**: p. 22.
82. Becker, A., et al., *Development of 5-benzylpaullones and paullone-9-carboxylic acid alkyl esters as selective inhibitors of mitochondrial malate dehydrogenase (mMDH).* Eur J Med Chem, 2010. **45**(1): p. 335-42.
83. Godesi, S., et al., *Design, Synthesis and Biological Evaluation of Novel MDH Inhibitors Targeting Tumor Microenvironment.* Pharmaceuticals (Basel), 2023. **16**(5).
84. Reyes Romero, A., et al., *A fragment-based approach identifies an allosteric pocket that impacts malate dehydrogenase activity.* Commun Biol, 2021. **4**(1): p. 949.
85. Halford, S., et al., *A Phase I Dose-escalation Study of AZD3965, an Oral Monocarboxylate Transporter 1 Inhibitor, in Patients with Advanced Cancer.* Clin Cancer Res, 2023. **29**(8): p. 1429-1439.
86. Payen, V.L., et al., *Monocarboxylate transporters in cancer.* Mol Metab, 2020. **33**: p. 48-66.
87. Felmlee, M.A., et al., *Monocarboxylate Transporters (SLC16): Function, Regulation, and Role in Health and Disease.* Pharmacol Rev, 2020. **72**(2): p. 466-485.
88. Doherty, J.R. and J.L. Cleveland, *Targeting lactate metabolism for cancer therapeutics.* J Clin Invest, 2013. **123**(9): p. 3685-92.
89. Hirschhaeuser, F., U.G. Sattler, and W. Mueller-Klieser, *Lactate: a metabolic key player in cancer.* Cancer Res, 2011. **71**(22): p. 6921-5.
90. Mohammad, G.H., et al., *Pyruvate Kinase M2 and Lactate Dehydrogenase A Are Overexpressed in Pancreatic Cancer and Correlate with Poor Outcome.* PLoS One, 2016. **11**(3): p. e0151635.
91. Zhao, J., et al., *LDHA promotes tumor metastasis by facilitating epithelial-mesenchymal transition in renal cell carcinoma.* Mol Med Rep, 2017. **16**(6): p. 8335-8344.
92. Xie, H., et al., *Targeting lactate dehydrogenase--a inhibits tumorigenesis and tumor progression in mouse models of lung cancer*

and impacts tumor-initiating cells. Cell Metab, 2014. **19**(5): p. 795-809.
93. Fantin, V.R., J. St-Pierre, and P. Leder, *Attenuation of LDH-A expression uncovers a link between glycolysis, mitochondrial physiology, and tumor maintenance.* Cancer Cell, 2006. **9**(6): p. 425-34.
94. McCleland, M.L., et al., *An integrated genomic screen identifies LDHB as an essential gene for triple-negative breast cancer.* Cancer Res, 2012. **72**(22): p. 5812-23.
95. Oshima, N., et al., *Dynamic Imaging of LDH Inhibition in Tumors Reveals Rapid In Vivo Metabolic Rewiring and Vulnerability to Combination Therapy.* Cell Rep, 2020. **30**(6): p. 1798-1810 e4.
96. Kanno, T., et al., *Lactate dehydrogenase M-subunit deficiency: a new type of hereditary exertional myopathy.* Clin Chim Acta, 1988. **173**(1): p. 89-98.
97. Pretsch, W., et al., *A mutation affecting the lactate dehydrogenase locus Ldh-1 in the mouse. II. Mechanism of the LDH-A deficiency associated with hemolytic anemia.* Genetics, 1993. **135**(1): p. 161-70.
98. Joukyuu, R., et al., *Hereditary complete deficiency of lactate dehydrogenase H-subunit.* Clin Chem, 1989. **35**(4): p. 687-90.
99. Liu, S., et al., *Glycerol-3-phosphate biosynthesis regenerates cytosolic NAD(+) to alleviate mitochondrial disease.* Cell Metab, 2021. **33**(10): p. 1974-1987 e9.
100. Le, A., et al., *Inhibition of lactate dehydrogenase A induces oxidative stress and inhibits tumor progression.* Proc Natl Acad Sci U S A, 2010. **107**(5): p. 2037-42.
101. Granchi, C., et al., *N-Hydroxyindole-based inhibitors of lactate dehydrogenase against cancer cell proliferation.* Eur J Med Chem, 2011. **46**(11): p. 5398-407.
102. Granchi, C., et al., *Discovery of N-hydroxyindole-based inhibitors of human lactate dehydrogenase isoform A (LDH-A) as starvation agents against cancer cells.* J Med Chem, 2011. **54**(6): p. 1599-612.
103. Flack, M.R., et al., *Oral gossypol in the treatment of metastatic adrenal cancer.* J Clin Endocrinol Metab, 1993. **76**(4): p. 1019-24.
104. Van Poznak, C., et al., *Oral gossypol in the treatment of patients with refractory metastatic breast cancer: a phase I/II clinical trial.* Breast Cancer Res Treat, 2001. **66**(3): p. 239-48.
105. Jaroszewski, J.W., O. Kaplan, and J.S. Cohen, *Action of gossypol and rhodamine 123 on wild type and multidrug-resistant MCF-7 human*

breast cancer cells: 31P nuclear magnetic resonance and toxicity studies. Cancer Res, 1990. **50**(21): p. 6936-43.
106. Granchi, C., et al., *Small-molecule inhibitors of human LDH5.* Future Med Chem, 2013. **5**(16): p. 1967-91.
107. Vander Jagt, D.L., L.M. Deck, and R.E. Royer, *Gossypol: prototype of inhibitors targeted to dinucleotide folds.* Curr Med Chem, 2000. **7**(4): p. 479-98.
108. Kohlmann, A., et al., *Fragment growing and linking lead to novel nanomolar lactate dehydrogenase inhibitors.* J Med Chem, 2013. **56**(3): p. 1023-40.
109. Billiard, J., et al., *Quinoline 3-sulfonamides inhibit lactate dehydrogenase A and reverse aerobic glycolysis in cancer cells.* Cancer Metab, 2013. **1**(1): p. 19.
110. Boudreau, A., et al., *Metabolic plasticity underpins innate and acquired resistance to LDHA inhibition.* Nat Chem Biol, 2016. **12**(10): p. 779-86.
111. Rai, G., et al., *Discovery and Optimization of Potent, Cell-Active Pyrazole-Based Inhibitors of Lactate Dehydrogenase (LDH).* J Med Chem, 2017. **60**(22): p. 9184-9204.
112. Lau, J.L. and M.K. Dunn, *Therapeutic peptides: Historical perspectives, current development trends, and future directions.* Bioorg Med Chem, 2018. **26**(10): p. 2700-2707.
113. Wilcox, G., *Insulin and insulin resistance.* Clin Biochem Rev, 2005. **26**(2): p. 19-39.
114. Al Shaer, D., et al., *2021 FDA TIDES (Peptides and Oligonucleotides) Harvest.* Pharmaceuticals (Basel), 2022. **15**(2).
115. Wang, L., et al., *Therapeutic peptides: current applications and future directions.* Signal Transduct Target Ther, 2022. **7**(1): p. 48.
116. Moiola, M., M.G. Memeo, and P. Quadrelli, *Stapled Peptides-A Useful Improvement for Peptide-Based Drugs.* Molecules, 2019. **24**(20): p. 3654.
117. Philippe, G.J.B., D.J. Craik, and S.T. Henriques, *Converting peptides into drugs targeting intracellular protein-protein interactions.* Drug Discov Today, 2021. **26**(6): p. 1521-1531.
118. Hill, T.A., et al., *Constraining cyclic peptides to mimic protein structure motifs.* Angew Chem Int Ed Engl, 2014. **53**(48): p. 13020-41.
119. Wojcik, P. and L. Berlicki, *Peptide-based inhibitors of protein-protein interactions.* Bioorg Med Chem Lett, 2016. **26**(3): p. 707-713.

120. Nadal-Bufi, F., et al., *Peptide-based LDH5 inhibitors enter cancer cells and impair proliferation.* Cell Mol Life Sci, 2022. **79**(12): p. 606.
121. Woodford, M.R., et al., *The tumor suppressor folliculin inhibits lactate dehydrogenase A and regulates the Warburg effect.* Nat Struct Mol Biol, 2021. **28**(8): p. 662-670.
122. Bedard, P.L., et al., *Small molecules, big impact: 20 years of targeted therapy in oncology.* Lancet, 2020. **395**(10229): p. 1078-1088.
123. Zhong, L., et al., *Small molecules in targeted cancer therapy: advances, challenges, and future perspectives.* Signal Transduct Target Ther, 2021. **6**(1): p. 201.
124. Hoelder, S., P.A. Clarke, and P. Workman, *Discovery of small molecule cancer drugs: successes, challenges and opportunities.* Mol Oncol, 2012. **6**(2): p. 155-76.
125. Friberg, A., et al., *Structural Evidence for Isoform-Selective Allosteric Inhibition of Lactate Dehydrogenase A.* ACS Omega, 2020. **5**(22): p. 13034-13041.
126. Shibata, S., et al., *Identification of the first highly selective inhibitor of human lactate dehydrogenase B.* Sci Rep, 2021. **11**(1): p. 21353.
127. Thabault, L., M. Liberelle, and R. Frederick, *Targeting protein self-association in drug design.* Drug Discov Today, 2021. **26**(5): p. 1148-1163.
128. Scott, D.E., et al., *Small molecules, big targets: drug discovery faces the protein-protein interaction challenge.* Nat Rev Drug Discov, 2016. **15**(8): p. 533-50.
129. Lu, H., et al., *Recent advances in the development of protein-protein interactions modulators: mechanisms and clinical trials.* Signal Transduct Target Ther, 2020. **5**(1): p. 213.
130. Guharoy, M. and P. Chakrabarti, *Conserved residue clusters at protein-protein interfaces and their use in binding site identification.* BMC Bioinformatics, 2010. **11**: p. 286.
131. Jubb, H.C., et al., *Mutations at protein-protein interfaces: Small changes over big surfaces have large impacts on human health.* Prog Biophys Mol Biol, 2017. **128**: p. 3-13.
132. Zhang, X., et al., *A novel inhibitor of STAT3 homodimerization selectively suppresses STAT3 activity and malignant transformation.* Cancer Res, 2013. **73**(6): p. 1922-33.
133. Pi, F., et al., *Discovery of a new method for potent drug development using power function of stoichiometry of homomeric biocomplexes or*

biological nanomotors. Expert Opin Drug Deliv, 2016. **13**(1): p. 23-36.
134. Derry, W.B., L. Wilson, and M.A. Jordan, *Substoichiometric binding of taxol suppresses microtubule dynamics.* Biochemistry, 1995. **34**(7): p. 2203-11.
135. La Manna, S., et al., *Peptides as Therapeutic Agents for Inflammatory-Related Diseases.* Int J Mol Sci, 2018. **19**(9): p. 2714.
136. Lee, A.C., et al., *A Comprehensive Review on Current Advances in Peptide Drug Development and Design.* Int J Mol Sci, 2019. **20**(10): p. 2383.
137. Shangary, S. and S. Wang, *Small-molecule inhibitors of the MDM2-p53 protein-protein interaction to reactivate p53 function: a novel approach for cancer therapy.* Annu Rev Pharmacol Toxicol, 2009. **49**: p. 223-41.
138. Vu, B., et al., *Discovery of RG7112: A Small-Molecule MDM2 Inhibitor in Clinical Development.* ACS Med Chem Lett, 2013. **4**(5): p. 466-9.
139. Chang, Y.S., et al., *Stapled alpha-helical peptide drug development: a potent dual inhibitor of MDM2 and MDMX for p53-dependent cancer therapy.* Proc Natl Acad Sci U S A, 2013. **110**(36): p. E3445-54.
140. Lunev, S., et al., *Oligomeric interfaces as a tool in drug discovery: Specific interference with activity of malate dehydrogenase of Plasmodium falciparum in vitro.* PLoS One, 2018. **13**(4): p. e0195011.
141. Sereikaite, V., et al., *Targeting the gamma-Aminobutyric Acid Type B (GABA(B)) Receptor Complex: Development of Inhibitors Targeting the K(+) Channel Tetramerization Domain (KCTD) Containing Proteins/GABA(B) Receptor Protein-Protein Interaction.* J Med Chem, 2019. **62**(19): p. 8819-8830.
142. Seidel, S.A., et al., *Microscale thermophoresis quantifies biomolecular interactions under previously challenging conditions.* Methods, 2013. **59**(3): p. 301-15.
143. Walpole, S., et al., *STD NMR as a Technique for Ligand Screening and Structural Studies.* Methods Enzymol, 2019. **615**: p. 423-451.
144. Bhunia, A., S. Bhattacharjya, and S. Chatterjee, *Applications of saturation transfer difference NMR in biological systems.* Drug Discov Today, 2012. **17**(9-10): p. 505-13.

145. Foley, E.D.B., et al., *Mass photometry enables label-free tracking and mass measurement of single proteins on lipid bilayers.* Nat Methods, 2021. **18**(10): p. 1247-1252.
146. Jerabek-Willemsen, M., et al., *Molecular interaction studies using microscale thermophoresis.* Assay Drug Dev Technol, 2011. **9**(4): p. 342-53.
147. Kim, S.H., et al., *Nano Differential Scanning Fluorimetry-Based Thermal Stability Screening and Optimal Buffer Selection for Immunoglobulin G.* Pharmaceuticals (Basel), 2021. **15**(1).
148. Soltermann, F., et al., *Quantifying Protein-Protein Interactions by Molecular Counting with Mass Photometry.* Angew Chem Int Ed Engl, 2020. **59**(27): p. 10774-10779.
149. Some, D., et al., *Characterization of Proteins by Size-Exclusion Chromatography Coupled to Multi-Angle Light Scattering (SEC-MALS).* J Vis Exp, 2019(148).
150. Jafari, R., et al., *The cellular thermal shift assay for evaluating drug target interactions in cells.* Nat Protoc, 2014. **9**(9): p. 2100-22.
151. Bastos, M. and A. Velazquez-Campoy, *Isothermal titration calorimetry (ITC): a standard operating procedure (SOP).* Eur Biophys J, 2021. **50**(3-4): p. 363-371.
152. Braz, V.A. and K.J. Howard, *Separation of protein oligomers by blue native gel electrophoresis.* Anal Biochem, 2009. **388**(1): p. 170-2.
153. Lawrence, S.H., et al., *Allosteric inhibition of human porphobilinogen synthase.* J Biol Chem, 2009. **284**(51): p. 35807-17.
154. He, M.M., et al., *Small-molecule inhibition of TNF-alpha.* Science, 2005. **310**(5750): p. 1022-5.
155. Toro, M.A., et al., *Probing the dimerization interface of Leishmania infantum trypanothione reductase with site-directed mutagenesis and short peptides.* Chembiochem, 2013. **14**(10): p. 1212-7.
156. Sindrewicz, P., et al., *Intrinsic tryptophan fluorescence spectroscopy reliably determines galectin-ligand interactions.* Sci Rep, 2019. **9**(1): p. 11851.
157. DeBerardinis, R.J. and N.S. Chandel, *Fundamentals of cancer metabolism.* Sci Adv, 2016. **2**(5): p. e1600200.
158. Sheng, S.L., et al., *Knockdown of lactate dehydrogenase A suppresses tumor growth and metastasis of human hepatocellular carcinoma.* FEBS J, 2012. **279**(20): p. 3898-910.

159. Dong, T., et al., *Tumor LDH-A expression and serum LDH status are two metabolic predictors for triple negative breast cancer brain metastasis.* Sci Rep, 2017. **7**(1): p. 6069.
160. Yang, Y., et al., *Targeting lactate dehydrogenase a improves radiotherapy efficacy in non-small cell lung cancer: from bedside to bench.* J Transl Med, 2021. **19**(1): p. 170.
161. Guo, Y., et al., *Combined Aberrant Expression of NDRG2 and LDHA Predicts Hepatocellular Carcinoma Prognosis and Mediates the Anti-tumor Effect of Gemcitabine.* Int J Biol Sci, 2019. **15**(9): p. 1771-1786.
162. Dennison, J.B., et al., *Lactate dehydrogenase B: a metabolic marker of response to neoadjuvant chemotherapy in breast cancer.* Clin Cancer Res, 2013. **19**(13): p. 3703-13.
163. Wakabayashi, H., et al., *Hereditary deficiency of lactate dehydrogenase H-subunit.* Intern Med, 1996. **35**(7): p. 550-4.
164. Meng, B., et al., *Structural and functional analyses of human tryptophan 2,3-dioxygenase.* Proteins, 2014. **82**(11): p. 3210-6.
165. Navia, M.A., et al., *Three-dimensional structure of aspartyl protease from human immunodeficiency virus HIV-1.* Nature, 1989. **337**(6208): p. 615-20.
166. Darling, A.J., et al., *Reconstitution of herpes simplex virus type 1 ribonucleotide reductase activity from the large and small subunits.* Virus Genes, 1989. **2**(2): p. 187-94.
167. Cochran, A.G., *Antagonists of protein-protein interactions.* Chem Biol, 2000. **7**(4): p. R85-94.
168. Pellecchia, M., *Antagonists of protein-protein interactions made easy?* J Med Chem, 2013. **56**(1): p. 13-4.
169. Dobeli, H. and G.A. Schoenenberger, *Regulation of lactate dehydrogenase activity: reversible and isoenzyme-specific inhibition of the tetramerization process by peptides.* Experientia, 1983. **39**(3): p. 281-2.
170. Toleikis, Z., et al., *Determination of the volume changes induced by ligand binding to heat shock protein 90 using high-pressure denaturation.* Anal Biochem, 2011. **413**(2): p. 171-8.
171. Dahlin, J.L., et al., *PAINS in the assay: chemical mechanisms of assay interference and promiscuous enzymatic inhibition observed during a sulfhydryl-scavenging HTS.* J Med Chem, 2015. **58**(5): p. 2091-113.
172. Mayer, M. and B. Meyer, *Group epitope mapping by saturation transfer difference NMR to identify segments of a ligand in direct*

contact with a protein receptor. J Am Chem Soc, 2001. **123**(25): p. 6108-17.
173. Ward, R.A., et al., *Design and synthesis of novel lactate dehydrogenase A inhibitors by fragment-based lead generation.* J Med Chem, 2012. **55**(7): p. 3285-306.
174. Gao, K., et al., *A synthetic peptide as an allosteric inhibitor of human arginase I and II.* Mol Biol Rep, 2021. **48**(2): p. 1959-1966.
175. Trott, O. and A.J. Olson, *AutoDock Vina: improving the speed and accuracy of docking with a new scoring function, efficient optimization, and multithreading.* J Comput Chem, 2010. **31**(2): p. 455-61.
176. Cloonan, S.M., et al., *The antidepressants maprotiline and fluoxetine have potent selective antiproliferative effects against Burkitt lymphoma independently of the norepinephrine and serotonin transporters.* Leuk Lymphoma, 2010. **51**(3): p. 523-39.
177. Garcia-Quiroz, J. and J. Camacho, *Astemizole: an old anti-histamine as a new promising anti-cancer drug.* Anticancer Agents Med Chem, 2011. **11**(3): p. 307-14.
178. Tutton, P.J. and D.H. Barkla, *Influence of inhibitors of serotonin uptake on intestinal epithelium and colorectal carcinomas.* Br J Cancer, 1982. **46**(2): p. 260-5.
179. Sleire, L., et al., *Drug repurposing in cancer.* Pharmacol Res, 2017. **124**: p. 74-91.
180. Abadi, B., et al., *Antidepressants with anti-tumor potential in treating glioblastoma: A narrative review.* Fundam Clin Pharmacol, 2022. **36**(1): p. 35-48.
181. Ellegaard, A.M., et al., *Repurposing Cationic Amphiphilic Antihistamines for Cancer Treatment.* EBioMedicine, 2016. **9**: p. 130-139.
182. Faustino-Rocha, A.I., et al., *Antihistamines as promising drugs in cancer therapy.* Life Sci, 2017. **172**: p. 27-41.
183. Zheng, Y., et al., *The application of antidepressant drugs in cancer treatment.* Biomed Pharmacother, 2023. **157**: p. 113985.
184. Khin, P.P., et al., *Apoptotic effect of fluoxetine through the endoplasmic reticulum stress pathway in the human gastric cancer cell line AGS.* Naunyn Schmiedebergs Arch Pharmacol, 2020. **393**(4): p. 537-549.

185. Deuster, E., et al., *The Platelet-Activating Factor Receptor's Association with the Outcome of Ovarian Cancer Patients and Its Experimental Inhibition by Rupatadine.* Cells, 2021. **10**(9): p. 2337.
186. Fritz, I., et al., *Desloratadine and loratadine use associated with improved melanoma survival.* Allergy, 2020. **75**(8): p. 2096-2099.
187. Kachi, K., et al., *Anti-Allergic Drug Suppressed Pancreatic Carcinogenesis via Down-Regulation of Cellular Proliferation.* Int J Mol Sci, 2021. **22**(14): p. 7444.
188. Kabsch, W., *Xds.* Acta Crystallogr D Biol Crystallogr, 2010. **66**(Pt 2): p. 125-32.
189. McCoy, A.J., et al., *Phaser crystallographic software.* J Appl Crystallogr, 2007. **40**(Pt 4): p. 658-674.
190. Read, J.A., et al., *Structural basis for altered activity of M- and H-isozyme forms of human lactate dehydrogenase.* Proteins-Structure Function and Genetics, 2001. **43**(2): p. 175-185.
191. Liebschner, D., et al., *Macromolecular structure determination using X-rays, neutrons and electrons: recent developments in Phenix.* Acta Crystallogr D Struct Biol, 2019. **75**(Pt 10): p. 861-877.
192. Emsley, P., et al., *Features and development of Coot.* Acta Crystallogr D Biol Crystallogr, 2010. **66**(Pt 4): p. 486-501.
193. Group, C.C., *Molecular Operating Environment (MOE).* 2011: Montreal, Quebec, Canada.
194. Jaenicke, R., W. Vogel, and R. Rudolph, *Dimeric intermediates in the dissociation of lactic dehydrogenase.* Eur J Biochem, 1981. **114**(3): p. 525-31.
195. Sonn-Segev, A., et al., *Quantifying the heterogeneity of macromolecular machines by mass photometry.* Nat Commun, 2020. **11**(1): p. 1772.
196. Yang, Y. and A.A. Sauve, *NAD(+) metabolism: Bioenergetics, signaling and manipulation for therapy.* Biochim Biophys Acta, 2016. **1864**(12): p. 1787-1800.
197. Hitosugi, T., et al., *Tyrosine phosphorylation of mitochondrial pyruvate dehydrogenase kinase 1 is important for cancer metabolism.* Mol Cell, 2011. **44**(6): p. 864-77.
198. Birsoy, K., et al., *An Essential Role of the Mitochondrial Electron Transport Chain in Cell Proliferation Is to Enable Aspartate Synthesis.* Cell, 2015. **162**(3): p. 540-51.
199. Lemma, S., et al., *MDA-MB-231 breast cancer cells fuel osteoclast metabolism and activity: A new rationale for the pathogenesis of*

osteolytic bone metastases. Biochim Biophys Acta Mol Basis Dis, 2017. **1863**(12): p. 3254-3264.
200. Rodriguez-Enriquez, S., et al., *Energy metabolism transition in multi-cellular human tumor spheroids.* J Cell Physiol, 2008. **216**(1): p. 189-97.
201. Woitek, R. and F.A. Gallagher, *The use of hyperpolarised (13)C-MRI in clinical body imaging to probe cancer metabolism.* Br J Cancer, 2021. **124**(7): p. 1187-1198.
202. Dutta, P., et al., *Evaluation of LDH-A and glutaminase inhibition in vivo by hyperpolarized 13C-pyruvate magnetic resonance spectroscopy of tumors.* Cancer Res, 2013. **73**(14): p. 4190-5.
203. Hermans, D., et al., *Lactate dehydrogenase inhibition synergizes with IL-21 to promote CD8(+) T cell stemness and antitumor immunity.* Proc Natl Acad Sci U S A, 2020. **117**(11): p. 6047-6055.
204. Vettore, L., R.L. Westbrook, and D.A. Tennant, *New aspects of amino acid metabolism in cancer.* Br J Cancer, 2020. **122**(2): p. 150-156.
205. Tummino, T.A., et al., *Drug-induced phospholipidosis confounds drug repurposing for SARS-CoV-2.* Science, 2021. **373**(6554): p. 541-547.
206. Breiden, B. and K. Sandhoff, *Emerging mechanisms of drug-induced phospholipidosis.* Biol Chem, 2019. **401**(1): p. 31-46.
207. Azzarito, V., et al., *Inhibition of alpha-helix-mediated protein-protein interactions using designed molecules.* Nat Chem, 2013. **5**(3): p. 161-73.